
QCD SUM RULE STUDIES AT FINITE DENSITY AND TEMPERATURE

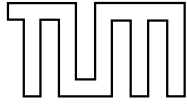
Doctoral Dissertation
by Youngshin Kwon
December 2009



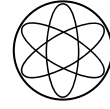
Physik-Department



TECHNISCHE
UNIVERSITÄT
MÜNCHEN



Technische Universität München



Physik Department
Institut für Theoretische Physik T39
Univ.-Prof. Dr. Wolfram Weise

QCD SUM RULE STUDIES AT FINITE DENSITY AND TEMPERATURE

Youngshin Kwon

Vollständiger Abdruck der von Fakultät für Physik der Technischen Universität München zur Erlangung des akademischen Grades eines

Doktors der Naturwissenschaften (Dr. rer. nat.)

genehmigten Dissertation.

Vorsitzender: Univ.-Prof. Dr. Reiner Krücken
Prüfer der Dissertation: 1. Univ.-Prof. Dr. Wolfram Weise
2. Univ.-Prof. Dr. Nora Brambilla

Die Dissertation wurden am 21.12.2009 bei der Technischen Universität München eingereicht und durch die Fakultät für Physik am 21.01.2010 angenommen.

Abstract

In-medium modifications of hadronic properties have a strong connection to the restoration of chiral symmetry in hot and/or dense medium. The in-medium spectral functions for vector and axial-vector mesons are of particular interest in this context, considering the experimental dilepton production data which signal the in-medium meson properties. In this thesis, finite energy sum rules are employed to set constraints for the in-medium spectral functions of vector and axial-vector mesons. Finite energy sum rules for the first two moments of the spectral functions are investigated with emphasis on the role of a scale parameter related to the spontaneous chiral symmetry breaking in QCD. It is demonstrated that these lowest moments of vector current spectral functions do permit an accurate sum rule analysis with controlled inputs, such as the QCD condensates of lowest dimensions. In contrast, the higher moments contain uncertainties from the higher dimensional condensates. It turns out that the factorization approximation for the four-quark condensate is not applicable in any of the cases studied in this work. The accurate sum rules for the lowest two moments of the spectral functions are used to clarify and classify the properties of vector meson spectral functions in a nuclear medium. Possible connections with the Brown-Rho scaling hypothesis are also discussed.

Zusammenfassung

Die Eigenschaften von Hadronen erfahren in Materie Abwandlungen, die eng mit der Wiederherstellung der chiralen Symmetrie in heißer und/oder dichter Materie verbunden sind. Spektralfunktionen in Materie von Vektor- und Axialvektormesonen sind von besonderem Interesse bei der Analyse von experimentellen Daten zur Dilepton-Produktion, die mit den Eigenschaften von Mesonen in Materie verknüpft sind. Summenregeln für endliche Energien werden angewandt, um Spektralfunktionen von Vektor- und Axialvektor-Mesonen in Materie zu untersuchen. Summenregeln für die ersten beiden Momente der Spektralfunktionen werden abgeleitet mit Hauptaugenmerk auf die Rolle des Skalenparameters für die spontane Brechung der chiralen Symmetrie in des QCD. Es wird gezeigt, dass diese beiden niedrigsten Momente der Vektorstrom-Spektralfunktionen eine präzise Summenregeln-Untersuchung bei Verwendung von bekannten Eingabegrößen, wie z.B. QCD-Kondensate niedrigster Dimensionen, erlauben.

Contents

1	Introduction	1
2	Theory of the strong interaction	4
2.1	Basics of QCD	4
2.2	Chiral symmetry	5
2.2.1	Spontaneous symmetry breaking	7
2.2.2	Chiral order parameter	8
2.2.3	Chiral effective Lagrangian	9
2.3	Currents and vector mesons	10
2.3.1	Vector mesons as gauge bosons	10
2.3.2	Weinberg sum rules	13
2.4	Partial restoration of chiral symmetry	15
2.4.1	Patterns of symmetry restoration	15
3	QCD sum rules	18
3.1	Overview	18
3.1.1	Operator Product Expansion	21
3.1.2	Dispersion relation	23
3.2	Finite energy sum rules	24
3.3	Sum rules for ρ -meson in vacuum	25
3.4	In-medium modifications of the sum rules	28
3.4.1	Condensates at low density	28
3.4.2	Condensates at low temperature	30
4	Vector mesons at finite density	31
4.1	Introduction	31
4.2	Derivation of QCD sum rules	33
4.3	Vacuum sum rules	37

4.3.1	Identifying the spontaneous chiral symmetry breaking scale	37
4.3.2	ρ -meson sum rules	38
4.3.3	Sensitivity to continuum threshold modeling	41
4.4	In-medium sum rules	43
4.4.1	ρ -meson sum rules	43
4.4.2	ω -meson sum rules	48
4.5	In-medium pion decay constant and chiral condensate	51
4.6	Note on four-quark condensates	53
4.7	Intermediate summary	54
5	Meson properties at finite temperature	56
5.1	Introduction	56
5.2	Reminder of QCD sum rules	57
5.3	T -dependence of OPE	59
5.4	Phenomenology at low T	61
5.4.1	Spectral function with zero width	63
5.4.2	Test on additional pole mass shift	64
5.4.3	Spectral function with finite width	65
5.4.4	Sensitivity to continuum threshold modeling	69
5.5	Spectral function from effective field theory	71
5.6	Note on higher order corrections	74
5.6.1	T^4 corrections	74
5.6.2	Massive states	75
5.7	Intermediate summary	75
6	Conclusion and outlook	77
	Appendix	80
A	Useful formulae	80
A.1	γ -matrix and trace techniques	80
A.2	Fourier transformation	83
A.3	Borel transformation	84
B	Expansion of the light quark propagator	85
C	QCD corrections	88
C.1	The running coupling $\alpha_s(\mu)$	88
D	First moment of quark distribution	90

<i>CONTENTS</i>	iii
Bibliography	95
Acknowledgments	101

Chapter 1

Introduction

The main subject of this thesis is to construct a reliable framework of in-medium QCD sum rules for hadrons with the aim of providing constraints for the in-medium spectral properties of the hadrons. In-medium modifications of hadronic properties are of interest per se in connection with various experiments. This topic also has a strong connection to the restoration of chiral symmetry in dense and hot hadronic matters.

Chiral symmetry is spontaneously broken in the QCD vacuum. As it is well-known from the Goldstone theorem, a spontaneous breaking of a continuous global symmetry is accompanied by massless Goldstone bosons. In QCD these Goldstone bosons are identified with the lightest pseudo-scalar mesons (pions and kaons). The non-trivial vacuum structure originally causes the spontaneous chiral symmetry breaking and is reflected by the non-zero value of chiral condensate which is the vacuum expectation value of quark-antiquark operator. Although the chiral condensate serves as a precise order parameter for spontaneously broken chiral symmetry, it is not a quantity directly observed from experiments. What we observe in the hadron spectroscopy are large mass splittings between parity partners (e.g. $\rho(770)$ - $a_1(1260)$ or $N(940)$ - $N^*(1535)$). Since the spatial parity transformation exchanges chiralities, all states of the theory should be degenerate with their parity partners if the chiral symmetry were unbroken.

Theoretical calculations, e.g. lattice gauge theory [1, 2], suggest that the spontaneously broken chiral symmetry should be restored in the vicinity of the deconfinement phase transition, i.e. at a few times normal nuclear matter density and/or at temperatures around 200 MeV. An important manifestation of chiral symmetry restoration is then that the hadronic spectral functions are modified with changing

thermodynamic conditions, and that chiral parity partners such as the ρ and a_1 mesons tend to become degenerate. In this context, dilepton production from relativistic heavy ion collisions has attracted great interest. Dileptons (e^+e^- or $\mu^+\mu^-$ pairs) as well as photons are believed to be ideal probes carrying pure information about the colliding regions at high density/temperature because dileptons hardly interact with the hadronic environments after cooling down. For heavy ion collisions at CERN SPS energies, hot and dense matter is formed in the initial stage of the collisions. The CERES/NA45 [3, 4, 6, 5] and NA60 [7, 8, 9, 10, 11, 12] experiments have shown a significant enhancement of dilepton yields with invariant masses between 0.3 GeV to 1 GeV. Dilepton productions from the two-body annihilation processes are dynamically enhanced through the vector meson resonances, such as ρ , ω and ϕ mesons, which can directly couple to lepton pairs. Therefore the invariant mass of the lepton pair emission is equivalent to the in-medium spectroscopy of the vector mesons. In particular the ρ mesons which are the lowest dipole excitations of the QCD vacuum, have been used to exploit in-medium changes of hadron properties.

The issue of in-medium hadronic properties persists as a fundamental theme ever since the suggestion of Brown and Rho [13] that hadron masses should drop to zero as a consequence of chiral symmetry restoration. The Brown-Rho's dropping mass of non-strange hadrons (BR scaling), based on the broken scale invariance of QCD, described the low-mass enhancement in the dilepton invariant mass spectra and was also supported by early studies using QCD sum rules [14]. There have also been other suggestions for a rising mass [15, 16] or even a structure with several peaks [17] thereafter. All of those scenarios are however influenced by strong collisional broadening of the spectral functions. For example, the ρ -meson spectral function, not to mention the a_1 -spectrum, has rather broad width already in the vacuum. The interactions of these mesons with hadrons in the medium would make their spectral widths even broader and hence the primary issue of a mass shift physically meaningless.

The controversial arguments of 'mass shift' versus 'broadening' can be better focused by introducing the chiral symmetry breaking scale, $\Lambda_{\text{CSB}} \approx 4\pi f_\pi$, which characterizes the convergence of the momentum expansion of chiral perturbation theory, and identifying Λ_{CSB} with the continuum threshold, $\sqrt{s_V}$, a scale separating the low energy resonance region from the high energy continuum in the spectral representation. The hypothetical relation, $\sqrt{s_V} = 4\pi f_\pi$, in vacuum is supported by the time-honored current algebras and spectral sum rules. The extension of

this relation to finite temperature or density is discussed in this thesis. Such a scale analysis, rather than the notions of in-medium mass and/or width, provides a better way to set constraints on the spectral functions in the nuclear medium.

QCD sum rules are often used to set constraints on the spectral properties of hadrons. The basis of this approach is Wilson's operator product expansion [18] (OPE) for the time-ordered product of two (or more) interpolating currents. Non-perturbative effects are taken into account by the non-zero values of condensates. The coefficients of the condensates are calculated in perturbation theory. At low temperature or density, non-perturbative corrections to the in-medium OPE are contributed by temperature- and density-dependent changes in the condensates.

The OPE includes higher dimensional operators (e.g. four-quark condensates) with unknown values, which make the sum rule analysis inaccurate. The finite energy sum rule (FESR) [19, 20, 21], one of the typical branches of QCD sum rule approaches, has the advantage that, if selecting only the lowest moments of the sum rules, the higher order condensates are excluded. Furthermore, one can determine the chiral gap scale $\sqrt{s_V}$ from the FESR regardless of any unphysical scale parameters such as the Borel mass. Several in-medium spectral functions that come from either effective theories or models are taken into account as an input into the phenomenological side of the sum rule analysis.

This dissertation is organized as follows: After this introduction, the basics of the strong interaction physics are summarized in chapter 2, focused on aspects of chiral symmetry. Chapter 3 is devoted by the general review of QCD sum rules in vacuum. It is shown how the QCD sum rules relate hadronic properties with QCD degrees of freedom. Current correlation functions as the usual starting point of the QCD sum rules are analytically continued in the complex energy plane via a dispersion relation. The extension of the sum rules to finite baryon density is discussed in chapter 4 [22]. We apply the in-medium FESR to the light vector mesons ($\rho(770)$ and $\omega(780)$) at normal nuclear matter density (0.17 fm^{-3}) in order to test the in-medium changes of their hadronic properties. In chapter 5, we analyze properties of the ρ - and a_1 -mesons at finite temperature using the in-medium FESR. Conclusions and an outlook are given in chapter 6.

Chapter 2

Theory of the strong interaction

2.1 Basics of QCD

The strong interaction sector of the standard model is described by quantum chromodynamics (QCD), a non-abelian $SU(3)_c$ gauge theory with quark-gluon degrees of freedom. The QCD Lagrangian is given by

$$\mathcal{L}_{\text{QCD}} = \bar{\psi}(i\gamma_\mu D^\mu - \mathbf{m})\psi - \frac{1}{4}G_{\mu\nu}^a G_a^{\mu\nu} \quad (a = 1, \dots, 8), \quad (2.1)$$

where $\mathbf{m} = \text{diag}(m_u, m_d, \dots)$ denotes the diagonal matrix of current quark masses and $G_{\mu\nu}^a$ is the non-abelian gluonic field-strength tensor,

$$G_{\mu\nu}^a = \partial_\mu A_\nu^a - \partial_\nu A_\mu^a + ig_s f^{abc} A_\mu^b A_\nu^c. \quad (2.2)$$

The QCD Lagrangian, \mathcal{L}_{QCD} , remains unchanged under an arbitrary rotation in $SU(3)$ color space

$$\psi \rightarrow \exp\left[i\theta^a \frac{\lambda_a}{2}\right] \psi, \quad (2.3)$$

by introducing the covariant derivative and the eight gluon fields A_a^μ in it,

$$D^\mu = \partial^\mu - ig_s \frac{\lambda^a}{2} A_a^\mu. \quad (2.4)$$

The matrices λ_a (called the Gell-Mann matrices) are the infinitesimal generators of the group $SU(3)$, which obey the relation $\text{Tr}[\lambda_a \lambda_b] = 2\delta_{ab}$.

The running coupling strength, $\alpha_s(\mu) = g_s^2(\mu)/(4\pi)$ depends on an energy scale μ (renormalization scale) at which the theory is probed. The μ -dependence of the strong coupling $g_s(\mu)$ is governed by the QCD β -function

$$\mu \frac{d}{d\mu} g_s(\mu) = \beta(g_s). \quad (2.5)$$

As long as g_s is small enough, $\beta(g_s)$ can be perturbatively calculated,

$$\beta(g_s) = -\frac{\beta_0}{(4\pi)^2}g_s^3 - \frac{\beta_1}{(4\pi)^2}g_s^5 + \dots, \quad (2.6)$$

where β_i 's are constant coefficients. Thus one arrives at the expression of the running coupling strength

$$\alpha_s(\mu) \simeq \frac{4\pi}{\beta_0 \ln(\mu^2/\Lambda_{\text{QCD}}^2)} + \dots, \quad (2.7)$$

where $\Lambda_{\text{QCD}} \sim 200$ MeV is the QCD scale parameter characterizing the change of α_s as a function of μ . As μ increases the coupling strength $\alpha_s(\mu)$ logarithmically decreases and then the interactions between quarks and gluons could be treated perturbatively. This is called the ‘‘asymptotic freedom’’. In the perturbative calculations, μ should be chosen so that the higher order terms in the expansion are effectively suppressed. Thus μ should be a characteristic scale of the system.

However, this theory is intricate at low energy scales (comparable to Λ_{QCD}) where the perturbation expansion is not applicable anymore due to the rapidly increasing $\alpha_s(\mu)$. A non-perturbative approach to QCD is lattice QCD which uses a discrete set of space-time points to reduce the analytically intractable path integrals of the continuum theory to a numerical computation. Otherwise it has been necessary in most nuclear physics phenomena to resort to effective theories or models of QCD that can be solved to some approximation. These effective methods are constructed by reflecting the symmetries of the QCD Lagrangian and the observable phenomenology.

2.2 Chiral symmetry

Apart from the local SU(3) gauge symmetry, the QCD Lagrangian has several global symmetries:

$$\text{SU}(N_f)_L \times \text{SU}(N_f)_R \times \text{U}(1)_V \times \text{U}(1)_A. \quad (2.8)$$

The global $\text{U}(1)_V$ symmetry yields the conservation of baryon number while the $\text{U}(1)_A$ symmetry is broken due to the axial anomaly which causes unexpectedly large mass of the η' meson (958 MeV) and can be connected to the instanton.

The QCD Lagrangian is chirally symmetric in the limit of massless quarks. Taking this limit for the u and d quark is reasonable since their masses are small in

comparison to characteristic hadronic mass scales, e.g. nucleon mass (~ 1 GeV). The strange quark has relatively larger mass but is still smaller than the hadronic scales. Therefore it is meaningful to examine the limit $m_u = m_d = m_s = 0$. The quark masses (estimated at a renormalization scale of $\mu \approx 2$ GeV) from Particle Data Group [23] are as follows:

$$m_u = 1.5 - 3.3 \text{ MeV} , \quad m_d = 3.5 - 6.0 \text{ MeV} ,$$

$$m_s = 105_{-35}^{+25} \text{ MeV} .$$

Chiral symmetry implies that the left- and right-handed quarks have a separate SU(3) symmetry

$$\mathcal{L}_{\text{QCD}} = \bar{\psi}_L i \not{D} \psi_L + \bar{\psi}_R i \not{D} \psi_R - \frac{1}{4} G_{\mu\nu}^a G_a^{\mu\nu} , \quad (2.9)$$

where the left- and right-handed quark fields are defined as

$$\psi_L = \frac{1}{2}(1 - \gamma_5)\psi , \quad \psi_R = \frac{1}{2}(1 + \gamma_5)\psi . \quad (2.10)$$

The Lagrangian in the massless limit is invariant under global SU(3) transformations in flavor space of the left- and right-handed quarks:

$$\psi_L \rightarrow \exp \left[i\theta_L^a \frac{\lambda_a}{2} \right] \psi_L , \quad \psi_R \rightarrow \exp \left[i\theta_R^a \frac{\lambda_a}{2} \right] \psi_R . \quad (2.11)$$

The conserved Noether currents are the left- and right-handed currents

$$J_{L,a}^\mu = \bar{\psi}_L \gamma^\mu \frac{\lambda_a}{2} \psi_L , \quad J_{R,a}^\mu = \bar{\psi}_R \gamma^\mu \frac{\lambda_a}{2} \psi_R , \quad (2.12)$$

with their vanishing divergences, $\partial_\mu J_L^\mu = \partial_\mu J_R^\mu = 0$. Alternatively the vector and axial-vector currents are often used,

$$J_{V,a}^\mu = J_{R,a}^\mu + J_{L,a}^\mu = \bar{\psi} \gamma^\mu \frac{\lambda_a}{2} \psi , \quad J_{A,a}^\mu = J_{R,a}^\mu - J_{L,a}^\mu = \bar{\psi} \gamma^\mu \gamma_5 \frac{\lambda_a}{2} \psi . \quad (2.13)$$

The corresponding charges are

$$Q_a^V = \int d^3x J_{V,a}^0(x) , \quad Q_a^A = \int d^3x J_{A,a}^0(x) , \quad (2.14)$$

which are generators of the SU(3)_L × SU(3)_R group and satisfy the Lie algebra,

$$\begin{aligned} [Q_a^V, Q_b^V] &= if_{abc} Q_c^V , \\ [Q_a^V, Q_b^A] &= if_{abc} Q_c^A , \\ [Q_a^A, Q_b^A] &= if_{abc} Q_c^V \end{aligned} \quad (2.15)$$

with the $SU(3)$ structure constants, f_{abc} .

Chiral $SU(3)_R \times SU(3)_L$ symmetry is explicitly broken by the small but non-zero quark masses. The divergence of the axial-vector current becomes

$$\partial_\mu J_{A,a}^\mu = i\bar{\psi} \left\{ m, \frac{\lambda_a}{2} \right\} \gamma_5 \psi . \quad (2.16)$$

This is the basis of the partial conservation of the axial-vector current (PCAC) hypothesis which plays a key role in low energy dynamics and also weak interactions.

2.2.1 Spontaneous symmetry breaking

In the limit of vanishing quark masses, chiral symmetry is an exact symmetry of the QCD Lagrangian. If the ground state (vacuum) of QCD were also symmetric under the group $SU(3)_L \times SU(3)_R$, then the chiral symmetry is realized in the so-called Wigner-Weyl mode. In this realization, one can expect degenerate hadronic multiplets of opposite parity since, for massless fermions, helicity eigenstates are also parity eigenstates. However such parity doublets are not observed in hadronic spectra. For example, the spectral functions of the ρ -meson ($J^P = 1^-$), 770 MeV, is quite different from that of its parity partner, a_1 meson ($J^P = 1^+$), 1230 MeV as seen in Fig. 2.1.

This evidence of broken chiral symmetry from the hadron spectrum can be interpreted via the Nambu-Goldstone realization in which the axial charge does not annihilate the physical vacuum,

$$Q_a^V |0\rangle = 0 , \quad Q_a^A |0\rangle \neq 0 . \quad (2.17)$$

Hence the chiral $SU(3)_L \times SU(3)_R$ group is dynamically reduced to the subgroup $SU(3)_V$. The axial charge acting on the vacuum yields non-vanishing pseudo-scalar states

$$Q_a^A |0\rangle = |\phi_a\rangle \neq 0 , \quad (2.18)$$

where the states $|\phi_a\rangle$ are degenerate with the vacuum $|0\rangle$ because $[Q_a^A, H_{\text{QCD}}] = 0$. The massless ϕ_a are called Goldstone bosons according to the Nambu-Goldstone theorem [24]: the spontaneous breaking of a continuous global symmetry is accompanied by massless Goldstone bosons. The Goldstone bosons for the spontaneous chiral symmetry breaking are identified with the pseudo-scalar octet mesons (π^\pm , π^0 , K^\pm , K^0 , \bar{K}^0 and η) which interact weakly at low energies. In real nature, the pseudo-scalar mesons acquire their finite masses due to the explicitly broken degeneracy by small (but non-zero) quark masses $m_q \neq 0$.

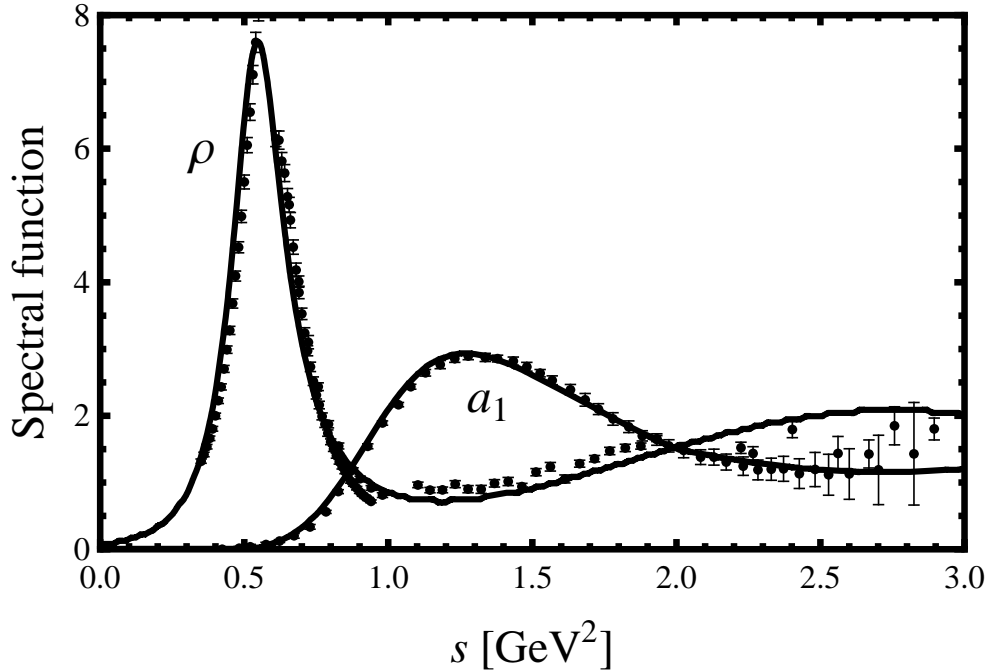


Figure 2.1: Vector and axial-vector spectral functions in vacuum (curves) as parameterized in Ref. [25], compared to $e^+e^- \rightarrow n\pi$ data with n even [26, 27] and data from hadronic τ decays [28, 29].

2.2.2 Chiral order parameter

Spontaneous breaking of the chiral symmetry originates from the fact that the QCD vacuum has non-trivial structure. An obvious order parameter of the chiral symmetry breaking is the vacuum expectation value of the scalar (light) quark-antiquark density,

$$\langle \bar{q}q \rangle = \langle \bar{q}_R q_L + \bar{q}_L q_R \rangle, \quad (2.19)$$

which mixes the left- and right-handed quarks. This quantity, the so-called chiral condensate (or quark condensate) must vanish if the QCD vacuum were trivial. The precise definition of the chiral condensate is

$$\langle \bar{q}q \rangle \equiv -i \text{Tr} \lim_{y \rightarrow x^+} S_F(x - y), \quad (2.20)$$

with the quark propagator $S_F(x - y) = -i \langle 0 | \mathcal{T} q(x) \bar{q}(y) | 0 \rangle$. Using the Wick theorem,

$$\mathcal{T} q(x) \bar{q}(y) = \mathcal{N} q(x) \bar{q}(y) + \overline{q(x) \bar{q}(y)}, \quad (2.21)$$

the time-ordered product (\mathcal{T}) is represented in terms of the normal-ordered product (\mathcal{N}) and the contraction of two field operators. The normal-ordered terms vanish

in perturbative theory. A non-vanishing normal-ordered terms hence stem from long-range, non-perturbative physics.

Another consequence of the spontaneous symmetry breaking is that the matrix element of the axial current between the vacuum and a Goldstone boson is non-vanishing

$$\langle 0 | J_{A,a}^\mu | \pi_b(p) \rangle = i p^\mu \delta_{ab} f_\pi e^{-i p x} . \quad (2.22)$$

Considering the flavor SU(2) subgroup ($a = 1 \cdots 3$), π_a denotes the pion field and $f_\pi = 92.4$ MeV the pion decay constant. The chiral condensate is connected to the pion decay constant f_π via the Gell-Mann–Oakes–Renner (GOR) relation [30],

$$m_\pi^2 f_\pi^2 = -\frac{1}{2} (m_u + m_d) \langle \bar{u}u + \bar{d}d \rangle + \mathcal{O}(m_{u,d}^2) , \quad (2.23)$$

and thus play the role of chiral order parameter at hadronic level.

2.2.3 Chiral effective Lagrangian

At low energy, processes involving the strong interaction as described by QCD are best analyzed in effective field theory approaches such as chiral perturbation theory. The basic idea of effective field theory is to use this pseudo-scalar meson (Goldstone boson) octet as the effective degrees of freedom at low energy. To describe the dynamics at low energy the chiral perturbative theory constructs an effective Lagrangian \mathcal{L}_{eff} by an expansion in powers of the meson momenta,

$$\mathcal{L}_{\text{eff}} = \frac{f_\pi^2}{4} \text{Tr}[\partial^\mu U^\dagger \partial_\mu U] + \frac{f_\pi^2}{2} B \text{Tr}[\mathbf{m}(U + U^\dagger)] + \mathcal{L}^{(4)} + \dots , \quad (2.24)$$

where f_π denotes the pion decay constant in the chiral limit and \mathbf{m} is the quark mass matrix. The Goldstone bosons are represented in \mathcal{L}_{eff} by a 3×3 special unitary matrix,

$$U = \exp [i\Phi(x)/f_\pi] \quad (2.25)$$

with

$$\Phi \equiv \pi_a \lambda_a = \begin{pmatrix} \frac{\pi^0}{\sqrt{2}} + \frac{\eta}{\sqrt{6}} & \pi^+ & K^+ \\ \pi^- & -\frac{\pi^0}{\sqrt{2}} + \frac{\eta}{\sqrt{6}} & K^0 \\ K^- & \bar{K}^0 & -\frac{2\eta}{\sqrt{6}} \end{pmatrix} . \quad (2.26)$$

This expansion is equivalent to QCD in the sense that it includes all possible terms permitted by the symmetries. The parameter B in Eq. (2.24) turns out to be connected with the quark condensate $\langle \bar{q}q \rangle$.

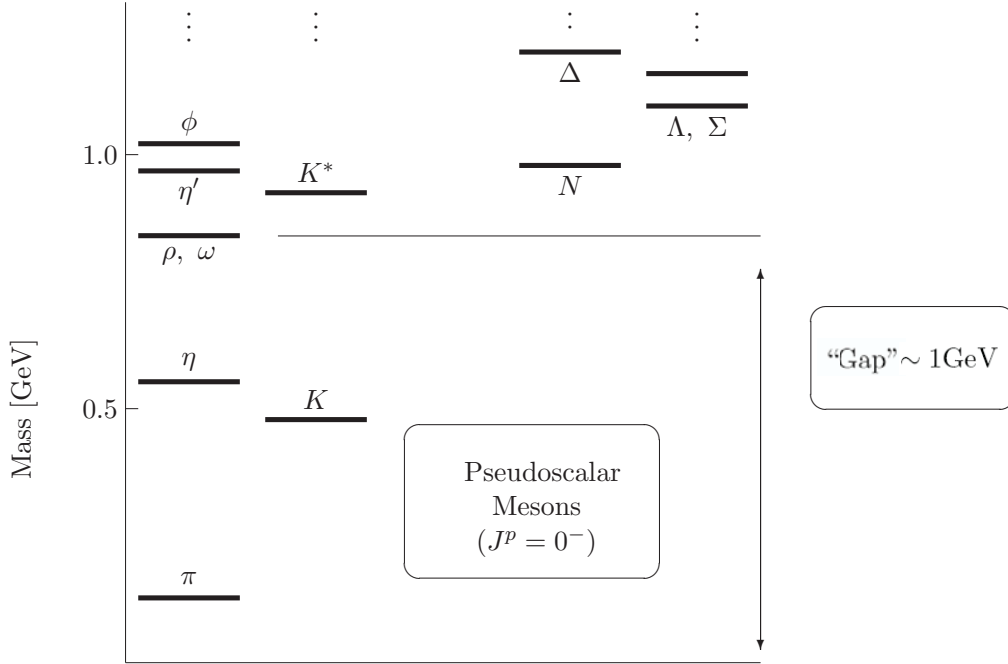


Figure 2.2: The spectrum of low-mass hadronic excitations built on the condensed QCD ground state. The characteristic gap $\Lambda_{\text{CSB}} \sim 1 \text{ GeV}$ is indicated.

The factor $(4\pi f_\pi)^{-1}$ appears in calculations of loop amplitude in the effective Lagrangian. This factor is generally found in meson loops and introduces the chiral scale

$$\Lambda_{\text{CSB}} \sim 4\pi f_\pi \sim 1 \text{ GeV} . \quad (2.27)$$

This choice of Λ_{CSB} as the symmetry breaking scale and the dimensional parameter that suppresses non-renormalized terms was motivated in Ref. [31], where it also served as a physically sensible cutoff. The energy scale of Λ_{CSB} , a characteristic gap, separates between light and heavy particles in the hadron spectrum of Fig. 2.2.

2.3 Currents and vector mesons

2.3.1 Vector mesons as gauge bosons

Before QCD was established as the fundamental theory of strong interactions it had been attempted to model strong interaction as a gauge theory in which the vector mesons $\rho(770)$, $\omega(780)$, $\phi(1020)$ and $K^*(890)$ played the role of the gauge

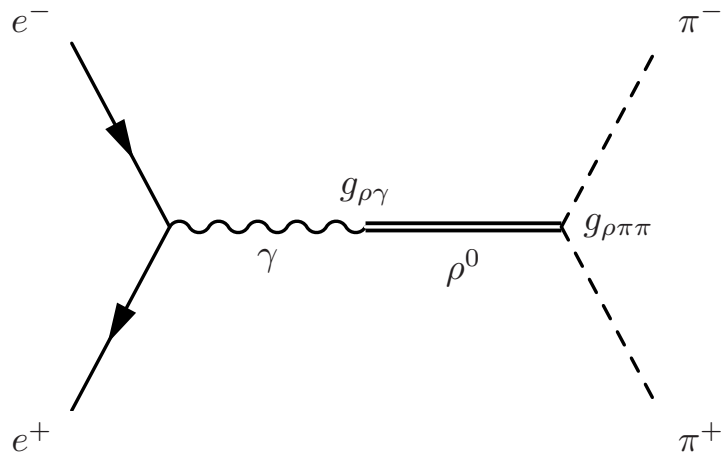


Figure 2.3: e^+e^- annihilation to $\pi^+\pi^-$. A virtual photon γ undergoes ρ -conversion with $g_{\rho\gamma}$ and ρ -meson dominates the process.

bosons. Starting from the great success of quantum electrodynamics (QED), J. J. Sakurai in 1960's predicted the existence of vector mesons coupled to the hadronic isospin and hypercharge currents.

In QED by introducing the covariant derivative ($D_\mu = \partial_\mu - ieA_\mu$), the electromagnetic field A_μ couples to a conserved electromagnetic current J_μ^{em} with an universal charge e . Employing this idea allows the vector field V_μ to couple to a conserved hadronic current with an universal coupling g_V . A typical example is the ρ -meson that couples to the hadronic isovector current, which is carried by the nucleon and pion. The interaction vertices of ρ -meson with nucleons and pions are characterized by universal couplings, $g_{\rho NN} = g_{\rho\pi\pi} \equiv g_\rho$. This phenomena is usually called the vector meson dominance (VMD).

The measurements of the electromagnetic form factor of the pions were interpreted as empirical evidence for an isoscalar vector meson, $\omega \rightarrow 3\pi$, by Nambu [32] in 1957 and for an isovector meson, $\rho^0 \rightarrow 2\pi$, by Frazer and Fulco [33] in 1959 (see Fig. 2.3). This interpretation of the form factors was generalized to hold for all photon-hadron interactions in terms of an operator identity reflecting gauge invariance. Concentrating on the $\rho\gamma$ -interaction, the operator identity, known as current-field identity, is obtained as

$$J_\mu^{(3)} = g_{\rho\gamma}\rho_\mu^0(x), \quad (2.28)$$

which relates the 3-component of the isospin current, $J_\mu^{(3)}$, to the ρ^0 -meson field with the coupling $g_{\rho\gamma}$. The electromagnetic current is identified with a linear

combination of isovector and isoscalar vector currents,

$$J_\mu^{em} = J_\mu^{(3)} + \frac{1}{2} J_\mu^Y . \quad (2.29)$$

It is clear that such a $\rho\gamma$ -interaction will arise from the gauge term $J_\mu^{em} A^\mu$.

The pionic matrix element of the isovectors current,

$$\langle \pi(q) | J_\mu^{(3)} | \pi(q') \rangle = (q' + q)_\mu F_\pi((q' - q)^2) + \dots , \quad (2.30)$$

defines the pion form factors $F_\pi(s)$. The normalization of the vector current imposes $F_\pi(0) = 1$, i.e. isovector charge conservation. Assuming that one can write down an unsubtracted dispersion relation for $F_\pi(s)$,

$$F_\pi(s) = g_{\rho\pi\pi} \frac{1}{m_\rho^2 - s} g_{\rho\gamma} + \dots , \quad (2.31)$$

and also that the ρ -pole dominates over the continuum, then at $s = 0$ one finds

$$g_{\rho\gamma} = \frac{m_\rho^2}{g_{\rho\pi\pi}} . \quad (2.32)$$

This is a second important VMD relation. Eq. (2.28), together with this, is rewritten as

$$J_\mu^{(3)} = \frac{m_\rho^2}{g_\rho} \rho_\mu^0 , \quad (2.33)$$

where the universality $g_\rho\pi\pi = g_\rho$ is assumed.

The process we are concerned with, $\rho^0 \rightarrow 2\pi$, can be described by the amplitude:

$$T_{\nu\mu}^{ij} = i \int d^4x e^{iq \cdot x} \langle 0 | \mathcal{T} J_{A,\nu}^i(x) J_{A,\mu}^j(0) | \rho(p) \rangle . \quad (2.34)$$

Taking its divergence, one obtains

$$\begin{aligned} q^\nu T_{\nu\mu}^{ij} &= - \int d^4x e^{iq \cdot x} \langle 0 | \mathcal{T} \partial^\nu J_{A,0}^i(x) J_{A,\mu}^j(0) | \rho(p) \rangle \\ &\quad - \int d^4x e^{iq \cdot x} \delta(x_0) \langle 0 | [J_{A,0}^i(x), J_{A,\mu}^j(0)] | \rho(p) \rangle . \end{aligned} \quad (2.35)$$

In the massless limit the first integral of the r.h.s vanishes. Using the relevant commutation relation, one can deduce the Ward identity

$$q^\nu T_{\nu\mu}^{ij} = -i f^{ijk} \langle 0 | J_{V,\mu}^k | \rho(p) \rangle . \quad (2.36)$$

The coupling of the ρ^0 -meson to the isovector current appears as

$$\langle 0 | J_{V,\mu} | \rho(p) \rangle = g_{\rho\gamma} \epsilon_\mu = \frac{m_\rho^2}{g_\rho} \epsilon_\mu , \quad (2.37)$$

where the isospin indices are omitted. Contracting again with the pion momentum q' , the amplitude becomes

$$q^\nu q'^\mu T_{\nu\mu} = \frac{m_\rho^2}{g_\rho} (q' \cdot \epsilon) \quad (2.38)$$

Introducing the $\rho\pi\pi$ coupling as:

$$\langle \pi(q'), \pi(q) | \rho(p) \rangle = \epsilon^\nu (q' - q)_\nu g_{\rho\pi\pi} , \quad (2.39)$$

and taking the limit $q', q \rightarrow 0$, one obtains the soft pion relation:

$$\frac{m_\rho^2}{g_\rho} = 2f_\pi^2 g_{\rho\pi\pi} . \quad (2.40)$$

Assuming ρ -universality from the VMD model, one finds the Kawarabayashi-Suzuki-Riazuddin-Fayyazuddin (KSRF) relation [34, 35]:

$$g_\rho^2 \equiv \frac{1}{f_V^2} = \frac{m_\rho^2}{2f_\pi^2} , \quad (2.41)$$

where $f_V = 1/g_\rho$ is defined for later convenience.

2.3.2 Weinberg sum rules

Further important consequences of the current algebras are the chiral sum rules derived by Weinberg [36]. These sum rules are based on the asymptotic behavior of the correlation function, assuming that the $SU(2)_L \times SU(2)_R$ chiral symmetry is asymptotically realized. Weinberg's sum rules are derived starting from the two-point correlation function which is particularly sensitive to properties of chiral symmetry breaking:

$$\begin{aligned} \Pi_{LR}^{\mu\nu} &= i \int d^4x e^{iq \cdot x} \langle 0 | \mathcal{T} J_L^\mu(x) (J_R^\nu(0))^\dagger | 0 \rangle \\ &= (g^{\mu\nu} q^2 - q^\mu q^\nu) \Pi_{LR}^{(1)} - q^\mu q^\nu \Pi_{LR}^{(0)} , \end{aligned} \quad (2.42)$$

with left- and right-handed currents defined by

$$J_L^\mu = \bar{u} \gamma^\mu (1 - \gamma_5) d , \quad J_R^\mu = \bar{u} \gamma^\mu (1 + \gamma_5) d . \quad (2.43)$$

The correlation function separates into two invariant correlators of the transverse and longitudinal parts, $\Pi_{LR}^{(1)}$ and $\Pi_{LR}^{(0)}$. In the asymptotic ($Q^2 \equiv -q^2 \rightarrow \infty$) and the chiral limit ($m_q = 0$), $\Pi_{LR}^{\mu\nu}$ tends to vanish since, in those limits, left- and

right-handedness become totally uncorrelated. The correlators can be expressed in terms of their spectral representation

$$\tilde{\Pi}_{LR}^{(j)}(Q^2) = \int_0^\infty ds \frac{\text{Im} \Pi_{LR}^{(j)}(s)}{\pi(s + Q^2)}. \quad (2.44)$$

The behavior of $\Pi_{LR}^{\mu\nu}$ in the asymptotic or chiral limit is converted into corresponding properties of the imaginary parts which are related to the absorption spectrum:

$$\begin{aligned} \int_0^\infty ds \left(\text{Im} \Pi_{LR}^{(1)}(s) + \text{Im} \Pi_{LR}^{(0)}(s) \right) &= 0, \\ \int_0^\infty ds s \text{Im} \Pi_{LR}^{(1)}(s) &= 0. \end{aligned} \quad (2.45)$$

These are commonly referred to as the first and second Weinberg sum rules. The correlation function in Eq. (2.42) can be rewritten as the difference of a vector current correlation function and an axial-vector current correlation function. Eq. (2.45) can be rewritten as

$$\begin{aligned} \int_0^\infty ds \left(\text{Im} \Pi_V^{(1)}(s) - \text{Im} \Pi_A^{(1)}(s) - \text{Im} \Pi_A^{(0)}(s) \right) &= 0, \\ \int_0^\infty ds s \left(\text{Im} \Pi_V^{(1)}(s) - \text{Im} \Pi_A^{(1)}(s) \right) &= 0, \end{aligned} \quad (2.46)$$

where $\text{Im} \Pi_V^{(0)} = 0$ in vacuum is used.

In his original paper [36], Weinberg assumed that only the lowest resonant state in the vector and axial-vector spectral functions contribute significantly to the sum rules,

$$\begin{aligned} \frac{1}{\pi} \text{Im} \Pi_V^{(1)}(s) &= f_V^2 m_V^2 \delta(s - m_V^2) + \dots, \\ \frac{1}{\pi} \text{Im} \Pi_A^{(1)}(s) &= f_A^2 m_A^2 \delta(s - m_A^2) + \dots, \\ \frac{1}{\pi} \text{Im} \Pi_A^{(0)}(s) &= f_\pi^2 \delta(s). \end{aligned} \quad (2.47)$$

The longitudinal part in the axial-vector spectral function is the contribution from the massless pion pole. The dots in the spectral functions in Eq. (2.47) implicitly assume that the sum over all other excited states is globally dual to the onset of the perturbative continuum. The vector and axial-vector spectral functions of the perturbative QCD continuum are the same in the chiral limit. Thus the first and second Weinberg sum rules, Eq. (2.46), constrain the couplings and masses of the

a_1 and ρ resonances as follows

$$\begin{aligned} f_V^2 m_V^2 - f_A^2 m_A^2 &= f_\pi^2, \\ f_V^2 m_V^4 - f_A^2 m_A^4 &= 0. \end{aligned} \quad (2.48)$$

The simplified Weinberg sum rules Eq. (2.48), together with the KSRF relation $f_V^2 m_V^2 = 2f_\pi^2$, lead to the prediction for the axial-vector mass,

$$m_A = \sqrt{2} m_V, \quad (2.49)$$

which is satisfied by the known masses within an accuracy of about 10%.

2.4 Partial restoration of chiral symmetry

The spontaneous breaking of the chiral symmetry is signaled by the non-vanishing values in physical vacuum of the quark condensates. Calculations based on chiral perturbation theory and QCD sum rules indicate that the magnitudes of these condensates are reduced when the hadrons are put in a medium, hence giving rise to partial restoration of chiral symmetry [37, 38].

The chiral condensate, however, is not the quantity that can be directly observed in experiments. Therefore it is important to explore in-medium modification of hadron properties as consequence of chiral symmetry restoration [39]. There is a lot of interest to understand the pattern of partial restoration of chiral symmetry in hot and/or dense medium [40, 41].

2.4.1 Patterns of symmetry restoration

Theoretical studies to modifications of in-medium hadronic masses were spurred since the suggestion of Brown and Rho [13], namely Brown-Rho (BR) scaling, based on the restoration of scale invariance of QCD, that masses of hadrons would scale in a nuclear medium as,

$$\frac{M_N^*}{M_N} \approx \frac{m_V^*}{m_V} \approx \frac{f_\pi^*}{f_\pi}, \quad (2.50)$$

where the in-medium quantities are denoted by asterisks. Here M_N and m_V indicate the masses of nucleon and vector mesons (e.g. ρ , ω) respectively. The pion decay constant f_π as an order parameter of chiral symmetry is believed to vanish when the chiral symmetry is completely restored. The in-medium behavior of pole mass shift was tested by using the QCD sum rule approach [14, 42].

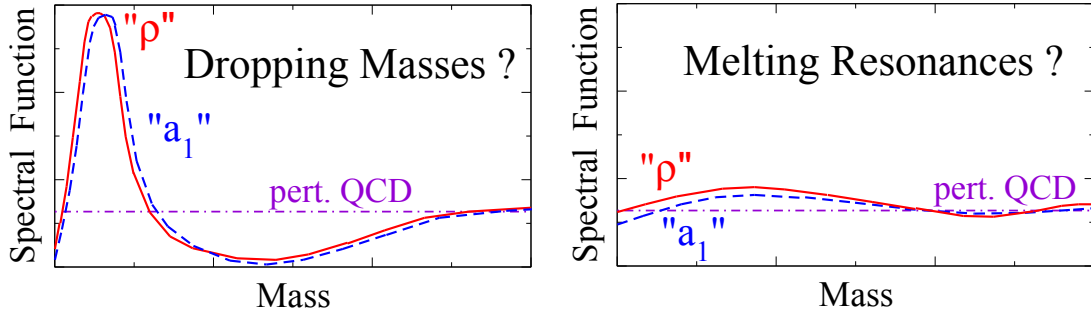


Figure 2.4: Schematic pictures in Ref. [44] to interpret possible patterns of chiral symmetry restoration in terms of vector and axial-vector spectral functions.

To get some insight of chiral symmetry restoration, it is useful to study the properties of a hadron in parallel with those of its parity partner, e.g. $\rho(770)$ - $a_1(1230)$, which become degenerate at some critical point of thermodynamic conditions due to chiral symmetry. In this context the BR scaling, which suggests masses going to zero, is not the only possible scenario. The masses of parity partners may move towards each other [43] but stay non-zero.

The mass shift scenario introduced above is based on the assumption that the narrow resonances are well defined in medium as well as in vacuum. However this condition is generally not realized because the imaginary part of the hadron self-energy usually grows with increasing temperature and/or density. It means that the decay width of the particle experiences in-medium broadening. This broadening would also decrease the maximum peak value of the spectral density. There may be also a decrease in the thresholds s_V^* and s_A^* of the continuum. Therefore the vector and axial-vector mesons are expected to melt away into the continuum. The continuum would merge with the broadened particle poles to give a very broad distribution of strength in the spectral densities. This disappearance of the particles into the continuum makes the difference between vector and axial-vector correlators vanish. Hence it is difficult to judge whether their masses are changed or not.

In a medium, thermal (or virtual) pions can couple to the vector and axial-vector current. The correlation function which is connected with the spectral density through the dispersion relation mixes the vector and axial-vector channel by absorbing and emitting the pions. Hence increasing temperature or density makes the mixing important until full chiral symmetry restoration is reached at which vector and axial-vector correlators become identical. The finite temperature

correlators are described by the factorization of T -dependence [45]:

$$\begin{aligned}\Pi_V^{\mu\nu}(q, T) &= (1 - \epsilon(T)) \Pi_V^{\mu\nu}(q, 0) + \epsilon(T) \Pi_A^{\mu\nu}(q, 0) , \\ \Pi_A^{\mu\nu}(q, T) &= (1 - \epsilon(T)) \Pi_A^{\mu\nu}(q, 0) + \epsilon(T) \Pi_V^{\mu\nu}(q, 0) ,\end{aligned}\tag{2.51}$$

where the T -dependent mixing parameter is obtained by the thermal pion loop

$$\epsilon(T) = \frac{2}{f_\pi^2} \int \frac{d^3p}{E(2\pi)^3} \frac{1}{e^{E/T} - 1} ,\tag{2.52}$$

with $E = \sqrt{m_\pi^2 + p^2}$. In the massless limit of pions, $\epsilon(T)$ is simplified as

$$\epsilon(T) = \frac{T^2}{6f_\pi^2} .\tag{2.53}$$

Although this parity mixing effect contaminates the vector correlator with the axial-vector and vice versa, remain their pole masses unchanged in distinction from BR scaling. In this scenario, the critical temperature T_c is determined (up to corrections of higher order in $\epsilon(T)$) as the temperature at which the mixing becomes maximal, i.e. $\epsilon(T_c) = 1/2$. Interestingly, to this T^2 order, Eq. (2.53) gives $T_c \approx 160$ MeV, not far from values $T_c \sim 170 - 190$ MeV deduced from lattice QCD [1, 2].

Chapter 3

QCD sum rules

The QCD sum rule approach was introduced by Shifman, Vainshtein and Zakharov (SVZ) in the late 1970's for the purpose of relating hadron properties to QCD [46]. This framework is powerful to study hadrons in their lowest-mass state with given quantum numbers. A QCD sum rule is a relation derived from a correlation function in QCD and its analytic property. In this framework the QCD duality connects hadronic quantities to the non-perturbative nature of QCD represented by QCD condensates. In this chapter the general formalism of the QCD sum rules is reviewed.

3.1 Overview

The starting point of the QCD sum rule approach is the construction of an interpolating current field with quark degrees of freedom that has strong overlap with the hadron of interest. Such a field is in general constructed guided by the valence quark content and given quantum numbers such as spin, isospin, parity etc. In our case the interpolating fields for ρ and ω mesons are simply given by the isovector and isoscalar current operators:

$$J_\rho^\mu = \frac{1}{2} (\bar{u}\gamma^\mu u - \bar{d}\gamma^\mu d) , J_\omega^\mu = \frac{1}{6} (\bar{u}\gamma^\mu u + \bar{d}\gamma^\mu d) . \quad (3.1)$$

The interpolating current fields are not saturated by the ground state hadrons with the given quantum numbers. These interpolating current fields can also annihilate other resonances and continuum states with the same constituent quark contents and quantum numbers. Therefore one should distinguish one state that

we are interested in from other states with same quantum numbers. One useful prescription for that is the so-called Borel transformation method that is commonly used in QCD sum rules. As will be shown later, the Borel transformation suppresses higher-mass states relative to the lowest-mass state. Consequently, these Borel sum rules are useful for determining the spectral properties of the lowest-mass state with a given set of quantum numbers.

Time-ordered correlation functions of the interpolating current fields play the role of a bridge between hadronic phenomenology and QCD. The generic two-point correlation function of a scalar interpolating current field has the form

$$\Pi(q^2) = i \int d^4x e^{iq \cdot x} \langle \Omega | \mathcal{T} [J(x) J(0)] | \Omega \rangle , \quad (3.2)$$

where $|\Omega\rangle$ is the nonperturbative QCD ground state. Additional complications for the vector interpolating current fields will be addressed later.

The correlation function, Eq. (3.2), can be calculated in terms of the QCD degrees of freedom, using the operator product expansion (OPE) on one hand. Using OPE for large space-like momenta, the correlator is expressed as a sum of coefficient functions, calculated in QCD perturbation theory, that multiply condensates of composite operators

$$\Pi_{\text{OPE}}(q^2) = \sum_n C_n(q^2) \langle \mathcal{O}_n \rangle , \quad (3.3)$$

where \mathcal{O}_n are local operators; $\mathbb{1}$, $\bar{q}q$, $G_{\mu\nu}^a G_a^{\mu\nu}$, \dots . The coefficients, $C_n(q^2)$, are c -numbers known as Wilson coefficients and contain information on the short distance physics. Non-perturbative long distance effects are reflected in the ground-state expectation values of the local operators, so-called condensates:

$$\langle \bar{q}q \rangle, \quad \langle G_{\mu\nu}^a G_a^{\mu\nu} \rangle, \quad \dots . \quad (3.4)$$

The quark condensate describes the scalar quark-antiquark density of the vacuum, which is the order parameter of spontaneous chiral symmetry breaking. The gluon condensate measures the density of gluon pairs which is a manifestation of the breaking of scale invariance of QCD by quantum effects. This separation between short-range dynamics (Wilson coefficients) and long-range dynamics (condensates) is the essence of the QCD sum rules framework.

On the other hand, the correlation function can also be evaluated phenomenologically with hadronic degrees of freedom such as hadron masses, coupling constants between hadrons, decay constants, etc. Introducing the overlap strength λ

between the interpolating current and the physical hadron field ϕ by:

$$J = \lambda\phi + \sum_{i=1} \lambda_i^* \phi_i^* , \quad (3.5)$$

where the sum includes excited hadron states, the two-point correlation function is written as follows:

$$\Pi_{\text{phen}}(q^2) = \frac{\lambda^2}{m^2 - q^2 - i\epsilon} + \sum_{i=1} \frac{\lambda_i^{*2}}{m_i^{*2} - q^2 - i\epsilon} . \quad (3.6)$$

More generally a continuous spectrum can be represented in the form of Källén-Lehmann spectral representation:

$$\Pi_{\text{phen}}(q^2) = \int_0^\infty ds \frac{\rho_{\text{phen}}(s)}{s - q^2 - i\epsilon} , \quad (3.7)$$

where $\rho_{\text{phen}}(s)$ is the spectral density proportional to the imaginary part of the correlator

$$\rho_{\text{phen}}(s) = \frac{1}{\pi} \text{Im} \Pi_{\text{phen}}(s) . \quad (3.8)$$

In practice the phenomenological spectral density ρ_{phen} is parameterized so that the lowest resonance is separated and higher mass states are incorporated into the continuum

$$\rho_{\text{phen}}(s) = \rho_{\text{res}}(s) + \rho_{\text{cont}}(s) . \quad (3.9)$$

According to the QCD duality, the continuum from which the lowest lying resonance is well-separated is assumed to be given by the result obtained with the OPE. This assumption is supported by the basic QCD property: asymptotic freedom for sufficiently large s . The continuum can be estimated by introducing a scale, s_0 , below which the continuum contribution vanishes

$$\rho_{\text{cont}}(s) = \rho_{\text{OPE}}(s) \Theta(s - s_0) . \quad (3.10)$$

The OPE is valid in the region of large space-like momentum transfer whereas the spectral density is defined in the time-like momentum region. Thus, by using the analyticity of the correlation function, ρ_{OPE} is written in the form of the correlator

$$\tilde{\Pi}_{\text{OPE}}(Q^2) = \int_0^\infty ds \frac{\rho_{\text{OPE}}(s)}{s + Q^2} , \quad (3.11)$$

where the analytically continued correlation function, $\tilde{\Pi}_{\text{OPE}}(Q^2)$, is identified with $\Pi_{\text{OPE}}(q^2)$ for all $Q^2 = -q^2$. The spectral density, ρ_{OPE} , is defined as

$$\rho_{\text{OPE}}(s) = \frac{1}{\pi} \text{Im} \Pi_{\text{OPE}}(s) . \quad (3.12)$$

As mentioned in the beginning of this section, the interpolating current field J can couple not only to the lowest-mass state but also to the higher-mass excitations that have the same quantum numbers as J . In order to filter out this high-energy part of the excitations the Borel transformation is often used. The Borel transformation of a function $f(Q^2)$ is defined as

$$\hat{f}(M^2) \equiv \lim_{Q^2, n \rightarrow \infty} \frac{(Q^2)^{n+1}}{n!} \left(-\frac{d}{dQ^2} \right)^n f(Q^2), \quad M^2 \equiv \frac{Q^2}{n} = \text{finite}, \quad (3.13)$$

where M is called the Borel mass. By applying the Borel transformation to the correlation function on the phenomenological side, the contributions from higher excited states are exponentially suppressed:

$$\tilde{\Pi}_{\text{phen}}(Q^2) = \int_0^\infty ds \frac{\rho_{\text{phen}}(s)}{s + Q^2} \implies \hat{\Pi}_{\text{phen}}(M^2) = \int_0^\infty ds e^{-s/M^2} \rho_{\text{phen}}(s). \quad (3.14)$$

Moreover, on the OPE side, the Borel transformation improves the convergence of the expansion:

$$\tilde{\Pi}_{\text{OPE}}(Q^2) \sim \sum_n \frac{c_n}{(Q^2)^n} \implies \hat{\Pi}_{\text{OPE}}(M^2) \sim \sum_n \frac{c_n}{(n-1)!(M^2)^{n-1}}. \quad (3.15)$$

After the Borel transformation, contributions from higher-dimensional operators (larger n) in the OPE obtain additional factorial suppression factors.

Because of the exponential factor, smaller M^2 in Eq. (3.14) make the suppression stronger and thus the lowest resonance becomes more dominant in the correlation function. Conversely, the suppression in Eq. (3.15) is stronger for larger M^2 . Therefore the unphysical parameter M^2 is usually determined around the intermediate region where the sum rules are optimally improved both on the phenomenological side and OPE side.

3.1.1 Operator Product Expansion

Operator product expansion (OPE) is the primary element of QCD sum rules in order to express the non-perturbative nature of hadronic properties. In 1969 the OPE by Wilson [18] was investigated to define the time-ordered product of two fields in the limit $x \rightarrow 0$ in Eq. (3.2),

$$\lim_{x \rightarrow 0} \mathcal{T} J(x) J(0). \quad (3.16)$$

In a theory with no divergencies the result would just be $J^2(0)$. However, there are ultra-violet singularities so that the limit is physically ill-defined. Wilson's idea

was that $J(x)J(0)$ should behave like a singular function of x times a renormalized operator as $x \rightarrow 0$. The full result is an expansion of the form,

$$\mathcal{T}J(x)J(0) \sim \sum_n C_n(x) \mathcal{O}_n(0) , \quad (3.17)$$

as $x \rightarrow 0$. The sum is taken over a set of local renormalized composite fields which constrained by the symmetry properties of $J(x)$ and by the underlying quantum field theory. The \mathcal{O}_n terms are organized in order of increasing mass dimension, generally decreasing in importance as the dimension increases. In other words, because the total mass dimension of $J(x)J(0)$ is fixed. the coefficient $C_n(x)$ are ordered according to decreasing order of singularity when $x \rightarrow 0$. For simplicity omitting possible anomalous dimensions at this point, one finds

$$C_n(x) \propto |x|^a , \quad a = \dim[\mathcal{O}_n] - \dim[J(x)J(0)] . \quad (3.18)$$

In the calculation of OPE sandwiched by the ground state (vacuum), the Wilson coefficients are usually computed with the background field method [47, 48, 49]. In QCD sum rules, the external gauge field is introduced using the so-called fixed-point gauge,

$$(x - x_0)^\mu A_\mu^{\text{ext}}(x) = 0 , \quad (3.19)$$

where x_0 is an arbitrary fixed point and for simplicity we set $x_0 = 0$ from now on. The external gauge field A_μ^{ext} can be expressed in terms of gauge covariant terms such as $G_{\mu\nu}^{a \text{ ext}}$, $D_\alpha G_{\mu\nu}^{a \text{ ext}}$,

$$\begin{aligned} A_\mu^{\text{ext}}(x) &= x^\nu \int_0^1 d\alpha \alpha G_{\nu\mu}^{a \text{ ext}}(\alpha x) \\ &= \frac{x^\nu}{2} G_{\nu\mu}^{a \text{ ext}}(0) + \frac{x^\alpha x^\nu}{3} D_\alpha G_{\nu\mu}^{a \text{ ext}}(0) + \frac{1}{8} x^\alpha x^\beta x^\nu D_\alpha D_\beta G_{\nu\mu}^{a \text{ ext}}(0) + \dots \\ &= \sum_n \frac{1}{n!(n+2)} x^{\alpha_1} \dots x^{\alpha_n} x^\lambda D_{\alpha_1} \dots D_{\alpha_n} G_{\lambda\mu}^{a \text{ ext}}(0) . \end{aligned} \quad (3.20)$$

Therefore one can directly extract gauge invariant terms in the correlation function.

The external background gauge field is used to evaluate the non-perturbative quark propagator,

$$\begin{aligned} iS(x) &= iS^0(x) - ig_s \int d^4y S^0(x-y) A^{\text{ext}}(y) S^0(y) \\ &\quad + ig_s^2 \int d^4y' d^4y S^0(x-y') A^{\text{ext}}(y') S^0(y'-y) A^{\text{ext}}(y) S^0(y) + \dots , \end{aligned} \quad (3.21)$$

where $iS^0(x)$ indicates the free quark propagator. Inserting Eq. (3.20) into Eq. (3.21), one obtains the quark propagator in the external gauge field. Note that the heavy quark propagator has to be treated differently because $1/m_Q$ still plays the role of a perturbative expansion parameter. However the heavy quark is beyond the scope of this thesis. When a light quark is concerned, the quark propagator itself involves the non-perturbative effects which would be expressed by the quark condensate $\langle \bar{q}q \rangle$. The explicit form of the light quark propagator and its derivation are presented in Appendix B.

3.1.2 Dispersion relation

As mentioned before, $\Pi(q^2)$ in the OPE is calculated in the deep Euclidean domain ($Q^2 = -q^2 > 0$) and in terms of quarks and gluons. On the other hand, the all physical observables are measured in the Minkowski domain ($q^2 > 0$). The connection between the Euclidean predictions and the measurable quantities is established via dispersion relation.

Källén and Lehmann have shown that the two-point function obeys a dispersion relation which follows from the analytical properties [50, 51],

$$\Pi(q^2) = \frac{1}{\pi} \int_0^\infty ds \frac{\text{Im } \Pi(s)}{s - q^2 - i\epsilon} + a + bq^2 + \dots, \quad (3.22)$$

where $\Pi(q^2)$ is an analytic function in the complex q^2 -plane but for a cut in the real axis $0 \leq q^2 \leq \infty$. In general the Cauchy integral formula of $\Pi(q^2)$ leads to the dispersion relation that the real part of the complex function is expressed as an integral over the imaginary part,

$$\text{Re } \Pi(q^2) = \mathcal{P} \frac{1}{\pi} \int_0^\infty ds \frac{\text{Im } \Pi(s)}{s - q^2}, \quad (3.23)$$

where \mathcal{P} stands for the Cauchy principal value.

In Eq. (3.23) good convergence properties have been implicitly assumed, but in general it may require some subtracted terms in order to improve convergence and reliability of the sum rule method,

$$\text{Re } \Pi(q^2) = \mathcal{P} \frac{1}{\pi} \int_0^\infty ds \frac{\text{Im } \Pi(s)}{s - q^2} + a + bq^2 + \dots, \quad (3.24)$$

where the polynomial terms in the r.h.s. of Eq. (3.24) depend on the convergence properties of $\text{Im } \Pi(s)$ when $s \rightarrow \infty$. The coefficients of the polynomial have no discontinuities, in other words, the ambiguity of short-distance behavior is reflected

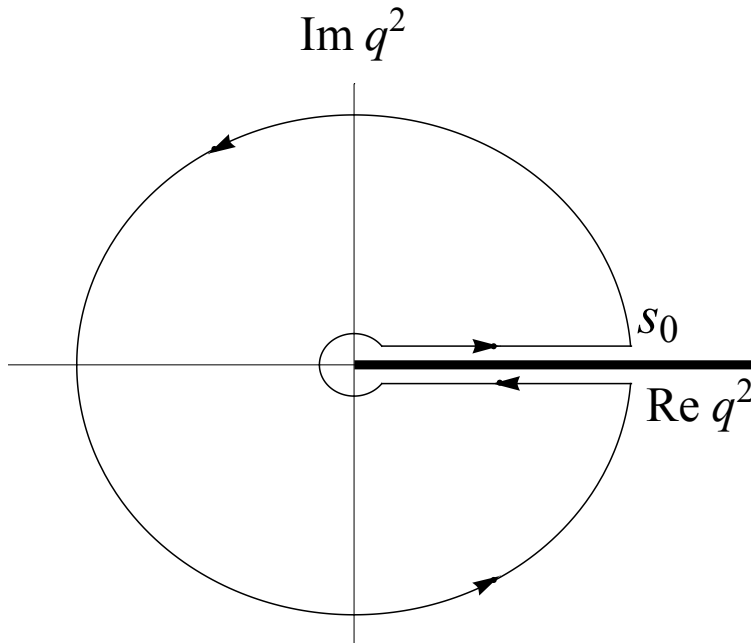


Figure 3.1: Contour integral in the complex q^2 -plane.

only in the evaluation of the real part of the two-point function, not in the imaginary part. The physical meaning of these coefficients depends on the choice of the local operator $J(x)$ in the two-point function. In some cases the coefficients are fixed by low-energy theorems, e.g. if $\Pi(0)$ is known, one can replace a in Eq. (3.24) with $\Pi(0)$,

$$\text{Re } \Pi(q^2) = \text{Re } \Pi(0) + \mathcal{P} \frac{1}{\pi} \int_0^\infty \frac{ds}{s} \frac{q^2}{s - q^2} \text{Im } \Pi(s) + bq^2 + \dots \quad (3.25)$$

In other cases, the constants are absorbed by renormalization constants. It is possible to get rid of the polynomial terms by taking an appropriate number of derivatives with respect to q^2 .

3.2 Finite energy sum rules

There exist several different types of QCD sum rule according to the weight factors applied to the spectral density. One of the most frequently used sum rules is the Borel sum rule (or equivalently Laplace sum rule), which is presented with Eqs. (3.14) and (3.15). In this type of the sum rules the exponential form of the weight factor in Eq. (3.14) enhances the role of the lowest state in the spectral integral.

Another type of QCD sum rule is the finite energy sum rule (FESR) [19, 20, 21] which we shall use throughout this thesis.

$$\mathcal{M}_n = \int_0^{s_0} ds s^n \frac{1}{\pi} \text{Im} \Pi(s) \quad (n = 0, 1, 2, \dots) . \quad (3.26)$$

A standard way to derive the finite energy sum rule is the use of the Cauchy integral theorem on a finite radius (s_0) contour in the complex q^2 -plane. Avoiding the cut on the real axis, the Cauchy theorem leads to

$$\frac{1}{2\pi i} \oint dq^2 q^{2n} \Pi(q^2) = 0 . \quad (3.27)$$

If the contribution of the small circle around the origin is neglected, one deduces the moment,

$$\int_0^{s_0} ds s^n \text{Im} \Pi(s) = -\frac{1}{2\pi i} \oint_{|q^2|=s_0} dq^2 q^{2n} \Pi(q^2) . \quad (3.28)$$

The l.h.s. of Eq. (3.28) is the contribution from the paths above and below the real axis which pick up the discontinuity of $\Pi(q^2)$. In practice it can be obtained from hadronic data or a parametrization of the spectral function. The r.h.s. is the contribution from the circle of radius s_0 . This r.h.s. is computed in perturbative QCD using the explicit form of the running coupling $\alpha_s(s)$. However, in contrast to the Borel sum rules in which the higher excited states are exponentially suppressed, the FESR has $(q^2)^n$ as the weight factor multiplying $\Pi(q^2)$ and hence diverges with increasing n . This high energy behavior that dominates the spectral function with increasing n is reflected in the non-perturbative corrections, e.g. condensates, to the r.h.s. of Eq. (3.28).

The FESR is useful to estimate the threshold of the perturbative continuum, s_0 , by using a given hadronic spectral function. The continuum threshold has the meaning of the scale that separates the low-lying resonance region from the high energy continuum.

3.3 Sum rules for ρ -meson in vacuum

As an simple example, we construct the sum rules for ρ -meson in vacuum. Let us start with the current-current correlation function,

$$\Pi^{\mu\nu}(q) = i \int_0^\infty d^4x e^{iq \cdot x} \langle \mathcal{T} J^\mu(x) J^\nu(0) \rangle \quad (3.29)$$

with vector isovector current,

$$J^\mu(x) = \frac{1}{2} (\bar{u}\gamma^\mu u - \bar{d}\gamma^\mu d) . \quad (3.30)$$

The tensor structure of $\Pi^{\mu\nu}(q)$ is represented in terms of an invariant (scalar) correlator $\Pi(q^2)$:

$$\Pi^{\mu\nu}(q) = \left(g^{\mu\nu} - \frac{q^\mu q^\nu}{q^2} \right) \Pi(q^2) = (q^\mu q^\nu - q^2 g^{\mu\nu}) \Pi'(-Q^2) , \quad (3.31)$$

with

$$\Pi'(-Q^2) = \frac{\Pi(q^2)}{-q^2} , \quad (3.32)$$

in order to satisfy the current conservation,

$$q_\mu \Pi^{\mu\nu} = 0 . \quad (3.33)$$

Then the OPE result for $\Pi(Q^2 = -q^2)$ is obtained as follows:

$$\begin{aligned} \Pi'_{\text{OPE}}(Q^2) &= -\frac{1}{8\pi^2} \left(1 + \frac{\alpha_s}{\pi} \right) \ln \left(\frac{Q^2}{\mu^2} \right) \\ &+ \frac{1}{2Q^4} (m_u \langle \bar{u}u \rangle + m_d \langle \bar{d}d \rangle) + \frac{1}{24Q^4} \left\langle \frac{\alpha_s}{\pi} G^2 \right\rangle \\ &- \frac{\pi\alpha_s}{2Q^6} \left[\langle (\bar{u}\gamma_\mu\gamma_5\lambda^a u - \bar{d}\gamma_\mu\gamma_5\lambda^a d)^2 \rangle \right. \\ &\quad \left. + \frac{2}{9} \langle (\bar{u}\gamma_\mu\lambda^a u + \bar{d}\gamma_\mu\lambda^a d) \sum_{q=u,d,s} \bar{q}\gamma^\mu\lambda^a q \rangle \right] . \end{aligned} \quad (3.34)$$

After the Borel transformation, the correlator is rewritten as,

$$\begin{aligned} \tilde{\Pi}'_{\text{OPE}}(M^2) &= \frac{1}{8\pi^2} \left(1 + \frac{\alpha_s}{\pi} \right) M^2 \\ &+ \frac{1}{2M^2} (m_u \langle \bar{u}u \rangle + m_d \langle \bar{d}d \rangle) + \frac{1}{24M^2} \left\langle \frac{\alpha_s}{\pi} G^2 \right\rangle \\ &- \frac{\pi\alpha_s}{4M^4} \left[\langle (\bar{u}\gamma_\mu\gamma_5\lambda^a u - \bar{d}\gamma_\mu\gamma_5\lambda^a d)^2 \rangle \right. \\ &\quad \left. + \frac{2}{9} \langle (\bar{u}\gamma_\mu\lambda^a u + \bar{d}\gamma_\mu\lambda^a d) \sum_{q=u,d,s} \bar{q}\gamma^\mu\lambda^a q \rangle \right] . \end{aligned} \quad (3.35)$$

Using Eqs. (3.14) and (3.15), the master equation of the Borel sum rule is obtained

$$\begin{aligned}
\int_0^\infty ds e^{-s/M^2} \rho_{\text{phen}} &= \frac{1}{8\pi^2} \left(1 + \frac{\alpha_s}{\pi}\right) M^2 \\
&+ \frac{1}{2M^2} (m_u \langle \bar{u}u \rangle + m_d \langle \bar{d}d \rangle) + \frac{1}{24M^2} \left\langle \frac{\alpha_s}{\pi} G^2 \right\rangle \\
&- \frac{\pi\alpha_s}{2M^4} \left[\langle (\bar{u}\gamma_\mu\gamma_5\lambda^a u - \bar{d}\gamma_\mu\gamma_5\lambda^a d)^2 \rangle \right. \\
&\quad \left. + \frac{2}{9} \langle (\bar{u}\gamma_\mu\lambda^a u + \bar{d}\gamma_\mu\lambda^a d) \sum_{q=u,d,s} \bar{q}\gamma^\mu\lambda^a q \rangle \right]. \tag{3.36}
\end{aligned}$$

The phenomenological spectral density ρ_{phen} can be optimized by using either experimental data or model calculations as an input.

The FESR for ρ -meson in vacuum is derived from Eq. (3.36) by assuming that the spectral density ρ_{phen} separates into a resonance part $\rho_{\text{phen}}^{\text{res}}$ with $s \leq s_0$ and a perturbative continuum,

$$\rho_{\text{phen}} = \rho_{\text{phen}}^{\text{res}} \Theta(s_0 - s) + \frac{1}{8\pi^2} \left(1 + \frac{\alpha_s}{\pi}\right) \Theta(s - s_0). \tag{3.37}$$

The Borel mass M must be sufficiently large so that Eq. (3.36) converges rapidly, but otherwise it is arbitrary. We choose $M > \sqrt{s_0}$ so that e^{-s/M^2} can be expanded in powers of s/M^2 for $s < s_0$,

$$\begin{aligned}
\int_0^\infty ds e^{-s/M^2} \rho_{\text{phen}} &= \int_0^{s_0} ds e^{-s/M^2} \rho_{\text{phen}}^{\text{res}} + \frac{1}{8\pi^2} \left(1 + \frac{\alpha_s}{\pi}\right) \int_{s_0}^\infty ds e^{-s/M^2} \\
&= \int_0^{s_0} ds \rho_{\text{phen}}^{\text{res}} - \frac{1}{M^2} \int_0^{s_0} ds s \rho_{\text{phen}}^{\text{res}} + \frac{1}{2M^4} \int_0^{s_0} ds s^2 \rho_{\text{phen}}^{\text{res}} + \dots \\
&\quad + \frac{1}{8\pi^2} \left(1 + \frac{\alpha_s}{\pi}\right) M^2 \left(1 - \frac{s_0}{M^2} + \frac{s_0^2}{2M^4} + \dots\right). \tag{3.38}
\end{aligned}$$

Then the term-by-term comparison in Eq. (3.36) gives the set of sum rules for the lowest two moments of the spectral density:

$$\begin{aligned}
\int_0^{s_0} ds \rho_{\text{phen}}^{\text{res}} &= \frac{s_0}{8\pi^2} \left(1 + \frac{\alpha_s}{\pi}\right), \\
\int_0^{s_0} ds s \rho_{\text{phen}}^{\text{res}} &= \frac{s_0^2}{16\pi^2} \left(1 + \frac{\alpha_s}{\pi}\right) + \frac{1}{24} \left\langle \frac{\alpha_s}{\pi} G^2 \right\rangle + \frac{1}{2} (m_u \langle \bar{u}u \rangle + m_d \langle \bar{d}d \rangle), \tag{3.39}
\end{aligned}$$

which are exactly the master equations of the FESR for $n = 0, 1$.

3.4 In-medium modifications of the sum rules

In the asymptotic region ($Q^2 \rightarrow \infty$) where the OPE is valid, all non-perturbative scales are represented as power corrections to the perturbative calculations. These non-perturbative contributions in the OPE appear to be more clearly separated into condensates. In the low density or temperature limit, medium-dependence of the OPE is estimated by corrections solely to the condensates. As far as these corrections are smaller than the vacuum value of the condensates, it does not spoil the convergence of the OPE.

3.4.1 Condensates at low density

The Hellmann-Feynman theorem [52] provides a useful way to consider quark densities in terms of the dependence of energies on the current quark mass. The theorem in quantum mechanics relates the parameter dependence between a given Hamiltonian ($H(\lambda)$) and the total energy ($E(\lambda)$),

$$\frac{dE(\lambda)}{d\lambda} = \langle \Psi | \frac{\partial H(\lambda)}{\partial \lambda} | \Psi \rangle , \quad (3.40)$$

where λ denotes an arbitrary (adiabatic) parameter and $|\Psi\rangle$ is the normalized ground state. To apply this theorem to the QCD Hamiltonian,

$$H_{\text{QCD}} = \int d^3x \mathcal{H}_{\text{QCD}}(x) = \int d^3x (\mathcal{H}_{\text{QCD}}^{\text{massless}} + m_q(\bar{u}u + \bar{d}d)) , \quad (3.41)$$

we regard the light quark mass m_q as the small parameter,

$$\frac{\partial E(m_q)}{\partial m_q} = \int d^3x \langle \Psi | \frac{\partial \mathcal{H}_{\text{QCD}}(m_q)}{\partial m_q} | \Psi \rangle = V \langle \Psi | \bar{u}u + \bar{d}d | \Psi \rangle , \quad (3.42)$$

where V is the volume. It reads in terms of the energy density $\mathcal{E} \equiv E/V$,

$$\frac{\partial \mathcal{E}}{\partial m_q} = \langle \Psi | \bar{u}u + \bar{d}d | \Psi \rangle \equiv \langle \bar{q}q \rangle_{\Psi} . \quad (3.43)$$

Considering the vacuum energy density \mathcal{E}_0 , the difference of $\langle \bar{q}q \rangle_{\Psi}$ and $\langle \bar{q}q \rangle_0$ is written as follows,

$$\langle \bar{q}q \rangle_{\Psi} = \langle \bar{q}q \rangle_0 + \frac{\partial}{\partial m_q} (\mathcal{E} - \mathcal{E}_0) . \quad (3.44)$$

The modification in the quark condensate is given by the change of the energy density with varying quark mass. In order to replace the variable to hadronic masses, one needs to know the quark-mass dependence of the hadronic masses. Restricting

ourselves to a system with nucleons and pions, the GOR relation, Eq. (2.23), and the definition of the nucleon σ -term, $\partial M_N/\partial m_q = \sigma_N/m_q$, can be used,

$$\begin{aligned} \frac{\langle \bar{q}q \rangle_\Psi}{\langle \bar{q}q \rangle_0} &= 1 + \frac{1}{\langle \bar{q}q \rangle_0} \left[\frac{\partial m_\pi^2}{\partial m_q} \frac{\partial}{\partial m_\pi^2} + \frac{\partial M_N}{\partial m_q} \frac{\partial}{\partial M_N} + \dots \right] (\mathcal{E} - \mathcal{E}_0) \\ &= 1 - \frac{1}{f_\pi^2} \frac{\partial (\mathcal{E} - \mathcal{E}_0)}{\partial m_\pi^2} + \frac{\sigma_N}{\langle \bar{q}q \rangle_0 m_q} \frac{\partial (\mathcal{E} - \mathcal{E}_0)}{\partial M_N} + \dots \\ &= 1 - \frac{1}{f_\pi^2} \left[\frac{\partial}{\partial m_\pi^2} + \frac{\sigma_N}{m_\pi^2} \frac{\partial}{\partial M_N} \right] (\mathcal{E} - \mathcal{E}_0) + \dots \end{aligned} \quad (3.45)$$

Using Eq. (3.45) and the energy density of a Fermi gas of nucleons, $\mathcal{E} - \mathcal{E}_0 \simeq M_N \rho_N$, for example, the density dependence of the quark condensate is expressed in leading order by the nucleon σ -term ($\sigma_N \approx 45$ MeV) in the following form,

$$\frac{\langle \bar{q}q \rangle_{\rho_N}}{\langle \bar{q}q \rangle_0} \simeq 1 - \frac{\sigma_N}{m_\pi^2 f_\pi^2} \rho_N, \quad (3.46)$$

which yields a reduction of the condensate by a factor of about 0.65 at normal nuclear matter density $\rho_N = \rho_0 = 0.17 \text{ fm}^{-3}$. At non-zero temperature the energy density \mathcal{E} can be easily replaced with the thermodynamic potential Ω (grand canonical ensemble) which is directly related to the pressure of the system via $\Omega = -P$. Consequently the leading expression in calculating the chiral condensate for a system of pions and nucleons appears in the form

$$\frac{\langle \bar{q}q \rangle_\Psi}{\langle \bar{q}q \rangle_0} = 1 + \frac{1}{f_\pi^2} \left(\frac{\partial P}{\partial m_\pi^2} + \frac{\sigma_N}{m_\pi^2} \frac{\partial P}{\partial M_N} \right) + \dots \quad (3.47)$$

A model-independent prediction for the in-medium gluon condensate is derived through the trace anomaly [53],

$$\theta_\mu^\mu = -\frac{1}{8} \left(11 - \frac{2}{3} N_f \right) \frac{\alpha_s}{\pi} G^2 + m_q \bar{q}q, \quad (3.48)$$

where θ_μ^μ denotes the trace of the energy momentum tensor and anomalous dimension has been neglected. The ground-state expectation value of θ_μ^μ for the nuclear matter with density ρ_N is

$$\langle \theta_\mu^\mu \rangle_{\rho_N} - \langle \theta_\mu^\mu \rangle_0 = \mathcal{E} - \mathcal{E}_0 \simeq M_N \rho_N. \quad (3.49)$$

Combining Eq. (3.48) with Eq. (3.49), one can obtain the leading order expression of the gluon condensate at finite density,

$$\begin{aligned} \left\langle \frac{\alpha_s}{\pi} G^2 \right\rangle_{\rho_N} - \left\langle \frac{\alpha_s}{\pi} G^2 \right\rangle_0 &\simeq -\frac{8}{9} [M_N \rho_N - m_q (\langle \bar{q}q \rangle_{\rho_N} - \langle \bar{q}q \rangle_0)] \\ &\simeq -\frac{8}{9} [M_N \rho_N - \sigma_N \rho_N] \\ &= -\frac{8}{9} M_N^{(0)} \rho_N, \end{aligned} \quad (3.50)$$

where $M_N^{(0)}$ is the nucleon mass in the chiral limit and $N_f = 3$ is used.

3.4.2 Condensates at low temperature

The temperature dependence of the vacuum condensates is known as far as the thermal environment is well approximated by the lowest excitation mode of the hadron gas, namely pions. The leading behavior of the chiral condensate at low temperature comes just from the pions. The first predictions of the T -dependent quark condensate were calculated in Ref. [54]. Later in Ref. [55] the thermodynamics of the pion gas was developed up to three-loop contributions in chiral perturbation theory. The pressure, as the thermodynamic potential, was derived from the chiral Lagrangian Eq. (2.24). Then Eq. (3.47), derived from the Hellmann-Feynman theorem, gives the leading expression of the T -dependent quark condensate.

$$\frac{\langle \bar{q}q \rangle_T}{\langle \bar{q}q \rangle_0} = 1 + \frac{1}{f_\pi^2} \left(\frac{\partial P}{\partial m_\pi^2} \right), \quad (3.51)$$

where the pressure of a noninteracting Bose gas of pions can be written as

$$\begin{aligned} P &= \frac{T^4}{2\pi^2} \int_0^\infty \frac{dx x^4}{\sqrt{x^2 + \frac{m_\pi^2}{T^2}}} \left(\exp \left[\sqrt{x^2 + \frac{m_\pi^2}{T^2}} \right] - 1 \right)^{-1} \\ &\simeq 3 \left(\frac{\pi^2}{90} T^4 - \frac{m_\pi^2}{24} T^2 + \frac{m_\pi^3}{12\pi} T + \dots \right). \end{aligned} \quad (3.52)$$

Substituting the pressure of the non-interacting pion gas in Eq. (3.51), we obtain

$$\langle \bar{q}q \rangle_T = \langle \bar{q}q \rangle_0 \left(1 - \frac{T^2}{8f_\pi^2} + \mathcal{O}(T^4) \right). \quad (3.53)$$

Higher order terms can be determined by taking into account the pion interactions in the framework of chiral perturbation theory.

The temperature dependence of the gluon condensate can be determined through its connection to the trace of the energy-momentum tensor,

$$\langle \theta_\mu^\mu \rangle_T - \langle \theta_\mu^\mu \rangle_0 = \mathcal{E} - 3P = T^5 \frac{d}{dT} \left(\frac{P}{T^4} \right), \quad (3.54)$$

where \mathcal{E} and P are the energy density and pressure of the pion gas. Inserting Eq. (3.48) and Eq. (3.52) into Eq. (3.54), the temperature dependence of the gluon condensate is found.

Chapter 4

Vector mesons at finite density

4.1 Introduction

As the lowest “dipole” excitations of the QCD vacuum, the light vector mesons (the ρ meson, in particular) have traditionally played an important prototype role in calculations and discussions based on QCD sum rules [46]. In-medium versions of these sum rules have been used to set constraints on the way in which vector meson masses undergo possible changes in dense and hot hadronic matter [14, 56, 57]. Questions were raised, however, concerning the interpretation of such studies. In-medium changes of meson properties, such as their mass shifts in nuclear matter, have their primary origin in long-distance physics described by meson-nucleon forward scattering amplitudes [58] and not in the short-distance physics represented by subleading terms of the operator product expansion (see also related discussions in Refs. [59, 60]). In-medium QCD sum rules have nonetheless been further developed and applied over the years [61, 15, 62, 63], including studies with emphasis on the density dependence of four-quark condensates [64, 65]. The present work aims in a different direction: namely, identifying the spontaneous chiral symmetry breaking scale, $4\pi f_\pi \sim 1$ GeV, and its possible change with increasing baryon density, in the context of QCD sum rules for the lowest moments of the vector meson spectral functions.

The issue of in-medium changes of hadron properties persists as a fundamental theme ever since the Brown-Rho (BR) scaling hypothesis [13] was launched, establishing a conceptual relationship between the shifts of hadron masses in matter and the sliding scale of spontaneous chiral symmetry breaking with changing thermodynamic conditions. Investigations along these lines included various

model calculations of vector meson spectral functions at finite temperatures and baryon densities (see Refs. [66, 41, 67] and further studies concerning BR scaling in the context of in-medium QCD sum rules, e.g. in Ref. [68]). Such calculations were performed with the aim of understanding the “low-mass enhancements” observed in dilepton spectra produced in high-energy heavy-ion collisions by the CERES/NA45 [3, 4, 6, 5] and NA60 [7, 8, 9, 10, 11, 12] experiments at the CERN SPS. These explorations, primarily focused on the behavior of the ρ meson in the strongly interacting hadronic medium, were conducted for a long time with two seemingly opposing quests: whether there is an in-medium shift of the ρ meson; or on the other hand, whether the strong collisional broadening of the spectral function due to interactions of the ρ meson with nucleons and mesons in the medium would render the primary issue of a mass shift physically meaningless.

In this chapter we point out that playing the notions of “mass shift” and “broadening” against one another may in fact not be the proper question to ask. For resonant states such as the ρ meson, which start out with a large decay width already in vacuum, identifying a mass in an even broader in-medium spectral distribution makes sense only in terms of the first moment of this spectral distribution. For the two lowest spectral moments, however, quite accurate statements can be made within the framework of QCD sum rules, as we shall demonstrate. We propose therefore to abandon the “mass shift” versus “broadening” dispute altogether and concentrate on an analysis of spectral moments in the context of QCD sum rules. Identifying the chiral symmetry breaking scale in such an analysis, both in vacuum and in-medium, permits addressing and examining the BR scaling hypothesis in a refined and better focused way.

The strategy is an update of previous work [69] which is in turn closely related to finite energy sum rules (FESR) [21, 70]. The advantage of these sum rules is that they do not have to rely on the existence of a window of stability for the Borel parameter usually employed in the sum rule analysis. Caution must nevertheless be exercised with FESR’s [71, 72] concerning their sensitivity to high-energy properties of spectral functions and the detailed modeling of the transition between resonance and continuum regions, a question that we shall also address. We concentrate here on the rho meson. Starting with vacuum sum rules for the ρ we recall how the delineation of scales between resonance and continuum parts of the spectral function can be related to the scale for spontaneous chiral symmetry breaking, $4\pi f_\pi \simeq 1.2$ GeV (the “chiral gap”), where $f_\pi = 92.4$ MeV is the pion decay constant. In-medium sum rules are examined using two complementary spectral

functions as generic examples: the one calculated in Ref. [57] using a chiral meson-nucleon effective Lagrangian with vector mesons as explicit degrees of freedom; and the one calculated in Ref. [66] using a model which emphasizes the role of particle-hole excitations including baryon resonances. Both types of spectral functions were applied earlier [41, 73] in descriptions of the CERES/NA45 dilepton data [3]. Updated versions of such spectral distributions have been used recently [74, 75] in comparisons with the more accurate NA60 data [7, 8]. The following sections are basically identical to our publication, Ref. [22].

4.2 Derivation of QCD sum rules

We begin with a brief introductory recollection (see section 3.3) of the QCD sum rule approach for excitations carrying the quantum numbers of the ρ -meson ($J^\pi = 1^-, I = 1$) and ω -meson ($J^\pi = 1^-, I = 0$). The corresponding quark currents

$$j_\rho^\mu(x) = \frac{1}{2}(\bar{u}\gamma^\mu u - \bar{d}\gamma^\mu d), \quad j_\omega^\mu(x) = \frac{1}{6}(\bar{u}\gamma^\mu u + \bar{d}\gamma^\mu d) \quad (4.1)$$

figure in the current-current correlation tensor

$$\Pi^{\mu\nu}(q) = i \int d^4x e^{iq \cdot x} \langle \mathcal{T} j_V^\mu(x) j_V^\nu(0) \rangle. \quad (4.2)$$

In vacuum this tensor can be reduced to a single scalar correlation function as in Eq. (3.31),

$$\Pi(q^2) = \frac{1}{3} g_{\mu\nu} \Pi^{\mu\nu}(q). \quad (4.3)$$

In nuclear matter with finite baryon density ρ_N , since the interaction with the nuclear environment breaks the Lorentz invariance of the system, the distinction needs to be made between longitudinal and transverse correlation functions. For vanishing three-momentum ($q^\mu = (\omega, \mathbf{q} = 0)$, the case considered here throughout), the longitudinal and transverse correlation functions coincide and will again be denoted as $\Pi(\omega, \mathbf{q} = 0)$.

The next step is to write $\Pi(q^2)$ as a twice-subtracted dispersion relation:

$$\Pi(q^2) = \Pi(0) + bq^2 + \frac{q^4}{\pi} \int ds \frac{\text{Im} \Pi(s)}{s^2(s - q^2 - i\epsilon)}. \quad (4.4)$$

Alternatively, the same quantity is expressed at large spacelike $q^2 = -Q^2 < 0$ in terms of the Wilson operator product expansion (OPE):

$$12\pi^2 \Pi(q^2 = -Q^2) = -c_0 Q^2 \ln \left(\frac{Q^2}{\mu^2} \right) + c_1 + \frac{c_2}{Q^2} + \frac{c_3}{Q^4} + \dots \quad (4.5)$$

In vacuum, the expansion coefficients are given as:

$$\begin{aligned}
c_0 &= d_V \left(1 + \frac{\alpha_s}{\pi} \right) + \dots , \\
c_1 &= -3 d_V (m_u^2 + m_d^2) , \\
c_2 &= d_V \frac{\pi^2}{3} \left\langle \frac{\alpha_s}{\pi} G^2 \right\rangle + 4 d_V \pi^2 (m_u \langle \bar{u}u \rangle + m_d \langle \bar{d}d \rangle) ,
\end{aligned} \tag{4.6}$$

with $d_V = 3/2$ for ρ -meson and $d_V = 1/6$ for ω -meson. These three leading coefficients are well determined. The dominant perturbative QCD piece c_0 is shown here including just the standard $\mathcal{O}(\alpha_s)$ correction. At a later stage and in all explicit calculations, the QCD corrections will be further extended up to and including $\mathcal{O}(\alpha_s^3)$ (see Appendix C).

The quark mass term c_1 is small and can safely be neglected. The coefficient c_2 involves the QCD condensates of lowest dimension four. The quark condensate times the quark mass is given accurately through the Gell-Mann–Oakes–Renner (GOR) relation [30] as

$$\begin{aligned}
\langle m_u \bar{u}u + m_d \bar{d}d \rangle &\simeq m_q \langle \bar{u}u + \bar{d}d \rangle \\
&= -m_\pi^2 f_\pi^2 = -(0.11 \text{ GeV})^4 .
\end{aligned} \tag{4.7}$$

The gluon condensate $\langle (\alpha_s/\pi) G^2 \rangle \sim (0.3 \text{ GeV})^4$ is (far less accurately) determined by charmonium sum rules. For a detailed discussion see Ref. [76] where an upper limit

$$\langle (\alpha_s/\pi) G^2 \rangle^{1/4} \lesssim 0.31 \text{ GeV}$$

is given.

In-medium corrections to leading order in the baryon density ρ_N are introduced by the replacement $c_2 \rightarrow c_2 + \delta c_2(\rho_N)$, with [14, 56, 57]

$$\delta c_2 = 2 d_V \pi^2 \left[A_1 M_N - \frac{4}{27} M_N^{(0)} + 2\sigma_N \right] \rho_N . \tag{4.8}$$

The first term in brackets is the leading density dependent perturbative QCD correction. It involves the first moment, $A_1 = 2\langle x \rangle_{u+d}$, of the parton distribution in the nucleon. Given the empirical (MRST) [77, 78] momentum fraction carried by u and d quarks in the nucleon, $\langle x \rangle_{u+d} \simeq 0.62$ at $Q^2 = 1 \text{ GeV}^2$, we use $A_1 \simeq 1.24$ (see Appendix D).

The second term on the r.h.s. of Eq. (4.8) is the correction to the gluon condensate at finite density which is derived in Eq. (3.50). It is proportional to the nucleon mass in the chiral limit for which we use $M_N^{(0)} = 0.88 \text{ GeV}$ from Refs. [79, 80]. The

	value	reference
M_N	939 MeV	
$m_q \langle \bar{q}q \rangle$	$-(0.11 \text{ GeV})^4$	GOR
$\langle \frac{\alpha_s}{\pi} G^2 \rangle$	$0.005 \pm 0.004 \text{ GeV}^4$	[76]
A_1	1.237	[78]
$M_N^{(0)}$	0.88 GeV	[79][80]
σ_N	$45 \pm 8 \text{ MeV}$	[81]

Table 4.1: Input summary

third term represents the leading density dependence of the quark condensate in Eq. (3.46). It is proportional to the nucleon sigma term, $\sigma_N = (45 \pm 8) \text{ MeV}$ [81]. By far the largest contribution to δc_2 evidently comes from the A_1 term, so that the large uncertainty in σ_N has only relatively minor consequences.

Following these considerations the input for c_2 and δc_2 is summarized in Table 4.1. The in-medium sum rule analysis will be done at normal nuclear matter density, $\rho_N = \rho_0 = 0.17 \text{ fm}^{-3}$.

The coefficient c_3 involves four-quark condensates in the following combination:

$$c_3 = -d_V \pi^3 \alpha_s \left[\langle (\bar{u} \gamma_\mu \gamma_5 \lambda^a u - \bar{d} \gamma_\mu \gamma_5 \lambda^a d)^2 \rangle + \frac{2}{9} \langle (\bar{u} \gamma_\mu \lambda^a u + \bar{d} \gamma_\mu \lambda^a d) \sum_{q=u,d,s} \bar{q} \gamma^\mu \lambda^a q \rangle \right]. \quad (4.9)$$

These condensates of dimension six are not known at any reasonable level of precision. What is commonly done at this point is to introduce a factorization approximation, truncating intermediate states by the QCD ground state and writing

$$\langle (\bar{q} \gamma_\mu \gamma_5 \lambda^a q)^2 \rangle = -\langle (\bar{q} \gamma_\mu \lambda^a q)^2 \rangle = \frac{16}{9} \kappa \langle \bar{q}q \rangle^2, \quad (4.10)$$

with κ introduced to parameterize deviations from exact factorization ($\kappa = 1$). The in-medium analogue including terms linear in the density ρ_N becomes

$$c_3 = -d_V \frac{896}{81} \kappa(\rho_N) \pi^3 \alpha_s \left(\langle \bar{q}q \rangle^2 + \frac{\sigma_N \langle \bar{q}q \rangle}{m_q} \rho_N \right), \quad (4.11)$$

with a density dependent κ parameter.

Clearly, any QCD sum rule analysis that aims for accuracy must try to avoid the uncertain four-quark condensate piece c_3 in the OPE hierarchy. This is indeed

possible when considering only the two lowest moments of the spectral function, $\text{Im } \Pi(s)$, as follows. We introduce the dimensionless spectral function

$$R(s) = -\frac{12\pi}{s} \text{Im } \Pi(s) . \quad (4.12)$$

Note that, in vacuum, $R(s)$ is identified with the normalized cross-section,

$$R(s) = \frac{\sigma(e^+e^- \rightarrow \text{hadrons})}{\sigma(e^+e^- \rightarrow \mu^+\mu^-)} , \quad (4.13)$$

where the cross section of $e^+e^- \rightarrow \mu^+\mu^-$ simply reads

$$\sigma(e^+e^- \rightarrow \mu^+\mu^-) = \frac{4\pi\alpha_{em}^2}{3s} . \quad (4.14)$$

Now assume as usual that there exists a delineation scale s_0 which separates the low-mass resonance region ($s \leq s_0$) from the high-mass continuum ($s > s_0$):

$$R(s) = R_V(s) \Theta(s_0 - s) + R_c(s) \Theta(s - s_0) . \quad (4.15)$$

This step function delineation between resonance and continuum seems schematic on first sight. In practice, the transition to the continuum is smooth and s_0 should be considered as an average scale characterizing the transition region. A detailed analysis, to be described later, shows that the step function ansatz is equivalently as valid as a more realistic modeling of the threshold "ramp", e.g. by the dotted line in Fig. 4.2.

Let the high-mass continuum be subject to a perturbative QCD treatment, following duality considerations:

$$R_c(s) \rightarrow c_0 \quad \text{for } s > s_0 . \quad (4.16)$$

Then perform a Borel transformation on Eqs. (4.4) and (4.5), leading to

$$12\pi^2\Pi(0) + \int_0^\infty ds R(s) e^{-s/M^2} = c_0 M^2 + c_1 + \frac{c_2}{M^2} + \frac{c_3}{2M^4} + \dots \quad (4.17)$$

Choose the (otherwise arbitrary) Borel scale parameter sufficiently large, $M > \sqrt{s_0}$, expand e^{-s/M^2} and arrange term by term in inverse powers of M . The result is a hierarchy of sum rules for *moments* of the low-mass part of the spectral function $R(s)$:

$$\int_0^{s_0} ds R_V(s) = s_0 c_0 + c_1 - 12\pi^2 \Pi(0) , \quad (4.18)$$

$$\int_0^{s_0} ds s R_V(s) = \frac{s_0^2}{2} c_0 - c_2 , \quad (4.19)$$

$$\int_0^{s_0} ds s^2 R_V(s) = \frac{s_0^3}{3} c_0 + c_3 . \quad (4.20)$$

These equations are written again to first order in α_s , with $c_0 = d_V(1 + \alpha_s/\pi)$. Corrections to order α_s^3 are included by the replacements $c_0 \rightarrow c_0 + d_V \varepsilon_n$ in the n -th moment, with ε_n given explicitly in Appendix C. In the detailed calculations the relevant running coupling is to be taken as $\alpha_s(s_0)$ with $s_0 \sim 1 \text{ GeV}^2$, the onset scale for the (multipion) continuum part of the quark-antiquark excitation spectrum. We use

$$\alpha_s(s_0 \sim 1 \text{ GeV}^2) = 0.50 \pm 0.03 , \quad (4.21)$$

referring to the most recent NNLO ($\overline{\text{MS}}$) analysis in [82, 83]. The error in $\alpha_s(s_0)$ is actually the major source of uncertainty in the sum rule calculation, all other corrections being considerably smaller in magnitude relative to the leading term.

The subtraction constant $\Pi(0)$ in Eq.(4.18) vanishes in vacuum. At finite density this is the Landau term, $\Pi(0) = \rho_N/(4M_N)$, analogous to the Thomson limit in Compton scattering.

Note that even for a broad spectral distribution $R(s)$, a squared “mass” associated with the low-energy sector of this spectrum can be defined through the ratio of the first and zeroth moments, Eqs. (4.18) and (4.19) (see also Ref. [62]):

$$\bar{m}^2 = \frac{\int_0^{s_0} ds s R(s)}{\int_0^{s_0} ds R(s)} . \quad (4.22)$$

4.3 Vacuum sum rules

4.3.1 Identifying the spontaneous chiral symmetry breaking scale

Consider now first the sum rule for the isovector current-current correlation function in vacuum. Following Ref. [70] we start from the working hypothesis that the scale s_0 delineating low-energy and continuum parts of the vector-isovector quark-antiquark spectrum should be identified with the scale for spontaneous chiral symmetry breaking in QCD:

$$\sqrt{s_0} = 4\pi f_\pi . \quad (4.23)$$

For illustration, recall the schematic (large N_c) example of a zero-width ρ meson,

$$R_\rho(s) = \frac{12\pi^2 m_\rho^2}{g^2} \delta(s - m_\rho^2) , \quad (4.24)$$

with the vector coupling constant g . Neglecting small quark masses as well as QCD and condensate corrections in Eqs. (4.18) and (4.19), one arrives at

$$\begin{aligned} \int_0^{s_0} ds R_\rho(s) &= \frac{3}{2}s_0 = 24\pi^2 f_\pi^2, \\ \int_0^{s_0} ds s R_\rho(s) &= \frac{3}{4}s_0^2 = 192\pi^4 f_\pi^4, \end{aligned} \quad (4.25)$$

and immediately recovers a celebrated current algebra result (the KSRF relation [34, 35]),

$$m_\rho = \sqrt{2} g f_\pi, \quad (4.26)$$

together with the universal vector coupling $g = 2\pi$.

While this schematic example underlines the validity of the hypothesis, Eq. (4.23), a more detailed test using a realistic spectral distribution $R(s)$ and the full sum rule analysis, including corrections, must of course be performed. We do this along the lines of Ref. [70] and update the results found in that work.

4.3.2 ρ -meson sum rules

The input into the sum rules is now the resonant ρ meson spectral function $R_\rho(s)$ calculated from one-loop chiral $\pi\pi$ dynamics with gauge coupling to vector mesons [84, 57]. The n -pion continuum $R_c(s)$ (with $n \geq 4$ even) is parameterized as in Eq. (4.15), with the gap scale s_0 to be determined by the sum rules for the lowest two moments, Eqs. (4.18) and (4.19). In order to obtain the ρ meson spectral function, the process, $e^+e^- \rightarrow \pi^+\pi^-$ as depicted in Fig. 4.1 was considered. The cross section of e^+e^- pair annihilation for a pion pair is calculated as

$$\sigma(e^+e^- \rightarrow 2\pi) = \frac{\alpha_{em}^2 \pi}{3s} \left(1 - \frac{4m_\pi^2}{s}\right)^{3/2} |F_\pi(s)|^2, \quad (4.27)$$

where α_{em} and s are the electromagnetic fine structure constant and the square of total energy, respectively and $F_\pi(s)$ reads the black blob of Fig. 4.1 as a pion form factor which, in the case, is taken into account in Vector Meson Dominance model (VMD).

Including the contribution that photon directly couple to a pion pair, $F_\pi(s)$ with dominantly intermediate ρ meson is represented by the following form:

$$F_\pi(s) = 1 - \frac{g}{g_\rho} \frac{s}{s - m_\rho^2 + im_\rho \Gamma_\rho(s)}, \quad (4.28)$$

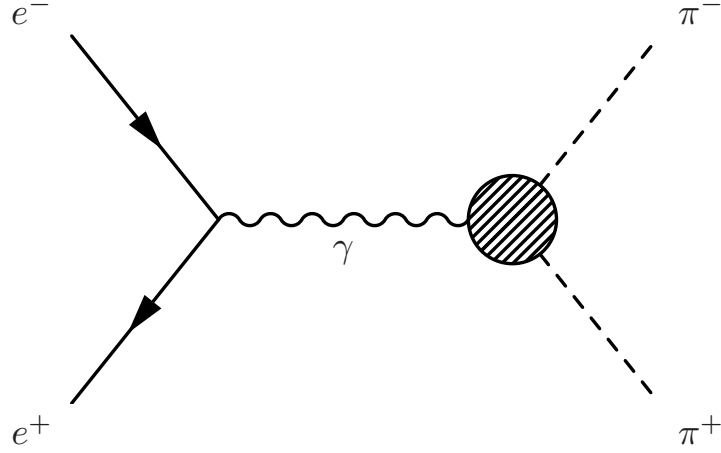


Figure 4.1: e^+e^- annihilation to $\pi^+\pi^-$. The pion-vertex has the form-factor that arises mainly through vector dominance.

where g and g_ρ are coupling constants for $\rho\pi\pi$ and $\rho\gamma$, respectively and the ρ decay width, $\Gamma_\rho(s)$, is given as

$$\Gamma_\rho(s) = \frac{g^2}{48\pi} \frac{s}{m_\rho} \left(1 - \frac{4m_\pi^2}{s}\right)^{3/2}. \quad (4.29)$$

If adopt $m_\pi = 140$ MeV and $m_\rho = 770$ MeV, we can take $g \simeq 6$ from Eq. (4.29), so that $\Gamma_\rho(\sqrt{s} = 770 \text{ MeV})$ may be about 150 MeV experimentally we know.

In addition, $g_\rho = 5.03$ is determined from $\rho \rightarrow e^+e^-$ decay width, then the cross section for $e^+e^- \rightarrow \pi^+\pi^-$, Eq. (4.27), is consistently obtained with experimental data (see Fig. 4.2). Therefore the ρ meson spectral function $R(s)$ with the finite width is obtained as

$$R(s) = \frac{1}{4} \left(1 - \frac{4m_\pi^2}{s}\right)^{3/2} |F_\pi(s)|^2. \quad (4.30)$$

The sum rule analysis proceeds as follows. The equations for the two lowest moments of $R(s)$,

$$\int_0^{s_0} ds R_\rho(s) = s_0 \left(c_0 + \frac{3}{2}\varepsilon_0\right) + c_1, \quad (4.31)$$

$$\int_0^{s_0} ds s R_\rho(s) = \frac{s_0^2}{2} \left(c_0 + \frac{3}{2}\varepsilon_1\right) - c_2, \quad (4.32)$$

are solved to determine s_0 . For the zeroth moment Eq. (4.31) gives $\sqrt{s_0} = 1.13 \pm 0.02$ GeV. Overall consistency requires that the same s_0 results also from Eq. (4.32)

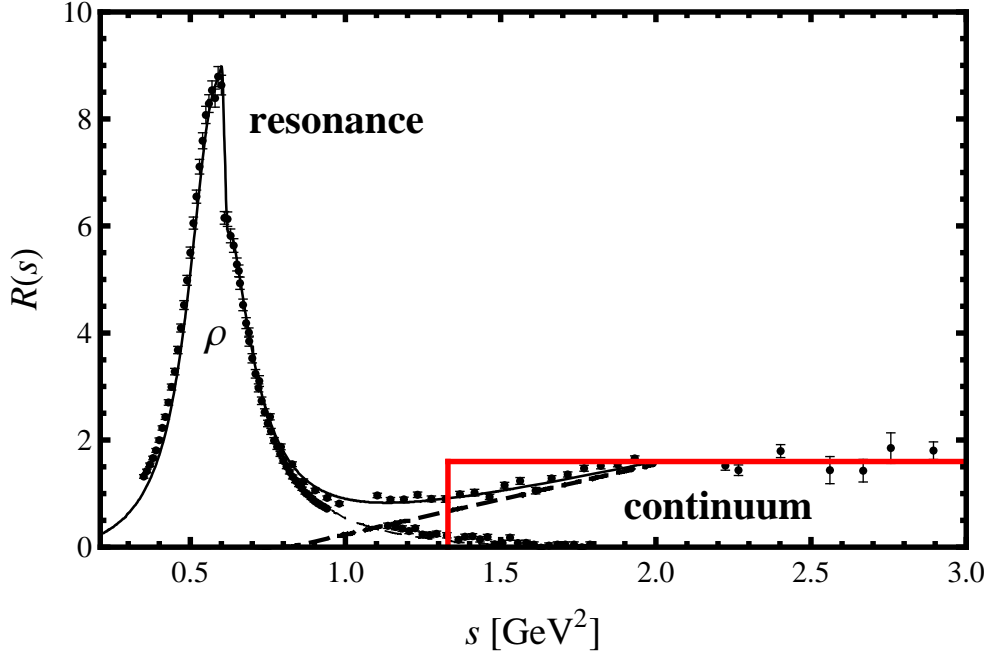


Figure 4.2: Vector-isovector spectral function in vacuum showing the ρ resonance and continuum parts as described in the text and compared to $e^+e^- \rightarrow \pi^+\pi^-$ (ρ resonance region) and $e^+e^- \rightarrow n\pi$ data with n even [26, 27].

within an error band determined by the uncertainties of the input summarized in Table 4.1 and Eq. (4.21). This test turns out to be successful. The detailed analysis of uncertainties performed with Eq. (4.32) for the first moment is shown in Fig. 4.3. The resulting $\sqrt{s_0} = 1.14 \pm 0.01$ GeV is within 2% of the empirical $4\pi f_\pi \simeq 1.16$ GeV using the physical value $f_\pi = 92.4$ MeV of the pion decay constant. The postulate, Eq. (4.23) identifying $\sqrt{s_0}$ with the scale characteristic of spontaneously broken chiral symmetry, appears to be working quantitatively.

The relation between first and the zeroth moment,

$$\int_0^{s_0} ds s R_\rho(s) = \mathcal{F}(s_0) \int_0^{s_0} ds R_\rho(s), \quad (4.33)$$

thus involves a uniquely determined function of s_0 :

$$\mathcal{F}(s_0) = \frac{s_0^2 (c_0 + \frac{3}{2}\varepsilon_1) - 2c_2}{2s_0 (c_0 + \frac{3}{2}\varepsilon_0) + 2c_1}, \quad (4.34)$$

up to the estimated uncertainties in the quantities c_i and ε_n (the largest error being associated with $\alpha_s(s_0)$). The squared mass given by $\bar{m}_\rho^2 = \mathcal{F}(s_0) \simeq 0.611 \pm 0.013$ GeV² or $\bar{m}_\rho \simeq 0.78 \pm 0.01$ GeV, is very close to the physical ρ meson mass as

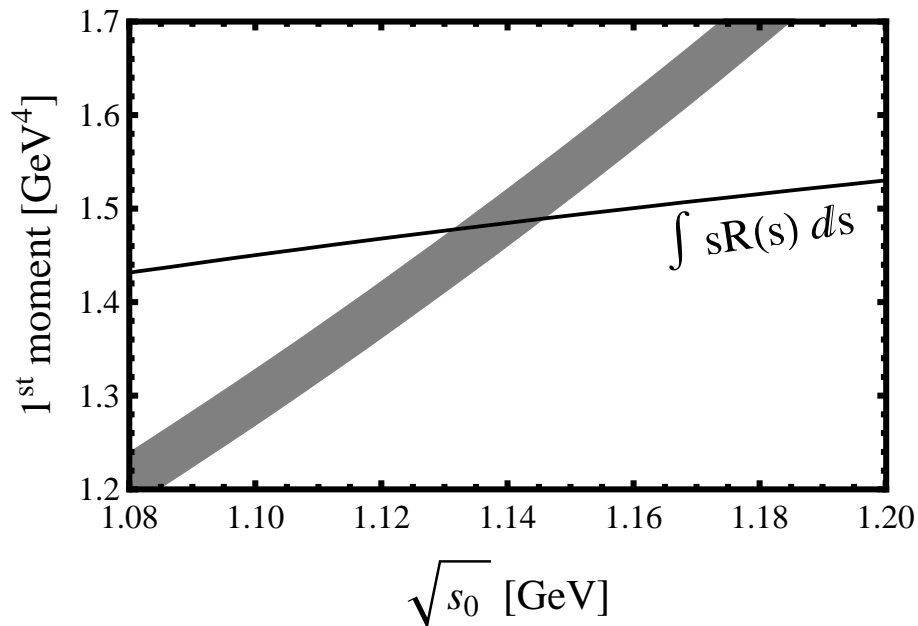


Figure 4.3: QCD sum rule analysis of the ρ meson spectral function in vacuum. First moment (solid line, left-hand side of Eq. (4.32)) is plotted versus right-hand side (grey band including uncertainties) as function of the gap scale $\sqrt{s_0}$ delineating low-mass resonance region from high-mass continuum.

expected. In fact the canonical relation $\bar{m}_\rho = \sqrt{s_0/2} = \sqrt{2} \cdot 2\pi f_\pi$ turns out to be satisfied again at the 2% level, demonstrating the smallness of the next-to-leading QCD corrections and of the condensate term c_2 .

4.3.3 Sensitivity to continuum threshold modeling

The question arises whether the quantitatively successful identification of the continuum threshold $\sqrt{s_0}$ with the chiral symmetry breaking scale (i.e. the consistency of the QCD sum rule analysis with current algebra results) is influenced by the schematic step-function parametrization, Eq. (4.15). A test can be performed replacing the step function by a ramp function to yield a smooth transition between resonance and continuum region, as follows:

$$R(s) = R_\rho(s) \Theta(s_2 - s) + R_c(s) W(s) , \quad (4.35)$$

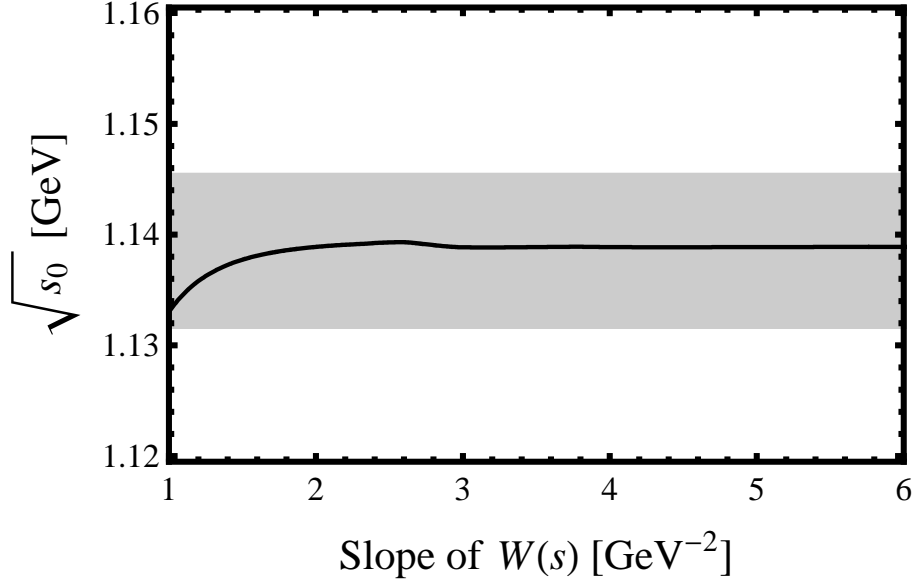


Figure 4.4: Dependence of $\sqrt{s_0}$ [determined from Eqs. (4.37)-(4.39)] on the slope $(s_2 - s_1)^{-1}$ of the ramp function $W(s)$ describing the onset of the continuum in the vacuum sum rule. The grey band indicates the uncertainty range of the result obtained with step function parametrization of the continuum.

where the weight function, $W(s)$, is defined as

$$W(x) = \begin{cases} 0 & \text{for } x \leq s_1 \\ \frac{x - s_1}{s_2 - s_1} & \text{for } s_1 \leq x \leq s_2 \\ 1 & \text{for } x \geq s_2 . \end{cases} \quad (4.36)$$

The step function behavior is recovered for $W(x)$ in the limit $s_1 \rightarrow s_2$.

Using the function $W(s)$, the modified sum rules for the lowest two moments of the spectrum $R(s)$ become

$$\begin{aligned} \int_0^{s_2} ds R_\rho(s) &= s_2 \left(c_0 + \frac{3}{2} \varepsilon_0 \right) + c_1 - 12\pi^2 \Pi(0) - (c_0 - R_\rho(s_2)) \int_{s_1}^{s_2} ds W(s) , \\ \int_0^{s_2} ds s R_\rho(s) &= \frac{s_2^2}{2} \left(c_0 + \frac{3}{2} \varepsilon_1 \right) - c_2 - (c_0 - R_\rho(s_2)) \int_{s_1}^{s_2} ds s W(s) . \end{aligned} \quad (4.38)$$

Sets of intervals $[s_1, s_2]$ are then determined so as to satisfy both sum rules [Eqs. (4.37) and (4.38)], and the scale s_0 defined by

$$s_0 = \frac{s_1 + s_2}{2} , \quad (4.39)$$

is now introduced to characterize the continuum threshold. As shown in Fig. 4.4, the resulting $\sqrt{s_0}$ is stable with respect to variations in the slope $(s_2 - s_1)^{-1}$ of the ramp function $W(s)$, thus confirming that the step function parametrization of the continuum is not restrictive: the smooth “ramping” into the continuum¹ produces values of $\sqrt{s_0}$ that fall within the narrow (less than 1%) uncertainty band of the step function approach. We note at this point that the best fit to the empirical spectral function has $s_2 - s_1 \simeq 1 \text{ GeV}^2$ (see Fig. 4.2). It can be concluded that the present sum rule analysis and the observed quantitative agreement of the continuum threshold with the chiral gap $4\pi f_\pi$ do not depend on details of the threshold modeling.

4.4 In-medium sum rules

In this section the approach just described is applied analogously to vector current spectral functions at finite density. We start again from Eqs. (4.31) and (4.32), now with inclusion of $\Pi(0) = \frac{\rho_N}{4M_N}$ and the density dependent corrections to the condensate terms, $c_2 \rightarrow c_2 + \delta c_2$ (see Eq. (4.8)).

4.4.1 ρ -meson sum rules

Two generic prototypes of in-medium isovector vector spectral functions, $\text{Im } \Pi(\omega = \sqrt{s}, \mathbf{q} = 0; \rho_N)$, are used for demonstration: the one derived from a chiral effective Lagrangian with vector meson couplings constrained by vector dominance [57] (referred to as KKW), and the one calculated with emphasis on particle-hole excitations incorporating baryon resonances [41] (referred to as RW). The analysis is performed at the baryon density of normal nuclear matter, $\rho_N = \rho_0 = 0.17 \text{ fm}^{-3}$. The KKW and RW spectral functions, taken at this density, are shown in comparison in Fig. 4.5.

The KKW and RW in-medium spectral distributions both consistently show a strong broadening as compared to the vacuum ρ meson. They differ in details at the low mass end of the spectrum. While KKW emphasizes the role of chiral in-medium $\pi\pi$ interactions, RW focuses on the role of nucleon-hole, $\Delta(1232)$ -hole and $N^*(1520)$ -hole excitations. At first sight, none of these broad distributions permit identifying an “in-medium mass” or a shift thereof with respect to the ρ

¹In this test the uncertainties of $\alpha_s(Q^2)$ and of the gluon condensate have been excluded for simplicity.

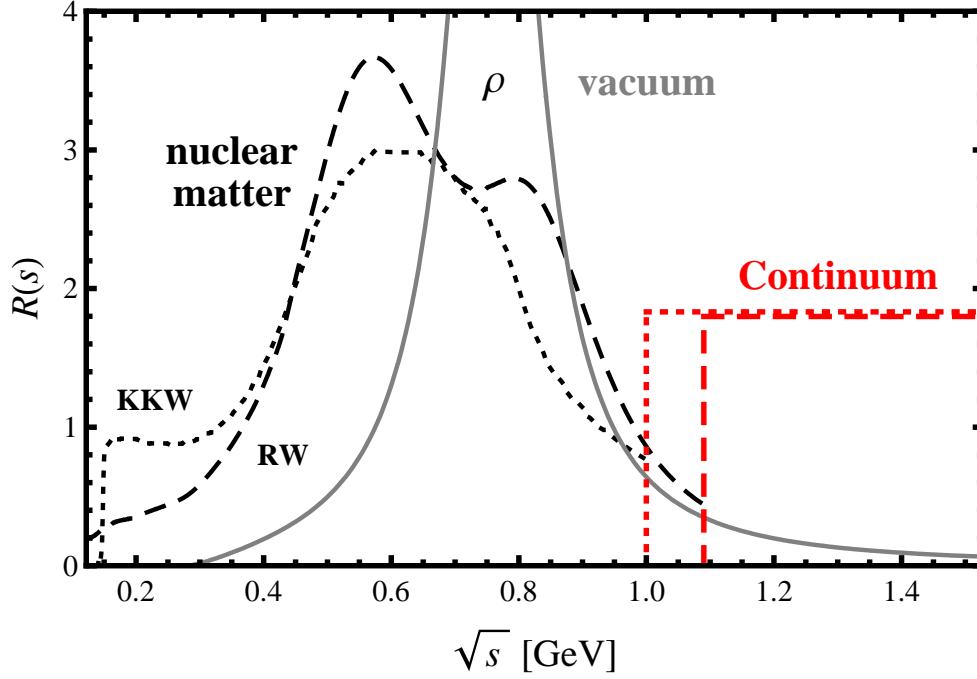


Figure 4.5: In-medium isovector vector spectral functions at nuclear matter density, $\rho_0 = 0.17 \text{ fm}^{-3}$, taken from Refs. [57] (KKW) and [41] (RW). The ρ meson spectrum in vacuum is also shown for comparison.

meson mass in vacuum. This has generally led to the conclusion of there being no ρ mass shift at finite density, but just an overwhelmingly large inelastic width due to interactions of the coupled $\rho \leftrightarrow \pi\pi$ system with nucleons in the nuclear medium.

We now perform the sum rule analysis, first with step function continuum, for the two leading moments of the KKW and RW spectral distributions:

$$\int_0^{s_0^*} ds R_\rho(s) = s_0^* \left(c_0 + \frac{3}{2}\varepsilon_0 \right) + c_1 - \frac{3\pi^2 \rho_N}{M_N}, \quad (4.40)$$

$$\int_0^{s_0^*} ds s R_\rho(s) = \frac{s_0^{*2}}{2} \left(c_0 + \frac{3}{2}\varepsilon_1 \right) - (c_2 + \delta c_2(\rho_N)), \quad (4.41)$$

where the gap scale $\sqrt{s_0^*}$ is permitted to adjust itself to the in-medium situation. Consistency of the first and zeroth spectral moments is again tested and observed to be satisfied within the uncertainties of the input. This determines s_0^* at given density $\rho_N = \rho_0$. Effects of smooth ramping into the continuum will again be examined later.

Fig. 4.6 shows the outcome of this procedure for the KKW spectral function.

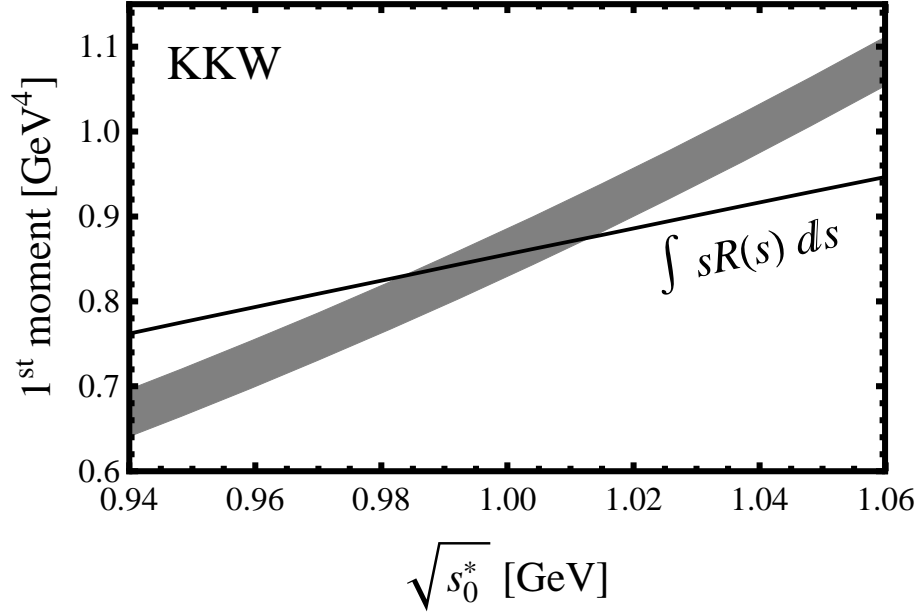


Figure 4.6: QCD sum rule analysis of the KKW in-medium ρ spectral function [57]. First moment [solid line, left-hand side of Eq. (4.41)] is plotted versus right-hand side [grey band including uncertainties] as function of the in-medium gap scale $\sqrt{s_0^*}$.

In this case, at nuclear matter density ρ_0 , the in-medium gap scale $\sqrt{s_0^*}$ is indeed seen to be shifted downward from its vacuum position, $\sqrt{s_0} \simeq 1.14$ GeV $\simeq 4\pi f_\pi$. One finds

$$\sqrt{s_0^*} = (1.00 \pm 0.02) \text{ GeV} \quad (\text{KKW at } \rho_N = \rho_0). \quad (4.42)$$

For comparison, the cross check with the sum rule for the zeroth moment gives $\sqrt{s_0^*} = (1.02 \pm 0.03)$ GeV, consistent with Eq. (4.42).

The analogue of Eq. (4.33) becomes:

$$\int_0^{s_0^*} ds sR(s, \rho_N) = \mathcal{F}(s_0^*, \rho_N) \int_0^{s_0^*} ds R(s, \rho_N) \quad (4.43)$$

with

$$\mathcal{F}(s_0^*, \rho_N) = \frac{s_0^{*2} (c_0 + \frac{3}{2}\varepsilon_1) - 2(c_2 + \delta c_2(\rho_N))}{2 [s_0^* (c_0 + \frac{3}{2}\varepsilon_0) + c_1 - 3\pi^2 \rho_N / M_N]}, \quad (4.44)$$

The average in-medium “mass” determined from the ratio $\mathcal{F}(s_0^*, \rho_N)$ of the first and zeroth spectral moments is found to be

$$\bar{m}^*(\rho_N) = \sqrt{\mathcal{F}(s_0^*, \rho_N)} = (0.67 \pm 0.02) \text{ GeV} \quad (4.45)$$

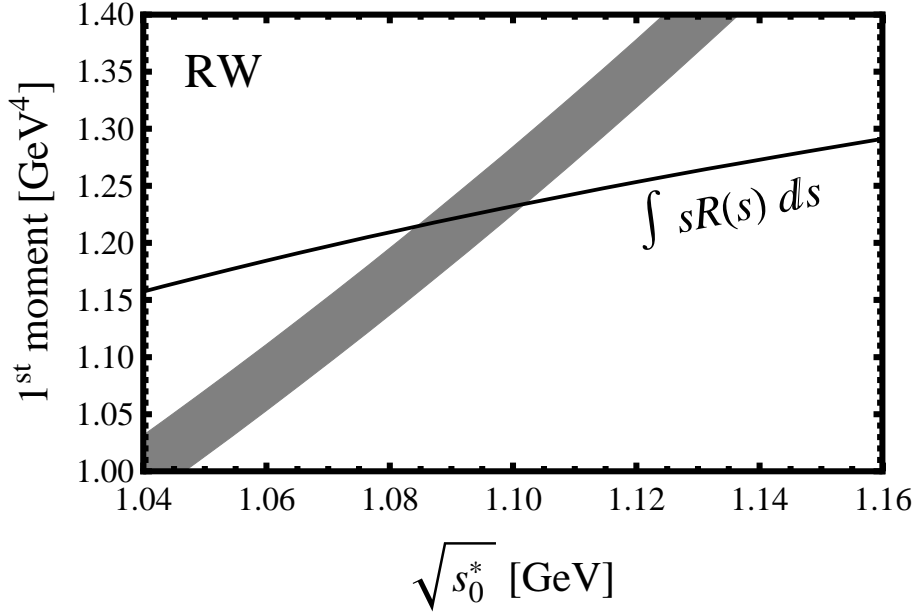


Figure 4.7: QCD sum rule analysis of the RW in-medium ρ spectral function [41]. First moment [solid line, left-hand side of Eq. (4.41)] is plotted versus right-hand side [grey band including uncertainties] as function of the in-medium gap scale $\sqrt{s_0^*}$.

for the KKW spectral function at density $\bar{\rho}_N = \rho_0$. One notes now that the ratio of in-medium and vacuum 1st spectral moments behaves as

$$\frac{\bar{m}^*}{\bar{m}_\rho(vac)} = \sqrt{\frac{\mathcal{F}(s_0^*, \rho_N)}{\mathcal{F}(s_0, \rho_N = 0)}} \simeq 0.85 \pm 0.02 \quad (4.46)$$

at $\rho_N = \rho_0$.

The successful identification $\sqrt{s_0} = 4\pi f_\pi$ in vacuum suggests a corresponding generalization to the in-medium case: $\sqrt{s_0^*} = 4\pi f_\pi^*$, in terms of the pion decay constant, $f_\pi^* \equiv f_t(\rho_N)$, related to the time component of the axial current at finite density. Then one observes $\sqrt{s_0^*/s_0} = f_\pi^*/f_\pi = 0.88 \pm 0.02$. One finds, within uncertainties,

$$\frac{\bar{m}^*}{\bar{m}_\rho(vac)} \simeq \frac{f_\pi^*}{f_\pi} \sim 1 - (0.15 \pm 0.02) \frac{\rho_N}{\rho_0}, \quad (4.47)$$

suggesting that the BR scaling tendency is indeed visible for the KKW in-medium spectral function, contrary to first impression when looking just at the very broad overall spectral distribution [57]. In this context we refer to the subsequent section for an update on the relationship between the in-medium pion decay constant and the density dependence of the chiral condensate.

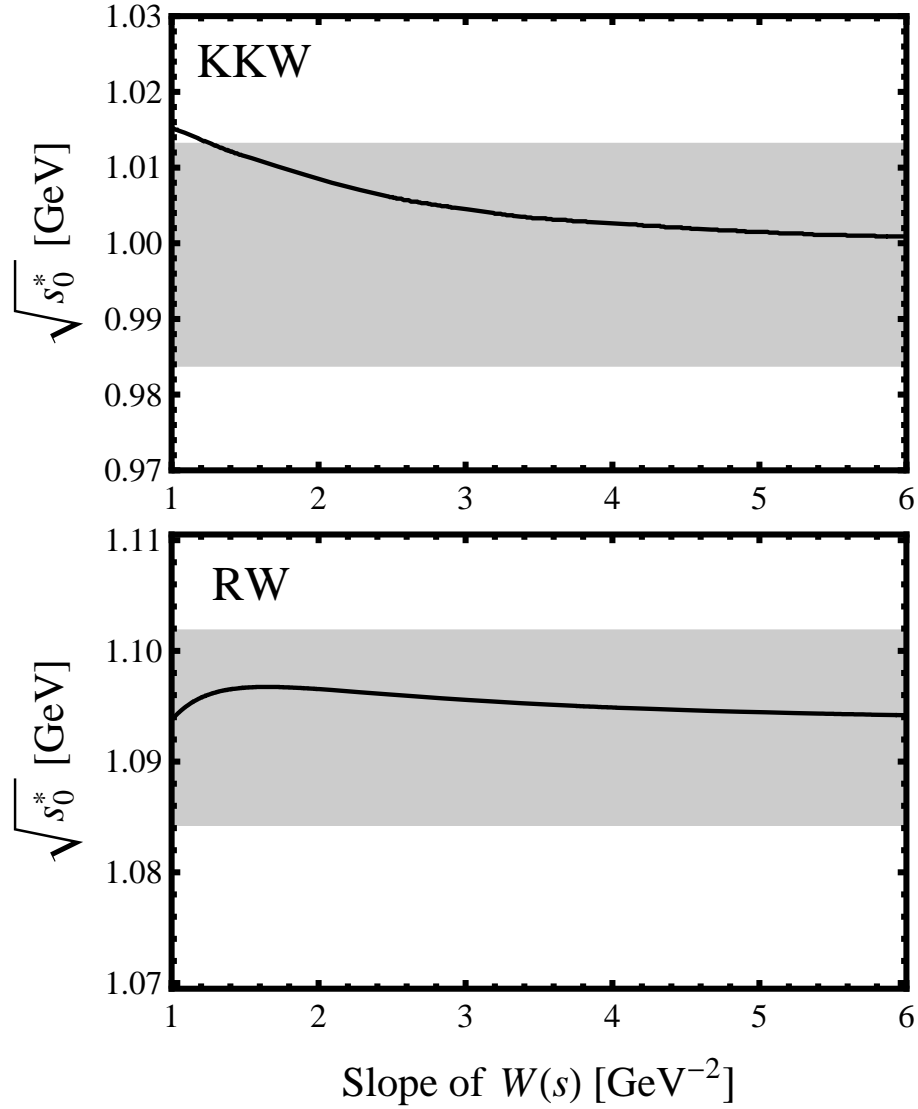


Figure 4.8: Dependence of $\sqrt{s_0^*}$, as in Fig. 4.4, on the slope $(s_2 - s_1)^{-1}$ of the ramp function $W(s)$, now describing the onset of the continuum in the in-medium sum rules. Upper panel: result for the KKW spectral function. Lower panel: for the RW spectral function. The grey bands indicate the uncertainty ranges of the results obtained with step function parameterizations of the continuum.

The KKW spectrum is based entirely on chiral pion dynamics with vector mesons. Baryon resonances are assumed to develop large widths and “dissolve” in nuclear matter so that they become part of the continuous background. In contrast, the RW spectral function starts from a different scenario in which baryon resonances play a distinguished role, assuming that they maintain their quasiparticle properties in matter. It is thus instructive to conduct, as before, a corresponding sum rule analysis for the moments of the RW spectrum under such aspects.

The result is displayed in Fig. 4.7. One deduces

$$\sqrt{s_0^*} = (1.09 \pm 0.01) \text{ GeV} \quad (\text{RW at } \rho_N = \rho_0) \quad (4.48)$$

and $\sqrt{s_0^*/s_0} = 0.97 \pm 0.01$, together with $\frac{\bar{m}^*}{\bar{m}_{\rho(vac)}} \simeq 0.96 \pm 0.02$ at $\rho_N = \rho_0$. [For comparison, the sum rule for the zeroth moment gives $\sqrt{s_0^*} = (1.11 \pm 0.02) \text{ GeV}$, consistent with Eq. (4.48)]. So the RW spectral function exhibits dominantly broadening with almost no in-medium shift of the ratio of the moments. Notably, both RW and KKW based spectral functions work quite well in comparison with dilepton data taken at SPS energies (assuming models for the expansion dynamics of the hot and dense matter which have their own uncertainties). This implies that it is presumably not possible to distinguish between the BR scaling scenario and other (opposing) views from those data.

The “ramping” test in order to establish stability with respect to the modeling of the continuum is performed as for the vacuum case described in the previous section, with the same ramping function $W(s)$ employed also for the in-medium case. The results of this test for the KKW and RW spectral functions are shown in Fig. 4.8. One finds again that the determination of $\sqrt{s_0^*}$, using a variety of smooth transitions to the continuum, is insensitive to details of the threshold modeling within the narrow band of uncertainties.

4.4.2 ω -meson sum rules

Applying the FESR to the ω -meson spectral function is straightforward. In this subsection we exhibit the results for the in-medium ω spectrum. The difference between ρ - and ω -sum rules, which comes from their isospin, is reflected solely in the overall factor d_V of Eq. (4.6).

$$\int_0^{s_0^*} ds R_\omega(s) = s_0^* \left(c_0 + \frac{1}{6} \varepsilon_0 \right) + c_1 - \frac{3\pi^2 \rho_N}{M_N}, \quad (4.49)$$

$$\int_0^{s_0^*} ds s R_\omega(s) = \frac{s_0^{*2}}{2} \left(c_0 + \frac{1}{6} \varepsilon_1 \right) - (c_2 + \delta c_2(\rho_N)), \quad (4.50)$$

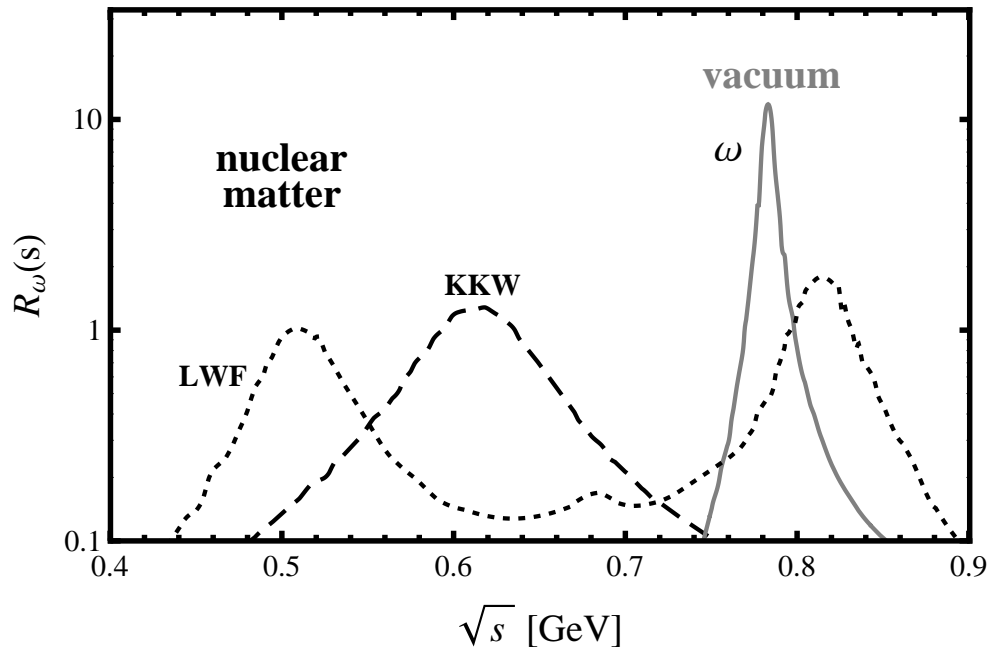


Figure 4.9: In-medium isoscalar vector spectral functions at nuclear matter density, $\rho_0 = 0.17 \text{ fm}^{-3}$, taken from Refs. [57] (KKW) and [17] (LWF). The ω meson spectrum in vacuum is also shown for comparison.

The isoscalar vector spectral function has been computed using several different approaches it at finite density. The first one starts from the same frameworks as in the ρ -meson case (again, referred to as KKW) [57] namely the effective Lagrangian combining chiral SU(3) dynamics with vector meson dominance. For the KKW spectrum the ω self-energy was evaluated at tree-level which needs as input the inelastic reactions $\omega N \rightarrow \pi N$ and $\omega N \rightarrow 2\pi N$ to determine the effective couplings. Furthermore KKW employed a heavy baryon approximation, i.e. an expansion in inverse power of the nucleon mass. The other approach is based on the coupled channel method [17] (referred to as LWF) solving the Bethe-Salpeter equation with local interaction kernels to calculate the ω self-energy. LWF showed that one additional peak in both the imaginary part of the self energy and the spectral function can be identified at $\sim 0.55 \text{ GeV}$. This branch of the ω spectral function is due to the excitation of the $S_{11}(1535)$ resonance. The KKW and LWF spectral functions at normal nuclear matter density, $\rho_N = \rho_0 = 0.17 \text{ fm}^{-3}$, are displayed in Fig. 4.9. As in the ρ -meson case the broadly distributed spectral functions prevent a determination of the in-medium mass and also its shift.

Fig. 4.10 displays the result of the in-medium QCD sum rule analysis for the

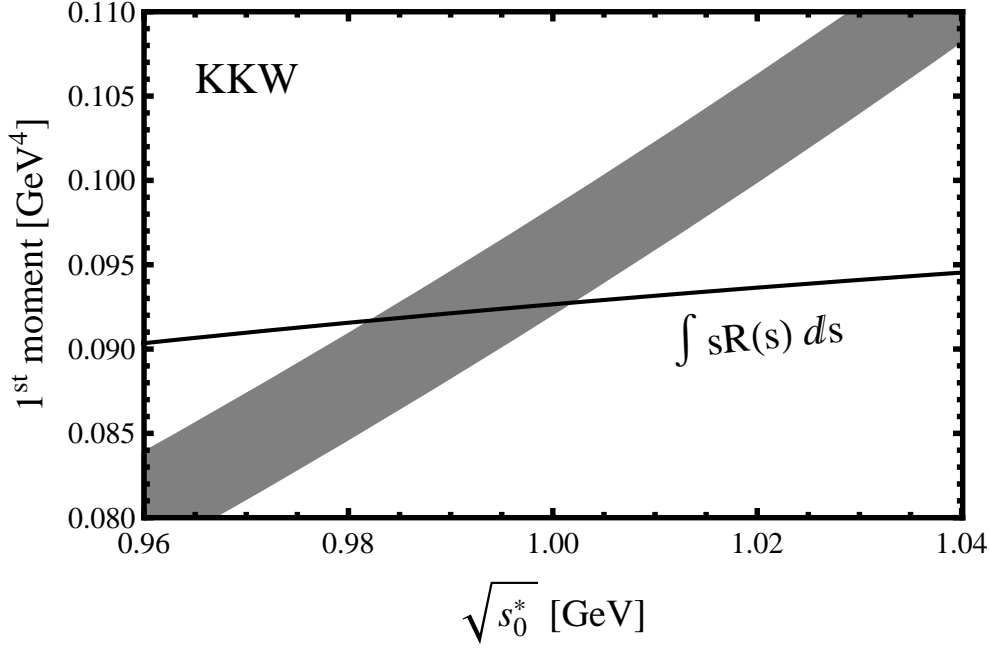


Figure 4.10: QCD sum rule analysis of the KKW in-medium ω spectral function [57] at $\rho_N = \rho_0 = 0.17 \text{ fm}^{-3}$. First moment [solid line, left-hand side of Eq. (4.50)] is plotted versus right-hand side [grey band including uncertainties] as function of the in-medium gap scale $\sqrt{s_0^*}$.

KKW ω spectrum. In consistency with the KKW ρ -meson case, the gap scale $\sqrt{s_0^*}$ is found to be reduced at nuclear matter density,

$$\sqrt{s_0^*} = (0.99 \pm 0.02) \text{ GeV} \quad (\text{KKW at } \rho_N = \rho_0) . \quad (4.51)$$

Using Eq. (4.43), the average in-medium ω -meson mass becomes

$$\bar{m}_\omega^*(\rho_N) = 0.64 \pm 0.02 \text{ GeV} \quad (4.52)$$

for the KKW ω -spectral function at density $\rho_N = \rho_0$, which reproduces the BR scaling,

$$\frac{\bar{m}_\omega^*}{\bar{m}_{\omega_{vac}}} = 0.86 \pm 0.02 \simeq \frac{f_\pi^*}{f_\pi} . \quad (4.53)$$

The LWF method yields a second peak at masses around 0.55 GeV due to a coupling to $N^*(1535)$ -nucleon hole configuration. Fig. 4.11 shows the result of $\sqrt{s_0^*}$ determined from the FESR for the LWF ω -spectrum,

$$\sqrt{s_0^*} = (1.09 \pm 0.02) \text{ GeV} \quad (\text{LWF at } \rho_N = \rho_0) . \quad (4.54)$$

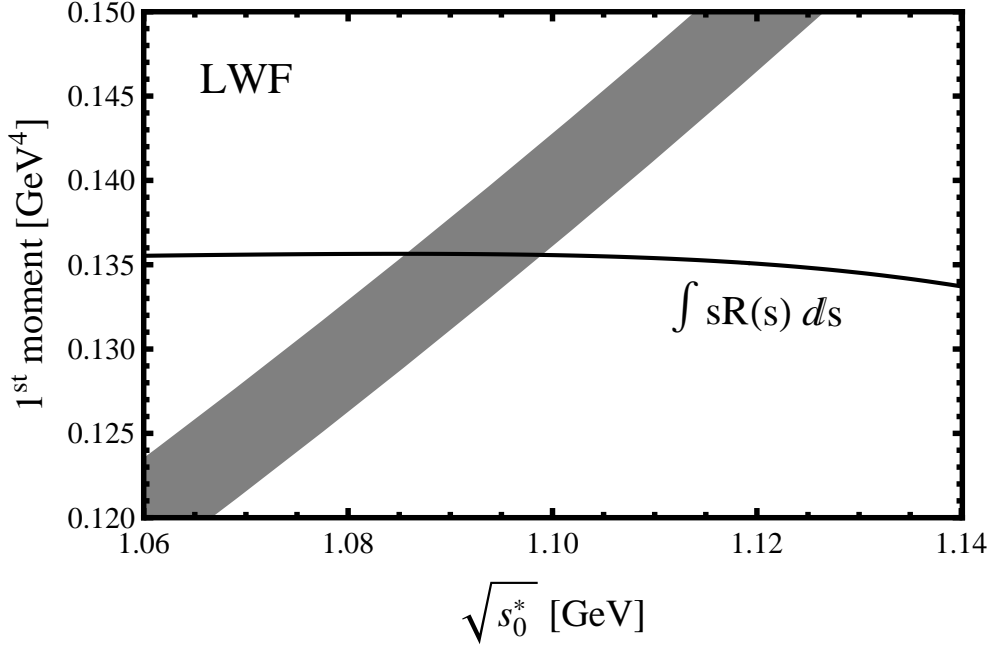


Figure 4.11: QCD sum rule analysis of the LWF in-medium ω spectral function [17] at $\rho_N = \rho_0 = 0.17 \text{ fm}^{-3}$. First moment [solid line, left-hand side of Eq. (4.50)] is plotted versus right-hand side [grey band including uncertainties] as function of the in-medium gap scale $\sqrt{s_0^*}$.

In this case there is almost no average in-medium mass shift at $\rho_N = \rho_0$,

$$\frac{\bar{m}_\omega^*}{\bar{m}_{\omega_{vac}}} \simeq 0.95 \pm 0.02 . \quad (4.55)$$

The LWF spectral function shows the in-medium behavior of the ω -meson dominated by the width-broadening. Note that such a double peak spectral function contributed by dynamically generated resonances is beyond the linear density approximation. It would be also interesting if the theoretical approaches included the resonance decay process such as $N^* \rightarrow N\pi^0\gamma$, because in case the ω -meson is identified via its decay mode $\omega \rightarrow \pi^0\gamma$.

4.5 In-medium pion decay constant and chiral condensate

The present QCD sum rule study asserts that the delineation between low-energy resonance and high-energy continuum parts of the spectral function is related to

the chiral scale, $4\pi f_\pi$, which acts as an order parameter for the spontaneously broken chiral symmetry of the QCD vacuum. Its in-medium change with increasing baryon density is of fundamental interest and deserves an added short section with an updated discussion.

In the nuclear medium, the relevant quantity is the pion decay constant $f_t(\rho_N) \equiv f_\pi^*(\rho_N)$ related to the time component of the axial vector current. Its connection with the density dependent chiral (quark) condensate $\langle \bar{\psi}\psi \rangle_{\rho_N}$ is determined by the in-medium analogue of the GOR relation,

$$f_\pi^{*2} m_\pi^{*2} = -m_q \langle \bar{\psi}\psi \rangle_{\rho_N} , \quad (4.56)$$

to leading order in the quark mass. Here $m_\pi^*(\rho_N)$ is the (charge averaged) pion mass in the medium. A low-density theorem gives the leading ρ_N dependence of the quark condensate as

$$\langle \bar{\psi}\psi \rangle_{\rho_N} = \langle \bar{\psi}\psi \rangle_0 \left(1 - \frac{\sigma_N}{f_\pi^2 m_\pi^2} \rho_N \right) , \quad (4.57)$$

where $\sigma_N = 45 \pm 8$ MeV is the sigma term of the nucleon. Assuming that the pion mass is protected by its Goldstone boson nature at low density, we expect to leading order in the baryon density:

$$\frac{f_\pi^*(\rho_N)}{f_\pi} \simeq 1 - \frac{\sigma_N}{2m_\pi^2 f_\pi^2} \rho_N \simeq 1 - \frac{\rho_N}{6\rho_0} \simeq 0.83 \quad (4.58)$$

at $\rho_N = \rho_0 = 0.16 \text{ fm}^{-3}$ and taking $\sigma_N = 45$ MeV for orientation.

A chiral perturbation theory treatment of in-medium pion dynamics [85] suggested instead a difference between m_π^* and the vacuum pion mass m_π , which translates into a stronger density dependence of the pion decay constant, $f_t(\rho_N)/f_\pi = 1 - (0.26 \pm 0.04)\rho_N/\rho_0$. On the other hand, the charge averaged in-medium pion mass to leading order in the baryon density is given by

$$m_\pi^{*2}(\rho_N) = m_\pi^2 - T^{(+)} \rho_N , \quad (4.59)$$

with the isospin-even forward pion-nucleon amplitude $T^{(+)} = 4\pi(1 + m_\pi/M_N) a^{(+)}$ taken at threshold, $\omega = m_\pi$. Empirically [86], the corresponding scattering length $a^{(+)} = (1.6 \pm 1.3) \cdot 10^{-3} m_\pi^{-1}$ is compatible with zero. This feature derives from a subtle cancelation of non-leading terms which cannot be handled accurately in baryon chiral perturbation theory. Taken as an empirical constraint, $T^{(+)}(m_\pi) \simeq 0$ implies $m_\pi^*(\rho_N) \simeq m_\pi$ at low density and hence an approximate scaling of f_π^* with

the square root of the in-medium chiral condensate as in Eq. (4.58). This behavior is actually consistent with the observed energy shifts in deeply bound states of pionic atoms [87] and related theoretical calculations [88, 89] (see also Ref. [90]).

A recent theoretical study [91] gives further support to these considerations, through a more general derivation of $f_t(\rho_N)$ which does not have to rely on a detailed evaluation of the charge averaged in-medium pion mass. The basic result of Ref. [91] is

$$f_\pi^*(\rho_N) \equiv f_t(\rho_N) = f_\pi \sqrt{\frac{Z}{Z^*} \frac{\langle \bar{\psi}\psi \rangle_{\rho_N}}{\langle \bar{\psi}\psi \rangle_0}}, \quad (4.60)$$

where Z and Z^* are the wave function renormalization factors of the pion in vacuum and in-medium, respectively. Their ratio is determined by the pion self-energy $\Pi(\omega, \mathbf{q}, \rho_N)$, as follows:

$$\frac{Z}{Z^*} = 1 - \frac{\partial}{\partial \omega^2} \Pi(\omega, \mathbf{q} = 0, \rho_N) \Big|_{\omega=0}. \quad (4.61)$$

Using the low-density expression $\Pi = -T^{(+)} \rho_N$ and the parametrization $T^{(+)}(\omega) = -\sigma_N/f_\pi^2 + \beta\omega^2 + \dots$ one arrives at

$$\frac{f_\pi^*(\rho_N)}{f_\pi} \simeq 1 - \left(\frac{\sigma_N}{m_\pi^2 f_\pi^2} - \frac{\beta}{2} \right) \rho_N, \quad (4.62)$$

to leading order in the density. With the slope β determined by the constraint $T^{(+)}(\omega = m_\pi) = 0$ and assuming higher order terms in the expansion of $T^{(+)}$ to be small, we arrive back at Eq. (4.58): $f_\pi^*(\rho_0)/f_\pi = 0.83 \pm 0.03$ when the admittedly large uncertainty of the nucleon sigma term is included.

Higher order corrections in the density ρ_N , calculated using in-medium chiral perturbation theory [92], can be expressed in terms of a density dependent effective nucleon sigma term with a reduced value at normal nuclear matter density, $\sigma_N^{\text{eff}}(\rho_0) = (36 \pm 9)\text{MeV}$, leading to a 3-4% increase of the ratio $f_\pi^*(\rho_0)/f_\pi$ over the value, Eq. (4.58).

Notably, the in-medium QCD sum rule analysis assuming $\sqrt{s_0^*} = 4\pi f_\pi^*$ exhibits chiral scaling of this sort for the KKW spectral distribution, whereas this is not observed for the RW spectral function.

4.6 Note on four-quark condensates

Given spectral functions which consistently satisfy the sum rules for the zeroth and first moments, Eqs. (4.18) and (4.19), one can turn to the second moment,

Eq. (4.20), and try to deduce constraints for the four-quark condensate term c_3 , both in vacuum and in-medium. In particular, one can discuss deviations from the frequently used factorization assumption for those condensates. As mentioned, factorization means that the intermediate states produced by the quark operators entering Eq. (4.9) are truncated by the ground state (vacuum) only. Exact factorization means $\kappa = 1$ in Eqs. (4.10) and (4.11).

When performing the consistency analysis including the sum rule, Eq. (4.20), for the second moment, it turns out in all cases that the correction c_3 is required to be much larger than the value for a factorized four-quark condensate (with $\kappa = 1$): factorization proves to be unrealistic under any circumstances. For detailed estimates we take a value $\langle \bar{q}q \rangle \simeq -(0.2 \text{ GeV})^3$ and find the following results:

- i. In vacuum, a lower limit $\kappa \gtrsim 4.5$ is observed which implies strong deviations from factorization.
- ii. For both types of ρ -meson spectral functions (KKW and RW) the minimal κ required in-medium (typically $\kappa \gtrsim 3$) is somewhat smaller than in vacuum.

The range of uncertainty is generally large in all cases, with κ typically extending from its lower limit up to about twice that value.

One concludes that the four-quark condensates, entering the sum rule at the level of the 2nd moment of the spectral function, remain basically undetermined. This appears to be at variance with reported attempts to constrain such dimension-six condensates from Borel sum rules for the nucleon [93]. Our findings confirm that the assumption of ground state saturation for four quark condensates should be handled with caution. In the present work the sum rules are released from such a dispute by restricting procedures to the 0th and 1st moments of the spectral distribution for which quantitative statements can indeed be made.

4.7 Intermediate summary

The present work re-emphasizes the usefulness of QCD sum rules for moments of spectral functions (or equivalently, finite energy sum rules), with focus on the ρ and ω mesons both in vacuum and in the nuclear medium. The sum rules for the two lowest spectral moments involve only the leading (dimension-four) QCD vacuum condensates as (small) corrections. With inclusion of perturbative QCD terms up to order α_s^3 , these sum rules permit an accurate quantitative analysis,

unaffected by the large uncertainties from condensates of higher dimension (such as the four-quark condensates).

An important scale parameter in this analysis is the gap separating low-energy (resonance) and high-energy (continuum) regions of the spectral function. For the vector-isovector current correlation function, identifying this gap with the scale for spontaneous chiral symmetry breaking in vacuum, $4\pi f_\pi$, reproduces time-honored current algebra relations and chiral sum rules characteristic of low-energy QCD. The corresponding in-medium sum rules for the lowest two spectral moments permit to address the “mass shift” versus “collisional broadening” issue from a new, more quantitative perspective, meaningful even for broad spectral distributions such as that of the ρ meson at nuclear matter density. Systematic tests have been performed to confirm that the conclusions drawn from such analysis do not depend on the detailed threshold modeling of the transition between resonance and continuum parts of the spectral distributions, even with strong in-medium broadening.

Two prototype examples of in-medium rho meson spectral functions have been examined from this point of view in the present paper. Both of these show substantial broadening and redistribution of strength into the low-mass region, as compared to the vacuum spectrum. The sum rule analysis of the lowest spectral moments reveals qualitative differences with respect to their Brown-Rho (BR) scaling properties. At the same time, both of these spectral distributions account quite well for the low-mass enhancements observed in dilepton spectra from high-energy nuclear collisions. So one must draw the conclusion that BR scaling can presumably not be tested in such measurements.

Given the consistency constraints derived from the first two sum rules for the spectral moments, one can then proceed to the third sum rule equation in this hierarchy (involving the second spectral moment and QCD condensates of dimension six) and discuss limits for the four-quark condensates. The outcome of this study demonstrates that the frequently used factorization approximation for these condensates is questionable under any circumstances, both in vacuum and in-medium.

Chapter 5

Meson properties at finite temperature

5.1 Introduction

In this chapter we analyze the in-medium spectral properties of the vector and axial-vector correlation functions at finite temperature and zero baryon density. As discussed in chapter 2, the Weinberg sum rules, based on current algebra, established the relation between vector and axial-vector spectral functions. Using the operator product expansion, these sum rules are reproduced in the language of QCD. In order to explore the implications of the chiral symmetry restoration with increasing temperature we make an extension of these sum rules to finite temperature.

At low temperatures, $T < T_c$ (where T_c is the temperature of the hadron–quark-gluon phase transition), the dynamics of QCD is essentially non-perturbative and is characterized by the spontaneous breaking of chiral symmetry. It is well known that the pion in the hadronic phase plays a special role in strong interacting phenomena due to its small mass in comparison with the typical hadronic scale (~ 1 GeV). At finite temperature, T itself appears as a new scale of hadronic system. However, since even the critical temperature turns out to be $T_c \sim 0.2$ GeV, at low temperature the pions dominate the heat bath. Other hadronic states are exponentially suppressed by the Boltzmann factor $\exp(-M/T)$. Non-perturbative thermal contributions to the sum rules are reflected in terms of the modification of condensates in the operator product expansion.

On the other hand, the spectral functions in the phenomenological side of the

QCD sum rules are usually given in parameterized form. Several guidelines are useful for the parametrization of these spectral functions in terms of hadronic resonance and continuum contributions. One well-established information is that the chiral partners become degenerate when the broken chiral symmetry gets restored.

In Ref. [45] it is shown that the thermal pions induce a mixing of vector and axial-vector correlators at low temperature. We therefore take into account this mixing ansatz between ρ and a_1 mesons, which are chiral partners, keeping in mind the change of the chiral scale $\sqrt{s_V} \approx 4\pi f_\pi$ as temperature increases.

5.2 Reminder of QCD sum rules

As in chapter 4, we start from the time-ordered current correlation function, which in turn is now thermal-expectation valued,

$$\Pi^{\mu\nu}(q) = i \int d^4x e^{iq \cdot x} \langle \mathcal{T} j^\mu(x) j^\nu(0) \rangle_T, \quad (5.1)$$

with the vector current $j_V^\mu(x) = \frac{1}{2} (\bar{u}\gamma^\mu u - \bar{d}\gamma^\mu d)$ and the axial-vector current $j_A^\mu = \frac{1}{2} (\bar{u}\gamma^\mu\gamma_5 u - \bar{d}\gamma^\mu\gamma_5 d)$ carrying the quantum numbers of ρ - and a_1 -meson, respectively. The bracket $\langle \mathcal{O} \rangle_T$ indicates the thermal average of an operator \mathcal{O} ,

$$\langle \mathcal{O} \rangle_T = \frac{\text{Tr } \mathcal{O} \exp(-H/T)}{\text{Tr } \exp(-H/T)}, \quad (5.2)$$

where H is the Hamiltonian and the trace can be evaluated by summing over the full set of eigenstates of the Hamiltonian.

In vacuum the tensor correlation function, Eq. (5.1), can be related to one invariant correlator, $\Pi(q^2) = \frac{1}{3} g_{\mu\nu} \Pi^{\mu\nu}$. In the thermal medium longitudinal and transverse parts of the correlator have to be distinguished due to the broken Lorentz invariance. In a preferred reference frame of the medium, i.e. vanishing three momentum $\mathbf{q} = 0$ of the vector and axial-vector modes, however, longitudinal and transverse correlation functions coincide and will again be denoted as single invariant form $\Pi(\omega, \mathbf{q} = 0)$. This scalar correlator is written in the form of a twice-subtracted dispersion relation:

$$\Pi(q^2) = \Pi(0) + b q^2 + \frac{q^4}{\pi} \int ds \frac{\text{Im } \Pi(s)}{s^2(s - q^2 - i\epsilon)}. \quad (5.3)$$

On the other hand, the operator product expansion (OPE) is used in order to obtain the theoretical estimates of the correlator at large space-like momentum

$q^2 = -Q^2 < 0$:

$$12\pi^2\Pi(Q^2) = -c_0Q^2 \ln\left(\frac{Q^2}{\mu^2}\right) + c_1 + \frac{c_2}{Q^2} + \frac{c_3}{Q^4} + \dots, \quad (5.4)$$

with the coefficients in vacuum,

$$\begin{aligned} c_0 &= \frac{3}{2}(1 + \varepsilon_N), \\ c_1 &= -\frac{9}{2}(m_u^2 + m_d^2), \\ c_2 &= \frac{\pi^2}{2} \left\langle \frac{\alpha_s}{\pi} G^2 \right\rangle \pm 6\pi^2 (m_u \langle \bar{u}u \rangle + m_d \langle \bar{d}d \rangle), \end{aligned} \quad (5.5)$$

where ε_N in c_0 indicates the radiative corrections in perturbative QCD. The explicit form of ε_N up to order $\alpha_s^3(s)$ is shown in Appendix C. The difference between vector and axial-vector channel is the sign of the quark condensate part. In the chiral limit, however, since c_1 and the second term of c_2 are omitted, first significant differences appear in c_3 involving the four-quark condensates:

$$\begin{aligned} c_3 &= -6\pi^3\alpha_s \left[\langle (\bar{u}\gamma_\mu\gamma_5\lambda^a u \mp \bar{d}\gamma_\mu\gamma_5\lambda^a d)^2 \rangle \right. \\ &\quad \left. + \frac{2}{9} \langle (\bar{u}\gamma_\mu\lambda^a u + \bar{d}\gamma_\mu\lambda^a d) \sum_{q=u,d,s} \bar{q}\gamma^\mu\lambda^a q \rangle \right]. \end{aligned} \quad (5.6)$$

The four-quark condensates are usually estimated in a factorization approximation, assuming that intermediate states are saturated by the QCD ground state:

$$\langle (\bar{q}\gamma_\mu\gamma_5\lambda^a q)^2 \rangle = -\langle (\bar{q}\gamma_\mu\lambda^a q)^2 \rangle = \frac{16}{9}\kappa \langle \bar{q}q \rangle^2, \quad (5.7)$$

with κ introduced to parameterize deviation from exact factorization ($\kappa = 1$). The factorization approximation is rather uncertain in medium. In section 4.6, we have discussed too large value of κ to make the ground-state saturation reliable even in the vacuum.

To make the QCD sum rule analysis accurate we cut off these unknown four-quark condensates contributions by arranging the sum rules moment by moment and adopting the lowest two moments of the spectral function:

$$\int_0^{s_0} ds R(s) = s_0 c_0 + c_1 - 12\pi^2 \Pi(0), \quad (5.8)$$

$$\int_0^{s_0} ds sR(s) = \frac{s_0^2}{2}c_0 - c_2, \quad (5.9)$$

where the dimensionless spectral function is defined as $R(s) = -\frac{12\pi}{s}\text{Im}\Pi(s)$. Here s_0 denotes again the characteristic scale that separates the low-mass resonance region ($s \leq s_0$) from the high-energy continuum ($s > s_0$). The last term on the right hand side in Eq. (5.8) stands for the pion pole contribution that vanishes for the vector and becomes $\Pi(0) = f_\pi^2$ for the axial-vector channel at $T = 0$.

It is instructive to reproduce the Weinberg sum rules, Eq. (2.46), using Eqs. (5.8) and (5.9). In vacuum and in the chiral limit, direct subtraction of the axial-vector sum rules from the vector one gives

$$\int_0^{s_V} ds R_V(s) - \int_0^{s_A} ds R_A(s) = c_0(s_V - s_A) + 12\pi^2 f_\pi^2, \quad (5.10)$$

$$\int_0^{s_V} ds s R_V(s) - \int_0^{s_A} ds s R_A(s) = \frac{c_0}{2}(s_V^2 - s_A^2). \quad (5.11)$$

Here $s_{V/A}$ indicate the square of the continuum thresholds for vector and axial-vector channel.

5.3 T -dependence of OPE

In the asymptotic region ($Q^2 \rightarrow \infty$) where the OPE is valid, all non-perturbative scales are represented as power corrections to the perturbative calculations. These non-perturbative contributions to the OPE appear to be more clearly separated into condensates. In the low density or temperature limit, medium-dependence of the OPE is estimated by corrections solely to the condensates. As far as these corrections are smaller than the vacuum value of the condensates, it does not spoil the convergence of the OPE.

To evaluate the T -dependent condensates, we follow the method by Hatsuda *et al.* [42]. Accordingly, in Eq. (5.2) the vacuum state and the lowest excitation of the hadron gas, namely pions, were taken into account as eigenstates of the Hamiltonian in order to calculate the thermal expectation values at low temperature.

$$\langle \mathcal{O} \rangle_T = \langle \mathcal{O} \rangle_0 + \sum_{a=1}^3 \int \frac{d^3p}{2E(2\pi)^3} \langle \pi^a(p) | \mathcal{O} | \pi^a(p) \rangle n_B, \quad (5.12)$$

where $n_B = (e^{E/T} - 1)^{-1}$ denotes Bose-Einstein distributions of thermal pions and $E^2 = m_\pi^2 + p^2$. The pionic matrix element in Eq. (5.12) can be evaluated in the soft pion limit:

$$\lim_{\mathbf{p} \rightarrow 0} \langle \pi^a(\mathbf{p}) | \mathcal{O} | \pi^b(\mathbf{p}) \rangle = -\frac{1}{f_\pi^2} \langle 0 | [Q_5^a, [Q_5^b, \mathcal{O}]] | 0 \rangle + \dots, \quad (5.13)$$

where Q_5^a is the axial charge operator defined by

$$Q_5^a = \int d^3x q^\dagger(x) \gamma_5 \frac{\lambda^a}{2} q(x) . \quad (5.14)$$

When applied to the scalar quark operator, $\bar{q}q$, Eq. (5.13) gives

$$\begin{aligned} \lim_{\mathbf{p} \rightarrow 0} \langle \pi^a(\mathbf{p}) | \bar{q}q | \pi^b(\mathbf{p}) \rangle &= -\frac{1}{f_\pi^2} \langle 0 | [Q_5^a, [Q_5^b, \bar{q}q]] | 0 \rangle + \dots \\ &= -\frac{1}{f_\pi^2} \delta^{ab} \langle \bar{q}q \rangle_0 , \end{aligned} \quad (5.15)$$

where the anti-commutation relations of Dirac fields were used:

$$\begin{aligned} \{q^i(x), q^{\dagger j}(y)\} &= \delta^{ij} \delta^3(x-y) , \\ \{q^{\dagger i}(x), q^{\dagger j}(y)\} &= 0 , \\ \{q^i(x), q^j(y)\} &= 0 . \end{aligned} \quad (5.16)$$

Inserting Eq. (5.15) into Eq. (5.12), we obtain the leading order T -dependence of the chiral quark condensate,

$$\begin{aligned} \langle \bar{q}q \rangle_T &= \langle \bar{q}q \rangle_0 \left(1 - \frac{3}{f_\pi^2} \int \frac{d^3p}{2E(2\pi)^3} \frac{1}{e^{E/T} - 1} \right) \\ &= \langle \bar{q}q \rangle_0 \left(1 - \frac{3T^2}{4\pi^2 f_\pi^2} \int_{\frac{m_\pi}{T}}^\infty dy \frac{\sqrt{y^2 - \frac{m_\pi^2}{T^2}}}{e^y - 1} \right) . \end{aligned} \quad (5.17)$$

Eq. (5.17) is consistent with the results from the effective field theories [54, 55, 95].

Application of Eq. (5.12) to the gluon operator,

$$\left\langle \frac{\alpha_s}{\pi} G^2 \right\rangle_T = \left\langle \frac{\alpha_s}{\pi} G^2 \right\rangle_0 + \frac{T^2}{4\pi^2} \int_{\frac{m_\pi}{T}}^\infty dy \frac{\sqrt{y^2 - \frac{m_\pi^2}{T^2}}}{e^y - 1} \sum_a \langle \pi^a | \frac{\alpha_s}{\pi} G^2 | \pi^a \rangle , \quad (5.18)$$

is evaluated with the QCD trace anomaly as well as the soft pion theorem,

$$\theta_\mu^\mu = -\frac{1}{8} \left(11 - \frac{2}{3} N_f \right) \frac{\alpha_s}{\pi} G^2 + \sum_q m_q \bar{q}q , \quad (5.19)$$

which is used to calculate the pionic matrix element of Eq. (5.18) for gluon operator [94],

$$\begin{aligned} -\frac{9}{8} \langle \pi^a | \frac{\alpha_s}{\pi} G^2 | \pi^b \rangle &= \langle \pi^a | \theta_\mu^\mu | \pi^b \rangle - \langle \pi^a | m_q \bar{q}q | \pi^b \rangle \\ &= 2 m_\pi^2 \delta^{ab} - m_\pi^2 \delta^{ab} \\ &= m_\pi^2 \delta^{ab} . \end{aligned} \quad (5.20)$$

Then, for $N_f = 3$, T -dependent gluon condensate reads

$$\left\langle \frac{\alpha_s}{\pi} G^2 \right\rangle_T = \left\langle \frac{\alpha_s}{\pi} G^2 \right\rangle_0 - \frac{2m_\pi^2 T^2}{3\pi^2} \int_{\frac{m_\pi}{T}}^{\infty} dy \frac{\sqrt{y^2 - \frac{m_\pi^2}{T^2}}}{e^y - 1}, \quad (5.21)$$

in which the second term of r.h.s. gives a numerically minor contribution to the sum rules. In the actual calculation the Gell-Mann–Oakes–Renner (GOR) relation is used for evaluating the value of vacuum quark condensate, $m_q \langle \bar{q}q \rangle = -(0.11 \text{ GeV})^4$, while the charmonium sum rules [76] constrain the gluon condensate, $\langle \frac{\alpha_s}{\pi} G^2 \rangle = 0.005 \pm 0.004 \text{ GeV}^4$.

Apart from the in-medium modifications of the scalar condensates, new spin-dependent operators appear in the OPE due to the absence of Lorentz invariance in the heat bath. Such operators are classified by their canonical dimension and the twist ($\tau = \text{dimension} - \text{spin}$). Then the first moment of our sum rules, Eq. (5.11), involves the twist-2 (dimension 4) operator,

$$\langle \mathcal{ST}(\bar{u}\gamma_\mu D_\nu u + \bar{d}\gamma_\mu D_\nu d) \rangle_T, \quad (5.22)$$

where the symbol \mathcal{ST} makes the operator symmetric and traceless with respect to their Lorentz indices. The precise relation between the pion matrix element of the twist-2 quark operators and the quark distribution function in the pion reads

$$\langle \pi | \mathcal{ST} \bar{q}\gamma_\mu D_\nu q(\mu) | \pi \rangle = -i(p_\mu p_\nu - \text{traces}) A_1^\pi(\mu), \quad (5.23)$$

with

$$A_1^\pi(\mu) = 2 \int_0^1 dx x [q(x, \mu) + \bar{q}(x, \mu)]. \quad (5.24)$$

Combining this correction with Eqs. (5.21) and (5.17), all the leading T -dependence of OPE is written by the replacement $c_2 \rightarrow c_2 + \delta c_2(T)$,

$$\delta c_2 = -\frac{3}{2} \left(\frac{2}{9} \mp 3 + A_1^\pi \right) m_\pi^2 T^2 \int_{\frac{m_\pi}{T}}^{\infty} dy \frac{\sqrt{y^2 - \frac{m_\pi^2}{T^2}}}{e^y - 1}. \quad (5.25)$$

The minus sign in front of the second term in the bracket, which is the leading T -dependence of quark condensate, is for vector channel and plus sign for axial-vector channel respectively.

5.4 Phenomenology at low T

M. Dey *et. al.* [45] have presented the mixing scenario of the correlation functions for vector and axial-vector channel which has been well-established at low

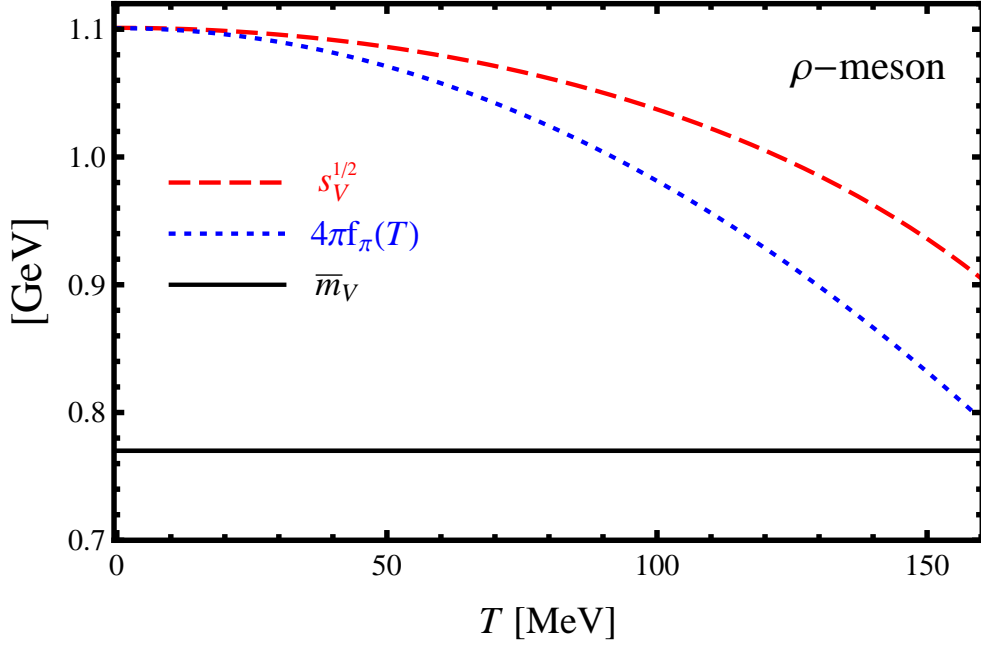


Figure 5.1: Vector continuum threshold $\sqrt{s_V}$ as a function of T as obtained from $0th$ (black solid line) and $1st$ (red dashed line) moment of the sum rules. T -dependence of chiral scale $\Lambda_{CSB} \approx 4\pi f_\pi(T)$ (blue dotted line) is also displayed.

temperature, and the spectral function inherits this mixing phenomenon:

$$R_{V/A}(s, T) = R_{V/A}(s) (1 - \epsilon) + R_{A/V}(s) \epsilon . \quad (5.26)$$

The mixing parameter ϵ is given by the thermal pion loop

$$\epsilon = \frac{2}{f_\pi^2} \int \frac{d^3p}{E(2\pi)^3} \frac{1}{e^{E/T} - 1} . \quad (5.27)$$

In the chiral limit ($m_\pi \rightarrow 0$) it reduces to $\epsilon = T^2/(6f_\pi^2)$. At critical temperature T_c where $\epsilon \simeq 0.5$, the vector and axial-vector spectral functions are fully mixed and become degenerate, $R_V(T) = R_A(T)$. The authors in Ref. [45] have predicted the vector meson mass not to change at low temperature using the mixing ansatz at the order of T^2 . To demonstrate this feature, we perform the finite energy sum rules introduced in the previous sections.

5.4.1 Spectral function with zero width

It is instructive to first test the simplest spectral ansatz for ρ and a_1 mesons assuming zero width:

$$\begin{aligned} R_V(s) &= 12\pi^2 f_V^2 m_V^2 \delta(s - m_V^2) , \\ R_A(s) &= 12\pi^2 f_A^2 m_A^2 \delta(s - m_A^2) . \end{aligned} \quad (5.28)$$

The vector and axial-vector couplings, $f_{V/A}$, are determined by

$$f_V^2 m_V^2 = 2f_\pi^2 , \quad f_A^2 m_A^2 \simeq f_\pi^2 + \frac{s_A - s_V}{8\pi^2} , \quad (5.29)$$

the left one of which is nothing but the KSRF relation and the right one is easily obtained by inserting Eq. (5.28) and KSRF relation into Eq. (5.10), the first Weinberg sum rule, with additional correction due to difference between s_A and s_V . Then applying Eqs. (5.26), (5.28) and (5.29) to Eqs. (5.8) and (5.9), the lowest two moments of the T -dependent vector meson sum rule become:

$$12\pi^2 f_V^2 m_V^2 (1 - \epsilon) = \frac{3}{2} s_V - 12\pi^2 f_\pi^2 \epsilon , \quad (5.30)$$

$$12\pi^2 f_V^2 m_V^4 (1 - \epsilon) = \frac{3}{4} s_V^2 - c_2 . \quad (5.31)$$

The a_1 -meson contribution has been omitted because, in actual calculation, $\sqrt{s_V}$ is always determined in the range $s_V \leq m_A^2$ so that the a_1 -meson pole does not affect the integral of the spectral moments.

With this setup, $\sqrt{s_V} \simeq 1.1$ GeV of the vector channel at $T = 0$ is evaluated from the sum rules by using $f_\pi \simeq 87$ MeV in the chiral limit and $m_V = 770$ MeV. The finite temperature behavior of $\sqrt{s_V}$ from the sum rules is depicted in Fig. 5.1. The two sum rules give consistent result at low temperature. In comparison with the chiral scale $\Lambda_{\text{CSB}} \approx 4\pi f_\pi$ that we have identified with $\sqrt{s_V} = 4\pi f_\pi$ from Eq. (5.30) at $T = 0$, the temperature evolution of $\sqrt{s_V}$ tends to progress downward on a different way from $f_\pi(T) = f_\pi(1 - 0.5\epsilon)$ in chiral perturbation theory [54]. However it might be possible that some additional spectral effects beyond the parity mixing that are excluded here, give rise to better agreement.

Defining an average mass as the normalized first moment of the spectral function,

$$\bar{m}^2 \equiv \frac{\int ds s R}{\int ds R} , \quad (5.32)$$

we confirm that the ρ -meson mass remains unchanged for $T \neq 0$ and stays at the vacuum pole position $\bar{m}_V = 770$ MeV.

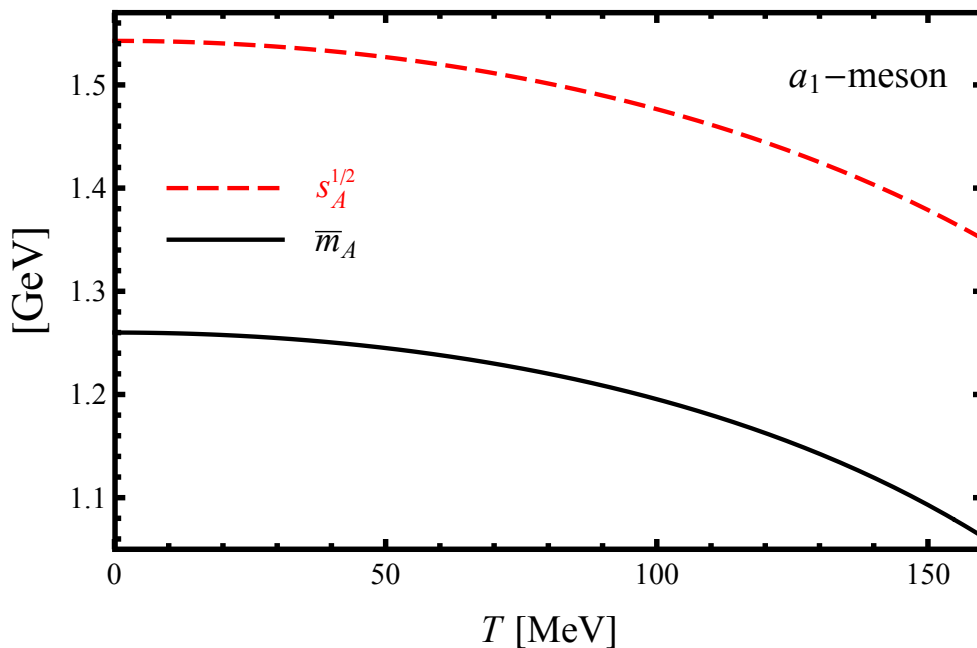


Figure 5.2: Axial-vector continuum threshold $\sqrt{s_A}$ (red dashed line) as a function of T as obtained from the sum rules. In contrast to the ρ meson mass, the a_1 -meson mass (black solid line) decreases with temperature.

In distinction from the ρ -meson case, the left hand side of the sum rules for the axial-vector channel involve both ρ and a_1 meson poles. The first moment of the sum rules with Eq. (5.29) and $m_A = 1.26$ GeV,

$$12\pi^2 [f_A^2 m_A^4 (1 - \epsilon) + f_V^2 m_V^4 \epsilon] = \frac{3}{4} s_A^2 - c_2, \quad (5.33)$$

gives $\sqrt{s_A} \simeq 1.54$ GeV at $T = 0$ and thus $f_A^2 \simeq 0.014$ which agrees with the empirical values of f_A^2 in Ref. [96]. As seen in Fig. 5.2, the average mass \bar{m}_A of the a_1 -meson defined by Eq. (5.32) is reduced with temperature as well as the continuum threshold $\sqrt{s_A}$. The a_1 -meson mass is still $\bar{m}_A \simeq 1.09$ GeV at the temperature $T_0 \simeq 151$ MeV where $\epsilon = 0.5$. The critical temperature at which \bar{m}_V and \bar{m}_A coincide is still considerably higher.

5.4.2 Test on additional pole mass shift

In addition to the parity mixing effect, the resonances themselves may involve temperature dependence which can be reflected in a shift of their pole positions. Just for a test, let us assume spectral functions with dropping pole masses instead

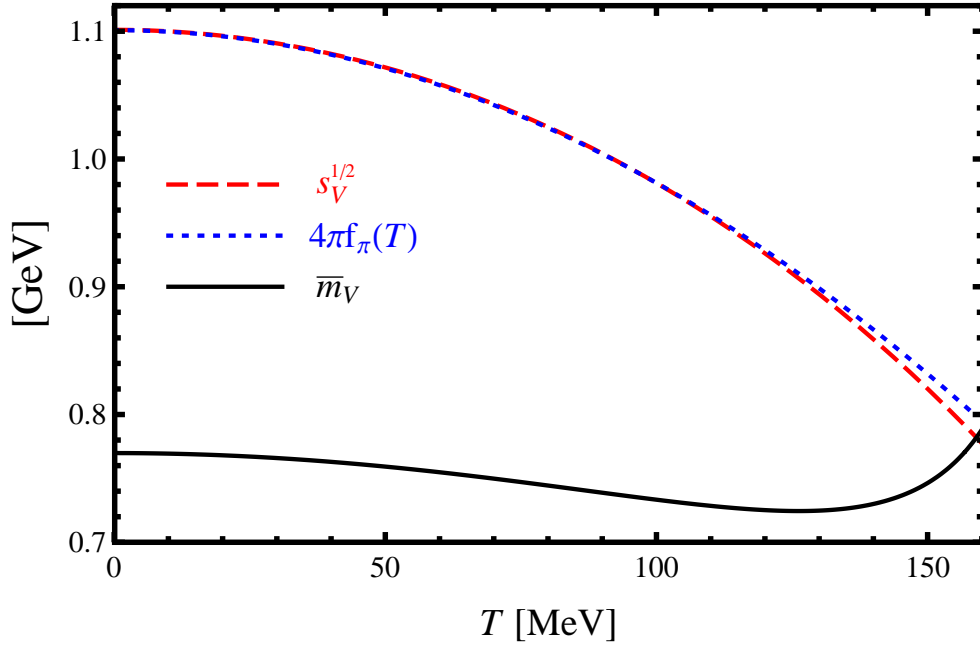


Figure 5.3: Vector continuum threshold $\sqrt{s_V}$ as a function of T using Eq. (5.34).

of Eq. (5.28),

$$\begin{aligned} R_V(s) &= 12\pi^2 f_V^2 m_V^2 \delta(s - m_V^2(1 - 0.5\epsilon)^2) , \\ R_A(s) &= 12\pi^2 f_A^2 m_A^2 \delta(s - m_A^2(1 - 0.5\epsilon)^2) , \end{aligned} \quad (5.34)$$

where we fixed the amplitudes and make pole masses drop with $\epsilon = T^2/(6f_\pi^2)$ according to the Brown-Rho scaling,

$$\frac{f_\pi(T)}{f_\pi} = \frac{m_\rho(T)}{m_\rho} = \dots . \quad (5.35)$$

It is remarkable that now the result gives nice agreement with the assertion $\sqrt{s_V} = 4\pi f_\pi(T)$ as shown in Fig. 5.3 although this prescription of the pole mass shift is ad hoc and the BR scaling for a_1 meson is ambiguous. The modification of the pole mass is related to the contribution of T^4 order. Therefore Fig. 5.3 can provide a hint that taking into account interactions in the thermal pion gas may again establish $\sqrt{s_V}$ as playing the role of chiral scale.

5.4.3 Spectral function with finite width

Now we examine the empirical spectral functions in vacuum displayed in Fig. 5.4, which are more realistic than δ -function resonances, but still use the simplifying

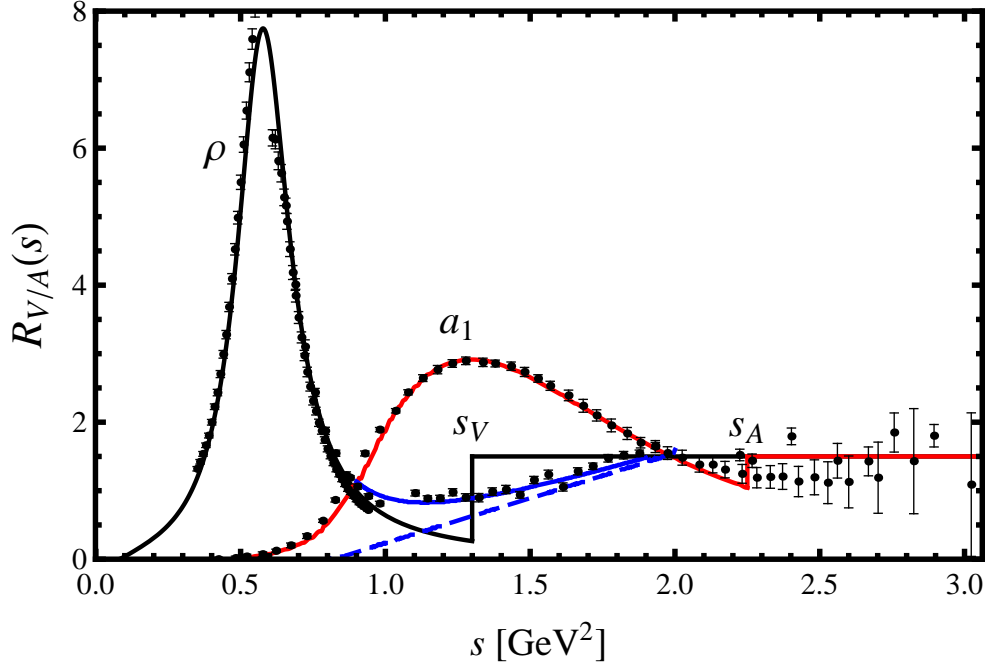


Figure 5.4: Vector (black curve) and axial-vector (red curve) spectral distributions in vacuum, compared to $e^+e^- \rightarrow n\pi$ data with n even [26, 27] and data from hadronic τ decays [28, 29]. Here s_V and s_A stand for the continuum thresholds in the vector and axial-vector channels, respectively. The ramping function (blue dashed line) shows a different example of threshold modeling (see text).

continuum with Heaviside step function. In section 4.3.3, we have shown that the choice of the modeling of the continuum threshold is not decisive for the results in the finite density case. Thus the continuum thresholds can be approximated by step functions although the ramping function, e.g. the blue solid curve in Fig. 5.4, reproduces the experimental data better. For the finite temperature sum rules, the results from the sum rules are also consistently stable regardless of the threshold modeling if the slope of the ramping continuum is larger than a certain minimal value as will be discussed in the subsequent section.

Fig. 5.5 exhibits the temperature-dependent ρ spectrum generated by Eq. (5.26) with $m_\pi = 139.6$ MeV and $f_\pi = 92.4$ MeV. The pole position of the vector meson stays at the mass pole in vacuum. However when it comes to an average mass defined by Eq. (5.32):

$$\bar{m}_V^2 = \frac{\frac{s_V^2}{2}c_0 - c_2}{s_Vc_0 + c_1 - 12\pi^2 f_\pi^2 \epsilon}, \quad (5.36)$$

the broad widths affect the mass distributions.

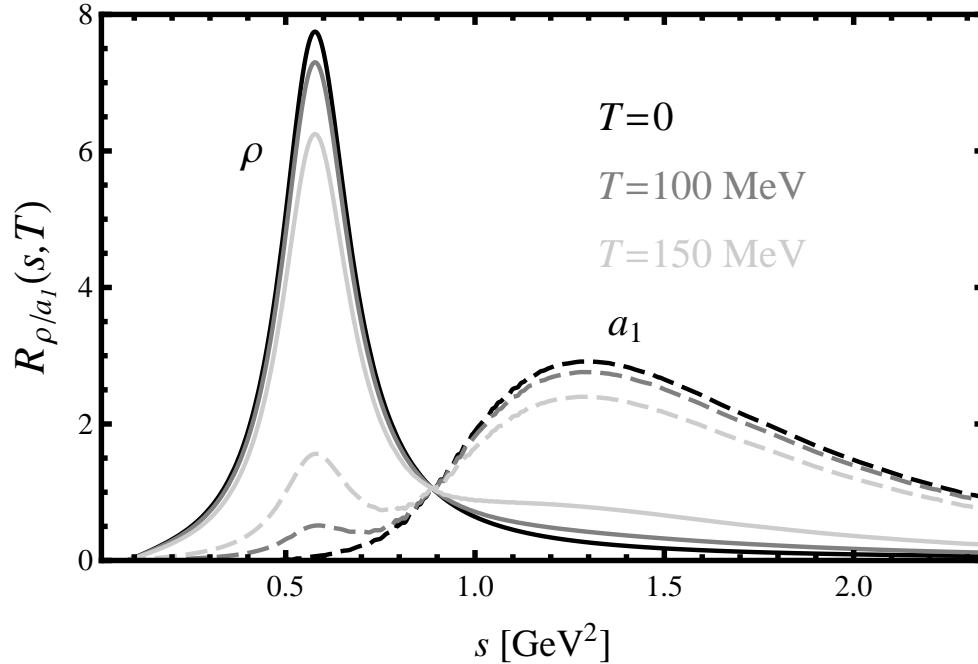


Figure 5.5: ρ - (solid curve) and a_1 -meson (dashed curve) resonance at finite temperatures are obtained by inserting the vacuum spectral functions depicted in Fig. 5.4 into Eq. (5.26).

As apparent from Fig. 5.6, the average vector mass tends to remain almost unchanged with temperature as $\sqrt{s_V}$ moves downward. Note that $\sqrt{s_V}$ from the first moment of the sum rules is taken as an optimal value in the Fig. 5.6 because, by considering 5% inconsistency between l.h.s. and r.h.s. of the sum rules, the results from the first moment are included within the error range of that from the zeroth moment. The errors in Fig. 5.6 practically come entirely from the uncertainties of the gluon vacuum condensate and the running strong coupling $\alpha_s(s)$. By identifying the continuum threshold $\sqrt{s_V}$ of the vector channel with the chiral scale $4\pi f_\pi$, the chiral symmetry restoration can be interpreted in terms of the shift of the scale s_V , and not by pole-mass shift or width broadening. As temperature increases the scale s_V shows evidently a tendency to reduce.

However, for higher temperature than about 160 MeV, there is no solution for the continuum threshold s_V and hence the average mass at that high T cannot be determined by Eq. (5.36). Such relatively high temperature is not the valid region in this consideration because in the OPE as well as in the spectrum the temperature dependence is induced just by the leading contribution of the thermal dilute pion gas. Moreover, the continuum at high temperature may contaminate

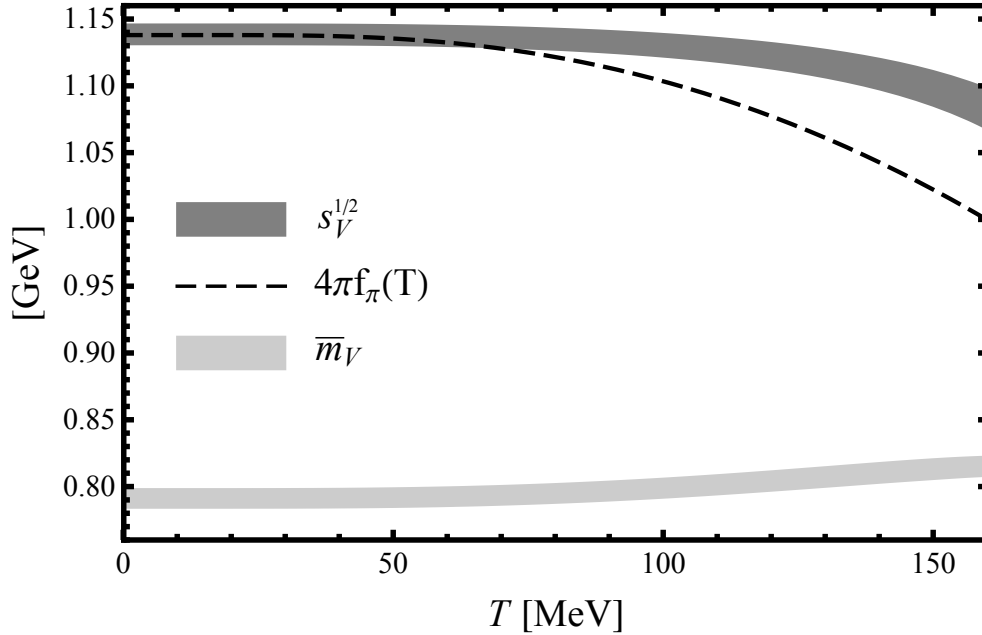


Figure 5.6: The average vector masses and its continuum threshold at various temperature are obtained by Eqs. (5.9) and (5.36). T -dependence of chiral scale $\Lambda_{CSB} \approx 4\pi f_\pi(T)$ (black dashed line) is also displayed.

the resonance part due to the decrease of the continuum threshold with increasing temperature. For the axial-vector channel, this problem already appears at too low temperature, $T \sim 60$ MeV.

The FESR is suitable for providing a way to relate the lowest hadronic spectral function with the onset of the perturbative continuum. In contrast to the Borel sum rule, where the contributions of excited resonances are suppressed with an exponential weight, the FESR needs to take into account the continuum contributions carefully. Thus, FESR is more sensitive to the spectral information in the vicinity of the continuum threshold. The a_1 -spectrum at $T = 0$ which we use here has a broad width. At $T \neq 0$ the resonance comes close to the continuum threshold which decreases with increasing temperature. Therefore the FESR no longer makes sense once the continuum at low temperature already melt away the a_1 resonance because there is no scale separation any more.

With physical pion mass ($m_\pi = 139.6$ MeV), direct subtraction of the FESR

for axial-vector from that of vector gives

$$\int_0^{s_V} ds R_V(s, T) - \int_0^{s_A} ds R_A(s, T) = c_0 (s_V - s_A) + 12\pi^2 f_\pi^2 (1 - 2\epsilon) , \quad (5.37)$$

$$\int_0^{s_V} ds s R_V(s, T) - \int_0^{s_A} ds s R_A(s, T) = \frac{c_0}{2} (s_V^2 - s_A^2) + 12\pi^2 (m_u \langle \bar{u}u \rangle_T + m_d \langle \bar{d}d \rangle_T) . \quad (5.38)$$

Keeping the mixing ansatz for spectral functions, Eq. (5.26), $\sqrt{s_V} \sim 1.12$ GeV and $\sqrt{s_A} \sim 1.48$ GeV at $T = 0$ are obtained from the above two equations. One notices that, as in the Weinberg sum rules, assuming $s_V = s_A \equiv s_0$ makes Eq. (5.37) trivial for non-vanishing temperatures.

$$\int_0^{s_0} ds (R_V(s, 0) - R_A(s, 0)) = 12\pi^2 f_\pi^2 , \quad (5.39)$$

$$\int_0^{s_0} ds s (R_V(s, T) - R_A(s, T)) = 12\pi^2 (m_u \langle \bar{u}u \rangle_T + m_d \langle \bar{d}d \rangle_T) . \quad (5.40)$$

The temperature dependence in Eq. (5.37), $1 - 2\epsilon$, was factored out in both sides of Eq. (5.39). While the term proportional to the chiral condensates in Eq. (5.38) implies the contribution of the in-medium shift of non-zero pion mass, the longitudinal contribution from the pion pole in Eq. (5.39) is still oversimplified. The temperature dependence of this longitudinal contribution must be of more complex form that would make the zeroth moment of our sum rules more accurate.

5.4.4 Sensitivity to continuum threshold modeling

Now we test how reliable the continuum threshold parameterized by the schematic step function is. A test can be performed replacing the step function by a ramping function to yield a smooth transition between resonance and continuum region, as follows:

$$R(s) = R_\rho(s) \Theta(s_2 - s) + R_c(s) W(s) , \quad (5.41)$$

where the weight function, $W(s)$, is defined as

$$W(x) = \begin{cases} 0 & \text{for } x \leq s_1 \\ \frac{x - s_1}{s_2 - s_1} & \text{for } s_1 \leq x \leq s_2 \\ 1 & \text{for } x \geq s_2 . \end{cases} \quad (5.42)$$

The step function behavior is recovered for $W(x)$ in the limit $s_1 \rightarrow s_2$.

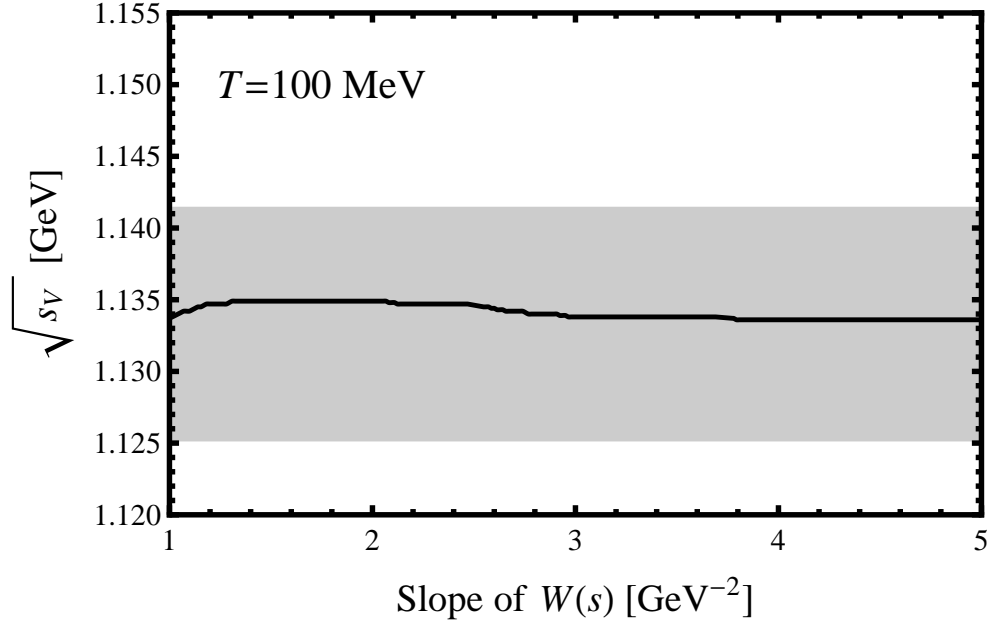


Figure 5.7: Dependence of $\sqrt{s_V}$ (determined from Eqs. (5.43), (5.44) and (5.45)) on the slope $(s_2 - s_1)^{-1}$ of the ramp function $W(s)$ describing the onset of the continuum at $T = 100$ MeV. The grey band indicates the uncertainty range of the result obtained with step function parametrization of the continuum.

Using the function $W(s)$, the modified sum rules for the lowest two moments of the spectrum $R(s)$ become

$$\int_0^{s_2} ds R_\rho(s) = s_2 \left(c_0 + \frac{3}{2} \varepsilon_0 \right) + c_1 - 12\pi^2 \Pi(0) - (c_0 - R_\rho(s_2)) \int_{s_1}^{s_2} ds W(s), \quad (5.43)$$

$$\int_0^{s_2} ds s R_\rho(s) = \frac{s_2^2}{2} \left(c_0 + \frac{3}{2} \varepsilon_1 \right) - c_2 - (c_0 - R_\rho(s_2)) \int_{s_1}^{s_2} ds s W(s). \quad (5.44)$$

Sets of intervals $[s_1, s_2]$ are then determined so as to satisfy both sum rules, Eqs. (5.43) and (5.44), and the scale s_V defined by

$$s_V = \frac{s_1 + s_2}{2}, \quad (5.45)$$

is now introduced to characterize the continuum threshold.

In any temperature region where the sum rules are valid the present analysis does not depend on details of the threshold modeling. Fig. 5.7 shows an example

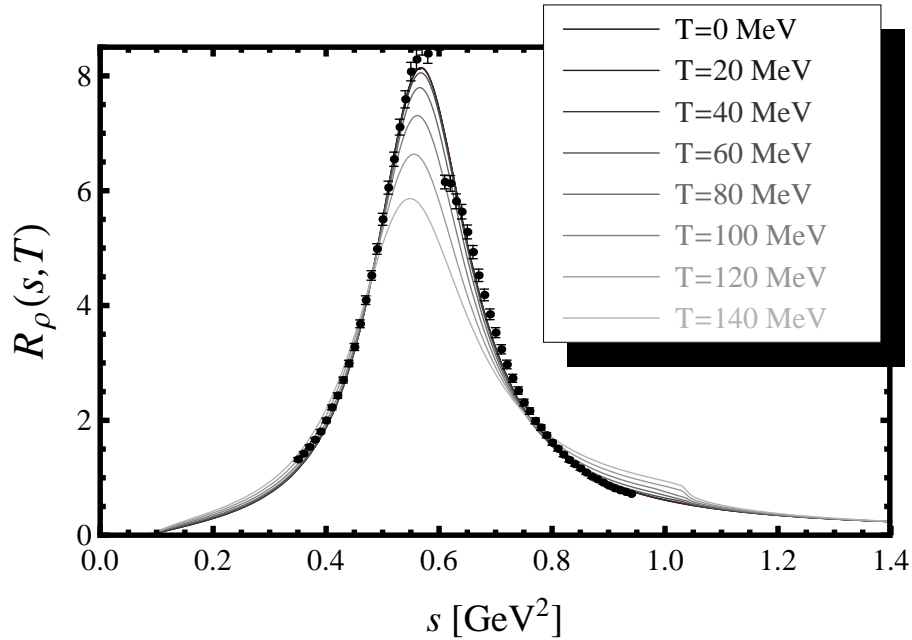


Figure 5.8: ρ -meson resonance at finite temperature from hidden local symmetry model.

demonstrating that the resulting $\sqrt{s_V}$ at finite temperature is stable with respect to variations in the slope $(s_2 - s_1)^{-1}$ of the ramp function $W(s)$. In this test the uncertainties of $\alpha_s(Q^2)$ and of the gluon condensate have been excluded for simplicity.

5.5 Spectral function from effective field theory

The spectral functions provided from phenomenological chiral models must be consistent with the finite energy sum rules. In this section we will investigate this important constraint using the chiral Lagrangian based on generalized hidden local symmetry (GHLS) [97, 98, 99, 100] which explicitly includes the axial-vector meson in addition to the pion and vector meson. Details of the formalism at one loop are found in Refs. [101, 102].

The vector (V_μ) and axial-vector (A_μ) mesons are identified with the GHLS gauge bosons L_μ and R_μ as $V_\mu = (R_\mu + L_\mu)/2$ and $A_\mu = (R_\mu - L_\mu)/2$. The definition of $N_f \times N_f$ special-unitary matrix U is given as

$$U = \xi_L^\dagger \xi_M \xi_R. \quad (5.46)$$

Under chiral symmetry, U transforms as

$$U \rightarrow g_L U g_R^\dagger, \quad (5.47)$$

where $g_{L,R} \in [\text{SU}(N_f)_{L,R}]_{\text{global}}$. Under the chiral transformation, ξ transforms as

$$\begin{aligned} \xi_{L,R} &\rightarrow h_{L,R} \cdot \xi_{L,R} \cdot g_{L,R}^\dagger, \\ \xi_M &\rightarrow h_L \cdot \xi_M \cdot h_R^\dagger, \end{aligned} \quad (5.48)$$

with $h_{L,R} \in [\text{SU}(N_f)_{L,R}]_{\text{local}}$. The GHLS gauge fields L_μ and R_μ transform as

$$\begin{aligned} L_\mu &\rightarrow i h_L \partial h_L^\dagger + h_L L_\mu h_L^\dagger, \\ R_\mu &\rightarrow i h_R \partial h_R^\dagger + h_R R_\mu h_R^\dagger. \end{aligned} \quad (5.49)$$

It is convenient to define the Mauer-Cartan one-form by

$$\begin{aligned} \hat{\alpha}_{L,R}^\mu &= D^\mu \xi_{L,R} \cdot \xi_{L,R}^\dagger / i, \\ \hat{\alpha}_M^\mu &= D^\mu \xi_M \cdot \xi_M^\dagger / (2i), \end{aligned} \quad (5.50)$$

which transforms as

$$\begin{aligned} \hat{\alpha}_{L,R}^\mu &\rightarrow h_{L,R} \hat{\alpha}_{L,R}^\mu h_{L,R}^\dagger, \\ \hat{\alpha}_M^\mu &\rightarrow h_L \hat{\alpha}_M^\mu h_L^\dagger. \end{aligned} \quad (5.51)$$

Using the above quantities, the GHLS Lagrangian is constructed as

$$\begin{aligned} \mathcal{L} &= a\mathcal{L}_V + b\mathcal{L}_A + c\mathcal{L}_M + d\mathcal{L}_\pi + \mathcal{L}_{\text{kin}}(L_\mu, R_\mu), \\ \mathcal{L}_V &= F^2 \text{Tr} [\hat{\alpha}_{\parallel\mu} \hat{\alpha}_{\parallel}^\mu], \\ \mathcal{L}_A &= F^2 \text{Tr} [\hat{\alpha}_{\perp\mu} \hat{\alpha}_{\perp}^\mu], \\ \mathcal{L}_M &= F^2 \text{Tr} [\hat{\alpha}_{M\mu} c], \\ \mathcal{L}_\pi &= F^2 \text{Tr} [(\hat{\alpha}_{\perp\mu} + \hat{\alpha}_{M\mu})(\hat{\alpha}_{\perp}^\mu + \hat{\alpha}_M^\mu)], \\ \mathcal{L}_{\text{kin}}(L_\mu, R_\mu) &= -\frac{1}{4g^2} \text{Tr} [L_{\mu\nu} L^{\mu\nu} + R_{\mu\nu} R^{\mu\nu}]. \end{aligned} \quad (5.52)$$

where $\hat{\alpha}_{\parallel,\perp}$ are defined as $\hat{\alpha}_{\parallel,\perp}^\mu = (\xi_M \hat{\alpha}_R^\mu \xi_M^\dagger \pm \hat{\alpha}_L^\mu) / 2$. The coefficients a , b , c and d are dimensionless parameters to be determined by the underlying QCD. The last term \mathcal{L}_{kin} corresponds to the kinetic term of the gauge bosons with the gauge coupling constant g and field strength tensors ($L_{\mu\nu}$ and $R_{\mu\nu}$).

The parity mixing in the ρ -meson spectrum is generated from the diagram depicted in Fig. 5.9 in which π and a_1 mesons propagate inside the loop which

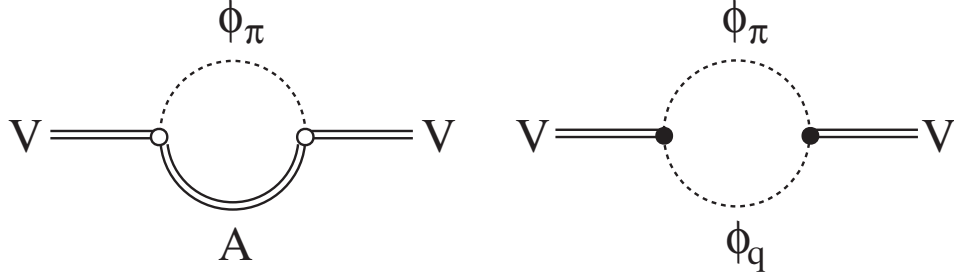


Figure 5.9: Diagrams contributing to the V - A mixing at one loop. Vector and axial-vector fields are denoted by V and A and pion by ϕ_π . Here A represents the transverse components of the a_1 meson, while ϕ_q stands for the longitudinal one [102].

traces in-medium modification of the a_1 meson. Fig. 5.8 shows the vector spectral function at several temperatures.

The spectrum exhibits a resonant peak which mainly represents the $V \rightarrow \pi\pi$ process at low temperatures. With rising temperature, the energy of the time-like virtual ρ meson splits into two branches corresponding to the processes, $\rho + \pi \rightarrow a_1$ and $\rho \rightarrow a_1 + \pi$, with thresholds $\sqrt{s} = m_{a_1} - m_\pi$ and $\sqrt{s} = m_{a_1} + m_\pi$. This results in the threshold effects seen as a shoulder at $\sqrt{s} = m_{a_1} - m_\pi$ and a bump above $\sqrt{s} = m_{a_1} + m_\pi$. The height of the spectrum gets reduced with increasing temperature, whereas the a_1 -meson contribution becomes enhanced via the mixing effect.

The average mass defined in Eq. (5.32) and the continuum threshold for the vector meson at finite temperature are summarized in Table 5.1. \bar{m}_V stays at the

T [MeV]	\bar{m}_V [GeV]	$\sqrt{s_V}$ [GeV]
0	0.787 ± 0.002	1.126 ± 0.007
40	0.787 ± 0.002	1.126 ± 0.007
60	0.787 ± 0.002	1.124 ± 0.007
80	0.787 ± 0.002	1.122 ± 0.007
100	0.787 ± 0.002	1.118 ± 0.008
120	0.786 ± 0.003	1.111 ± 0.008
140	0.786 ± 0.003	1.102 ± 0.008

Table 5.1: The average ρ -meson mass and its continuum threshold at various temperatures.

vacuum value in this temperature range, while $\sqrt{s_V}$ shows a systematic decrease toward higher temperature.

5.6 Note on higher order corrections

5.6.1 T^4 corrections

The vector mass to the order T^4 turned out to decrease as temperature increases due to additional pion interaction term [103]. In this consideration the mixing parameter ϵ is also modified by $\epsilon \rightarrow \epsilon(1 - \epsilon/2)$. This modification shifts the “critical” temperature T_0 defined as the temperature at which vector and axial-vector correlators become identical, i.e., the mixing parameter becomes 1/2.

The interacting pions with non-vanishing momentum contribute to the Lorentz non-invariant part of the correlation function. According to the Ref. [103] this contribution can be expressed in the frame of $\mathbf{q} = 0$:

$$\Pi_V(T) = \Pi_V(0) - \epsilon \left(1 - \frac{\epsilon}{2}\right) (\Pi_V(0) - \Pi_A(0)) + c \frac{T^4}{2Q^2}, \quad (5.53)$$

where $c = 8\pi^2 M_2/15$ and M_2 is the first moment of quark distributions in the pion:

$$M_2 = \frac{1}{2} \int_0^1 dx x [v(x) + 2s(x)] . \quad (5.54)$$

Applying Eq. (5.53) to the FESR, only Eq. (5.9) is affected by the new term:

$$\int_0^{s_0} ds s R(s) = \frac{s_0^2}{2} c_0 - c_2 + 6\pi^2 c T^4 . \quad (5.55)$$

On the OPE side, the T -dependence of the quark condensates is also improved up to order T^4 . The correction is obtained in the chiral perturbation theory as [55]:

$$\langle \bar{q}q \rangle_T = \langle \bar{q}q \rangle_0 \left(1 - \frac{3}{4}\epsilon - \frac{3}{32}\epsilon^2\right) . \quad (5.56)$$

However this correction is numerically small in the actual calculation.

The substitution of Eq. (5.55) with the numerator of Eq. (5.36) compensates for the increase of the vector average mass by the finite width effect. For instance the average mass at $T = 100$ MeV is obtained as $\bar{m}_V \simeq 0.818 \pm 0.009$ GeV which is slightly less than in Fig. 5.6.

5.6.2 Massive states

For higher temperature T the contributions from massive excitations such as K , η etc. in Eq. (5.2) become significant. Those contributions to the T -dependence of the quark- and gluon-condensates are obtained as in the Ref. [42]

$$\begin{aligned} \frac{\langle \bar{q}q \rangle_T}{\langle \bar{q}q \rangle_0} &= 1 - \frac{T^2}{8f_\pi^2} \left[B_1 \left(\frac{m_\pi}{T} \right) + \frac{7}{9} B_1 \left(\frac{m_K}{T} \right) \right], \\ \left\langle \frac{\alpha_s}{\pi} G^2 \right\rangle_T &= \left\langle \frac{\alpha_s}{\pi} G^2 \right\rangle_0 - \frac{T^2}{9} \left[m_\pi^2 B_1 \left(\frac{m_\pi}{T} \right) + \frac{5}{3} m_K^2 B_1 \left(\frac{m_K}{T} \right) \right], \end{aligned} \quad (5.57)$$

with

$$B_1(x) = \frac{6}{\pi^2} \int_x^\infty dy \frac{\sqrt{y^2 - x^2}}{e^y - 1}. \quad (5.58)$$

In practice the T -dependence of the gluon condensate is just a few percent of its vacuum value and negligible.

These numerically minor corrections in OPE hardly affect the sum rule equations and hence an appropriate value of $\sqrt{s_A}$ for a_1 -meson is still not determined even at low temperatures as well as for ρ -meson of which case is relatively better.

5.7 Intermediate summary

In this chapter the finite energy sum rules were analyzed to explore the behavior of ρ and a_1 mesons at finite temperature and thus the pattern of chiral symmetry restoration. The sum rules for the lowest two spectral moments involve only the leading QCD condensates as corrections. With inclusion of perturbative QCD terms up to order $\alpha_s^3(\mu)$, these sum rules permit an accurate quantitative analysis, unaffected by the large uncertainties from condensates of higher dimension such as the four-quark condensates.

The lowest order temperature dependent corrections are obtained by considering thermal pion loops. Only the parity mixing effect caused by non-vanishing $\rho\pi a_1$ coupling is considered in the temperature dependence of the ρ -meson spectral function to order T^2 . The ρ -meson pole mass can be further modified by the self energy with two pion intermediate state. However, such a contribution is of order T^4 because of the derivative in the $\rho\pi\pi$ coupling. Using the simplest ansatz (delta-function resonances) of vector and axial-vector vacuum spectrum and their mixing at finite temperature, the FESR reproduces the renowned current algebra and chiral sum rules. When the empirical decay widths are introduced in

the spectral functions, there is no solution for s_A even at low temperature in the axial-vector case. This can be interpreted that “resonance” and “continuum” merge and the a_1 dissolves. In this situation, it is hard to interpret the chiral symmetry restoration in terms of the degeneracy between vector and axial-vector spectral functions. However, the vector continuum threshold s_V in this analysis is an important scale parameter of spectral behavior through its identification with the chiral scale, $\sqrt{s_V} = 4\pi f_\pi$. Although the scale, s_V , at finite temperature agrees with the leading T -dependence of $4\pi f_\pi(T)$ only in the low temperature region, it is expected that, when higher order T -corrections are taken into account, the agreement would improve even at relatively high temperature.

Chapter 6

Conclusion and outlook

In this dissertation we have used the in-medium QCD sum rules in order to explore the spectral properties of vector and axial-vector mesons at finite density or temperature. Predictions rely on phenomenological information about the condensates and about the form of the spectral function. The in-medium spectral functions of vector mesons are model dependent. Shifts of the pole mass in the medium compete with strong collisional broadening effects. The existing experimental dilepton production data do not allow for a discrimination between the mass shift and broadening. We have therefore stressed the importance of determining which of the interpretations of in-medium hadronic properties are compatible with theoretical constraints based on QCD sum rule methodology.

For this purpose, we have used the finite energy sum rule (FESR) to determine the continuum threshold, the scale separating low-energy (resonance) and high-energy (continuum) regions of the spectral function. The continuum threshold for the vector channel is identified with the chiral symmetry breaking scale, $\sqrt{s_V} \simeq 1.14 \text{ GeV} \simeq 4\pi f_\pi$. In vacuum ($\rho_N = 0$ and $T = 0$), the FESR for the vector current and this hypothetical relation reproduce the celebrated current algebras such as the Weinberg sum rules and the KSRF relation.

In the nuclear medium, this scale analysis, instead of the discussion on the mass shift and broadening, was used to analyze the in-medium modification of the spectral function. In order to extend the sum rules to the dense or hot nuclear medium, the theoretical estimate in terms of the operator product expansion (OPE) is modified with the medium-dependent corrections of the condensates and with new operators due to the broken Lorentz invariance (e.g. twist-2 operator, $\bar{q}\gamma_\nu D_\mu q$). We have taken into account the lowest two spectral moments of the FESR which

involve the dimension-four operators (e.g. $\langle \frac{\alpha_s}{\pi} G^2 \rangle$ and $m_q \langle \bar{q}q \rangle$) as non-perturbative corrections. It is an advantage of the FESR that higher order condensates with uncertain values (e.g. four-quark condensates) can be excluded by selecting the lowest two moments of the sum rules.

In chapter 4, two prototype examples of the in-medium ρ -meson spectral functions at normal nuclear matter density ($\rho_N = \rho_0 = 0.17 \text{ fm}^{-3}$) and zero temperature have been examined. The first one (referred to as KKW) from a chiral effective Lagrangian with vector meson dominance emphasizes the role of chiral in-medium $\pi\pi$ interactions. The other one (referred to as RW) focuses on the role of nucleon-hole, $\Delta(1232)$ -hole and $N^*(1520)$ -hole excitations. Both of the in-medium spectral distributions show a strong broadening as compared to the vacuum ρ meson. We obtained from the FESR the in-medium continuum threshold for the KKW ρ spectral function, $\sqrt{s_V^*} = 1.00 \pm 0.02 \text{ GeV}$. Using the hypothetical identification, $\sqrt{s_V^*} = 4\pi f_\pi^*$, the in-medium pion decay constant, f_π^* , is seen to decrease by about 22 % at normal nuclear matter density. The average mass, defined as the square root of the normalized 1st spectral moment, shows the tendency of Brown-Rho (BR) scaling. On the other hand, the continuum threshold for the RW ρ spectral function was obtained as $\sqrt{s_V^*} = 1.09 \pm 0.01 \text{ GeV}$, not displaying BR scaling. So the broadening with almost no average mass shift dominates the RW ρ spectral function.

The results for the ω meson at $\rho_N = \rho_0$ are similar to the ρ meson case. For the KKW ω spectral function, the sum rule analysis has resulted in BR scaling with $\sqrt{s_V^*} = 0.99 \pm 0.02 \text{ GeV}$. The other approach for the in-medium ω spectral function (referred to as LWF) is based on the coupled channel method solving the Bethe-Salpeter equation to calculate the ω self-energy. The LWF ω spectral function at $\rho_N = \rho_0$ has a multi-peak structure due to the excitation of the $S_{11}(1535)$ resonance. For the LWF ω spectral function, we obtained $\sqrt{s_V^*} = 1.09 \pm 0.02 \text{ GeV}$. The LWF spectral function at finite density is broadly redistributed with almost no average mass shift. The sum rule analysis depends on the shape of in-medium spectral functions. All of these tested spectral functions at $\rho_N = \rho_0$ are compatible with dilepton spectra from relativistic heavy ion collisions. So one can presumably not distinguish certain scenarios for the in-medium modification of the spectral functions from those data.

We have also tested the factorization approximation for the four-quark condensates which is often used without a more detailed discussion. The continuum threshold, consistently determined from the first two sum rules for the spectral mo-

ments, should be a solution of the third sum rule equation which involves the second spectral moment and four-quark condensates. Inserting the continuum threshold to the third sum rule equation, we deduced the value for a four-quark condensate and the parameter κ defined as the ratio between the four-quark condensate and factorized four-quark condensate. The uncertainty of κ is large in all cases. A lower limit $\kappa \gtrsim 4.5$ in vacuum has been obtained to satisfy the sum rule equation. For the in-medium ρ -meson spectral functions (KKW and RW), the minimal κ was determined to be $\kappa \gtrsim 3$. These values are far from the exact factorization ($\kappa = 1$). This demonstrates that the factorization assumption is unreliable in vacuum and also in medium.

In chapter 5, the FESR was performed to analyze the behavior of ρ - and a_1 -mesons at finite temperature and zero baryon density. The leading expression of temperature dependence is estimated by the thermal pion loops. We have examined the in-medium spectral functions generated by the ρ - a_1 mixing effect. For the axial-vector spectral function, the sum rule equations have no solution for the continuum threshold even at low temperature. A possible interpretation is that the a_1 meson dissolves into the continuum. For the vector channel the continuum threshold, $\sqrt{s_V}$, from the T -dependent FESR shows a decrease with increasing temperature. Using the identification of $\sqrt{s_V} = 4\pi f_\pi$, the result agrees with the leading T -dependence of $f_\pi(T)$ from chiral perturbation theory in the low temperature region. It is expected that the agreement at relatively high temperature would improve by higher order T -corrections of the spectral function.

In summary, we repeat that QCD sum rules for the first two moments of (axial) vector spectral functions, when combined with the spontaneous chiral symmetry breaking scale of low-energy QCD, permit a quantitatively accurate analysis in vacuum, consistent with well established current algebra relations. The in-medium analogues of these sum rules can be used routinely to clarify and classify the properties of vector meson spectral functions in nuclear matter.

Appendix

A Useful formulae

A.1 γ -matrix and trace techniques

The γ matrices satisfy

$$\{\gamma^\mu, \gamma^\nu\} = \gamma^\mu \gamma^\nu + \gamma^\nu \gamma^\mu = 2g^{\mu\nu} \quad (\text{A.1})$$

with γ^0 hermitian, γ^i anti-hermitian.

$$\begin{aligned} \gamma_5 = \gamma^5 &= i\gamma^0\gamma^1\gamma^2\gamma^3 = -\frac{i}{4!} \epsilon_{\mu\nu\rho\tau} \gamma^\mu \gamma^\nu \gamma^\rho \gamma^\tau \\ &= -i\gamma_0\gamma_1\gamma_2\gamma_3 = i\gamma^3\gamma^2\gamma^1\gamma^0 = \gamma_5^\dagger \end{aligned} \quad (\text{A.2})$$

$$\begin{aligned} \gamma_5^2 &= I \\ \{\gamma_5, \gamma^\mu\} &= 0 \end{aligned} \quad (\text{A.3})$$

Commutators of γ matrices:

$$\begin{aligned} \sigma^{\mu\nu} &= \frac{i}{2} [\gamma^\mu, \gamma^\nu] \\ \gamma^\mu \gamma^\nu &= g^{\mu\nu} - i\sigma^{\mu\nu} \\ [\gamma_5, \sigma^{\mu\nu}] &= 0 \\ \gamma_5 \sigma^{\mu\nu} &= \frac{i}{2} \epsilon^{\mu\nu\rho\tau} \sigma_{\rho\tau} \end{aligned} \quad (\text{A.4})$$

Hermitian conjugates:

$$\begin{aligned} \gamma^0 \gamma^\mu \gamma^0 &= \gamma^{\mu\dagger} \\ \gamma^0 \gamma_5 \gamma^0 &= -\gamma_5^\dagger = -\gamma_5 \\ \gamma^0 (\gamma_5 \gamma^\mu) \gamma^0 &= (\gamma_5 \gamma^\mu)^\dagger \\ \gamma^0 \sigma^{\mu\nu} \gamma^0 &= (\sigma^{\mu\nu})^\dagger \end{aligned} \quad (\text{A.5})$$

For any two spinors ψ_1 and ψ_2 and any 4×4 matrix Γ ,

$$(\bar{\psi}_1 \Gamma \psi_2)^* = \bar{\psi}_2 (\gamma_0 \Gamma^\dagger \gamma_0) \psi_1 \quad (\text{A.6})$$

while the corresponding identity for two anti-commuting spin $\frac{1}{2}$ fields involves an extra minus sign.

Charge conjugation matrix:

$$\begin{aligned} C\Gamma^T C &= \Gamma \quad \text{for } \Gamma = \gamma_\mu, \sigma_{\mu\nu}, \gamma_5 \sigma_{\mu\nu} \\ C\Gamma^T C &= -\Gamma \quad \text{for } \Gamma = \gamma_5, \gamma_5 \gamma_\mu, (\not{x} \sigma^{\mu\nu} + \sigma^{\mu\nu} \not{x}) \end{aligned} \quad (\text{A.7})$$

$$C = C^* = -C^\dagger = -C^T = -C^{-1}, \quad C^2 = -I \quad (\text{A.8})$$

Contraction identities:

$$\begin{aligned} \not{a} \not{b} &= a \cdot b - i \sigma_{\mu\nu} a^\mu b^\nu \\ \gamma^\mu \gamma_\mu &= 4 \\ \gamma^\nu \gamma^\mu \gamma_\nu &= -2\gamma^\mu \\ \gamma^\tau \gamma^\mu \gamma^\nu \gamma_\tau &= 4g^{\mu\nu} \\ \gamma^\tau \gamma^\mu \gamma^\nu \gamma^\rho \gamma_\tau &= -2\gamma^\rho \gamma^\nu \gamma^\mu \\ \gamma^\tau \gamma^\mu \gamma^\nu \gamma^\rho \gamma^\sigma \gamma_\tau &= 2(\gamma^\sigma \gamma^\mu \gamma^\nu \gamma^\rho + \gamma^\rho \gamma^\nu \gamma^\mu \gamma^\sigma) \\ \gamma^\tau \sigma^{\mu\nu} \gamma_\tau &= 0 \\ \gamma^\tau \sigma^{\mu\nu} \gamma^\rho \gamma_\tau &= 2\gamma^\rho \sigma^{\mu\nu} \\ \sigma^{\mu\nu} \sigma_{\mu\nu} &= 12 \\ \sigma^{\tau\rho} \gamma^\mu \gamma^\nu \sigma_{\tau\rho} &= 4\gamma^\nu \gamma^\mu + 8g^{\mu\nu} = 16g^{\mu\nu} - 4\gamma^\mu \gamma^\nu \end{aligned} \quad (\text{A.9})$$

Traces:

$$\begin{aligned} \text{Tr}[I] &= 4 \\ \text{Tr}[\gamma^\mu] &= 0 \\ \text{Tr}[\gamma^5] &= 0 \end{aligned} \quad (\text{A.10})$$

The trace of an odd product of γ^μ matrices vanishes:

$$\begin{aligned}
\text{Tr}[\sigma^{\mu\nu}] &= 0 \\
\text{Tr}[\gamma^5\gamma^\mu] &= 0 \\
\text{Tr}[\gamma^5\gamma^\mu\gamma^\nu] &= 0 \\
\text{Tr}[\gamma^5\gamma^\mu\gamma^\nu\gamma^\rho\gamma^\tau] &= -4i\epsilon^{\mu\nu\rho\tau} = 4i\epsilon_{\mu\nu\rho\tau} \\
\text{Tr}[\gamma^\mu\gamma^\nu] &= 4g^{\mu\nu} \\
\text{Tr}[\gamma^\mu\gamma^\nu\gamma^\rho\gamma^\tau] &= 4(g^{\mu\nu}g^{\rho\tau} - g^{\mu\rho}g^{\nu\tau} + g^{\mu\tau}g^{\nu\rho}) \\
\text{Tr}[\gamma^\alpha\gamma^\beta\gamma^\mu\gamma^\nu\gamma^\rho\gamma^\tau] &= 4(g^{\alpha\beta}g^{\mu\nu}g^{\rho\tau} - g^{\alpha\beta}g^{\mu\rho}g^{\nu\tau} + g^{\alpha\beta}g^{\mu\tau}g^{\nu\rho} \\
&\quad - g^{\alpha\mu}g^{\beta\nu}g^{\rho\tau} + g^{\alpha\mu}g^{\beta\rho}g^{\nu\tau} - g^{\alpha\mu}g^{\beta\tau}g^{\nu\rho} \\
&\quad + g^{\alpha\nu}g^{\beta\mu}g^{\rho\tau} - g^{\alpha\nu}g^{\beta\rho}g^{\mu\tau} + g^{\alpha\nu}g^{\beta\tau}g^{\mu\rho} \\
&\quad - g^{\alpha\rho}g^{\beta\tau}g^{\mu\nu} + g^{\alpha\rho}g^{\beta\nu}g^{\mu\tau} - g^{\alpha\rho}g^{\beta\mu}g^{\nu\tau} \\
&\quad + g^{\alpha\tau}g^{\beta\rho}g^{\mu\nu} - g^{\alpha\tau}g^{\beta\nu}g^{\mu\rho} + g^{\alpha\tau}g^{\beta\mu}g^{\nu\rho})
\end{aligned} \tag{A.11}$$

Anti-symmetric tensor:

$$\begin{aligned}
\epsilon^{\mu\nu\rho\tau}\epsilon_{\mu\nu}{}^{\rho'\tau'} &= -2(g^{\rho\rho'}g^{\tau\tau'} - g^{\rho\tau'}g^{\rho'\tau}) \\
\epsilon^{\mu\nu\rho\tau}\epsilon_{\mu\nu\rho}{}^{\tau'} &= -6g^{\tau\tau'} \\
\epsilon^{\mu\nu\rho\tau}\epsilon_{\mu\nu\rho\tau} &= -24
\end{aligned} \tag{A.12}$$

A.2 Fourier transformation

This Appendix summarizes the explicit formulae of Fourier transformations often used in the QCD sum rule method. The general form of the Fourier transformation reads

$$\begin{aligned} \int d^4x \frac{e^{iq \cdot x}}{(x^2)^n} &= \frac{i(-1)^n 2^{4-2n} \pi^2}{\Gamma(n-1)\Gamma(n)} (q^2)^{n-2} \ln(-q^2) + P_{n-2}(q^2) \quad (n \geq 2), \\ \int d^4x e^{iq \cdot x} \frac{x_\mu x_\nu \cdots}{(x^2)^n} &= \left(\frac{\partial}{i\partial q^\mu} \frac{\partial}{i\partial q^\nu} \cdots \right) \int d^4x \frac{e^{iq \cdot x}}{(x^2)^n}, \end{aligned} \quad (\text{A.13})$$

where $P_m(q^2)$ is a polynomial in q^2 of degree m with divergent coefficients. According to Eq. (A.13), explicit formula is tabulated as follows. Note that polynomial terms and δ -function are neglected because these terms vanish under the Borel transformation.

$$\begin{aligned} \int d^4x \frac{e^{iq \cdot x}}{x^2} &= -\frac{4i\pi^2}{q^2}, \\ \int d^4x \frac{e^{iq \cdot x}}{x^4} &= i\pi^2 \ln(-q^2), \\ \int d^4x \frac{e^{iq \cdot x}}{x^6} &= -\frac{i\pi^2}{8} q^2 \ln(-q^2), \\ \int d^4x e^{iq \cdot x} \frac{x_\mu}{x^2} &= 8\pi^2 \frac{q_\mu}{q^4}, \\ \int d^4x e^{iq \cdot x} \frac{x_\mu}{x^4} &= 2\pi^2 \frac{q_\mu}{q^2}, \\ \int d^4x e^{iq \cdot x} \frac{x_\mu}{x^6} &= -\frac{\pi^2}{4} q_\mu \ln(-q^2), \\ \int d^4x e^{iq \cdot x} \frac{x_\mu x_\nu}{x^2} &= -8i\pi^2 \left(\frac{g_{\mu\nu}}{q^4} - 4 \frac{q_\mu q_\nu}{q^6} \right), \\ \int d^4x e^{iq \cdot x} \frac{x_\mu x_\nu}{x^4} &= -2i\pi^2 \left(\frac{g_{\mu\nu}}{q^2} - 2 \frac{q_\mu q_\nu}{q^4} \right), \\ \int d^4x e^{iq \cdot x} \frac{x_\mu x_\nu}{x^6} &= \frac{i\pi^2}{4} \left(g_{\mu\nu} \ln(-q^2) + 2q_\mu q_\nu \frac{1}{q^2} \right), \\ \int d^4x e^{iq \cdot x} \frac{x_\mu x_\nu}{x^8} &= -\frac{i\pi^2}{48} (g_{\mu\nu} q^2 \ln(-q^2) + 2q_\mu q_\nu \ln(-q^2)). \end{aligned} \quad (\text{A.14})$$

A.3 Borel transformation

In practical applications of the sum rule method there is a technical prescription needed in addition to dispersion relations in order to study the low-energy aspects of QCD. The prescription called Borel transformation consists in applying the following operator $\hat{\mathcal{B}}$ to the function of concern,

$$\hat{\mathcal{B}} \equiv \lim_{Q^2, n \rightarrow \infty} \frac{(Q^2)^{n+1}}{n!} \left(-\frac{d}{dQ^2} \right)^n, \quad M^2 \equiv \frac{Q^2}{n} \quad (= \text{finite}). \quad (\text{A.15})$$

Applying the Borel transformation to the sum rules, the correlator can be simplified as an exponentially weighted function,

$$\begin{aligned} \hat{\mathcal{B}} \left(\frac{1}{s + Q^2} \right) &= \lim_{Q^2, n \rightarrow \infty} \frac{(Q^2)^{n+1}}{n!} n! \left(\frac{1}{s + Q^2} \right)^{n+1} \\ &= \lim_{n \rightarrow \infty} \left(1 + \frac{s}{M^2 n} \right)^{-(n+1)} \\ &= e^{-s/M^2}. \end{aligned} \quad (\text{A.16})$$

On the other hand the OPE is expressed in the form of $1/Q^2$ -expansion. It is practically useful to present the transformation for typical functions in QCD sum rules,

$$\begin{aligned} \exp(-zQ^2) &\longrightarrow M^2 \delta(zM^2 - 1) \\ (Q^2)^n \ln Q^2 &\longrightarrow (-1)^{n+1} n! (M^2)^{n+1} \\ \alpha_s(Q^2) (Q^2)^n \ln(Q^2) &\longrightarrow (-1)^{n+1} n! \alpha_s(M^2) (M^2)^{n+1} + \dots \\ \frac{1}{(Q^2)^n} &\longrightarrow \frac{1}{(n-1)! (M^2)^{n-1}} \\ \frac{\alpha_s(Q^2)}{(Q^2)^n} &\longrightarrow \frac{1}{(n-1)! (M^2)^{n-1}} \frac{4\pi}{b \ln(M^2/\Lambda^2)} \left[1 + \mathcal{O} \left(\frac{1}{\ln(M^2/\Lambda^2)} \right) \right] \\ &\longrightarrow \frac{\alpha_s(M^2)}{(n-1)! (M^2)^n} + \dots \\ \frac{1}{(Q^2 + m^2)^n} &\longrightarrow \frac{1}{\Gamma(n) (M^2)^{n-1}} e^{-m^2/M^2} \end{aligned} \quad (\text{A.17})$$

where the dots denote higher order α_s corrections.

B Expansion of the light quark propagator

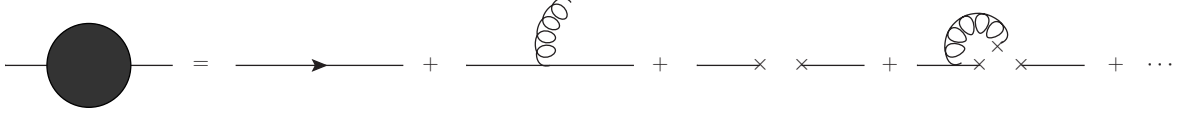


Figure B.1: The light quark propagator.

The quark propagator is diagrammatically represented in Fig. B.1. The first term of r.h.s. in Fig. B.1 indicates that the quark perturbatively propagates in free space, and it appears in momentum space as

$$S^0(p) = \frac{i}{\not{p} - m_q} . \quad (\text{B.1})$$

The perturbative quark propagator can be easily expanded with light quark mass, m_q ,

$$\frac{i}{\not{p} - m_q} \simeq \frac{i}{\not{p}} + i \frac{m_q}{p^2} + i \frac{m_q^2}{p^4} \not{p} . \quad (\text{B.2})$$

Fourier-transforming to space-time coordinates, it becomes

$$\text{Eq. (B.2)} \rightarrow \frac{i}{2\pi} \frac{\not{x}}{x^4} - \frac{m_q}{4\pi^2 x^2} + \frac{i m_q^2}{8\pi^2} \frac{\not{x}}{x^2} . \quad (\text{B.3})$$

The second part of the r.h.s. is the quark propagator that couples with one external gauge field

$$A_\mu^{\text{ext}}(x) = -\frac{1}{2} G_{\mu\nu}^{\text{ext}}(0) x^\nu , \quad (\text{B.4})$$

or in momentum space,

$$A_\mu^{\text{ext}}(k) = \int d^4x e^{ik \cdot x} A_\mu^{\text{ext}}(x) = \frac{i}{2} (2\pi)^4 G_{\mu\nu}^{\text{ext}} \partial^\nu \delta^4(x) . \quad (\text{B.5})$$

Therefore the diagram of the quark propagator with one external gluon field is calculated

$$\begin{aligned} & \int \frac{d^4k}{(2\pi)^4} \frac{i}{\not{p} - m_q} \left(i g_s \gamma^\mu \frac{i}{2} (2\pi)^4 G_{\mu\nu}^{\text{ext}} \partial^\nu \delta^4(k) \right) \frac{i}{\not{p} - \not{k} - m_q} \\ &= -\frac{i}{4} g_s G_{\mu\nu}^{\text{ext}} \frac{1}{(p^2 - m_q^2)^2} [\sigma^{\mu\nu} (\not{p} + m_q) + (\not{p} + m_q) \sigma^{\mu\nu}] \\ &= -\frac{i}{4} G_{\mu\nu}^{\text{ext}} \frac{1}{p^4} (\sigma^{\mu\nu} \not{p} + \not{p} \sigma^{\mu\nu}) - \frac{i}{2} g_s G_{\mu\nu}^{\text{ext}} \frac{1}{p^4} m_q \sigma^{\mu\nu} \\ &\quad - \frac{i}{2} g_s G_{\mu\nu}^{\text{ext}} \frac{m_q^2}{p^6} (\sigma^{\mu\nu} \not{p} + \not{p} \sigma^{\mu\nu}) + \mathcal{O}(m_q^3) . \end{aligned} \quad (\text{B.6})$$

Then the Fourier transformation gives the expression in coordinate space

$$\begin{aligned}
\text{Eq. (B.6)} \rightarrow & -\frac{i}{32\pi^2} \frac{1}{x^2} g_s G_{\mu\nu}^{\text{ext}} (\not{x}\sigma^{\mu\nu} + \sigma^{\mu\nu}\not{x}) \\
& - \frac{1}{32\pi^2} \left[\ln\left(-\frac{x^2\Lambda^2}{4}\right) + 2\gamma_{\text{EM}} \right] m_q g_s G_{\mu\nu}^{\text{ext}} \sigma^{\mu\nu} \\
& + \frac{i}{128\pi^2} \left[\ln\left(-\frac{x^2\Lambda^2}{4}\right) + 2\gamma_{\text{EM}} \right] m_q g_s G_{\mu\nu}^{\text{ext}} (\not{x}\sigma^{\mu\nu} + \sigma^{\mu\nu}\not{x}) .
\end{aligned} \tag{B.7}$$

On the other hand, the other terms of the r.h.s. in Fig. B.1 stand for the non-perturbative contribution to the propagator, obtained via the Taylor expansion of the normal-ordered operator,

$$\begin{aligned}
\langle q_i^a(x) \bar{q}_j^b(0) \rangle = & \langle q_i^a(0) \bar{q}_j^b(0) \rangle + x^\mu \langle D_\mu q_i^a(0) \bar{q}_j^b(0) \rangle \\
& + \frac{1}{2!} x^\mu x^\nu \langle (D_\mu D_\nu + D_\nu D_\mu) q_i^a(0) \bar{q}_j^b(0) \rangle + \dots ,
\end{aligned} \tag{B.8}$$

where a, b and i, j denote color indices and spinor indices respectively. The vacuum expectation values of the r.h.s. in Eq. (B.8) are encoded into the condensates. For example, the second term of Eq. (B.8) corresponds to the quark condensate which is described by the third diagram in Fig. B.1

$$\langle q_i^a(0) \bar{q}_j^b(0) \rangle = -\frac{1}{12} \langle \bar{q}q \rangle \delta^{ab} \delta_{ij} , \tag{B.9}$$

$$\langle D_\mu q_i^a(0) \bar{q}_j^b(0) \rangle = \frac{i}{48} m_q \langle \bar{q}q \rangle \delta^{ab} (\gamma^\mu)_{ij} . \tag{B.10}$$

To verify these, perform appropriate contractions for each equation, multiplying $\delta^{ba} \delta_{ji}$ to Eq. (B.9) and $\delta^{ba} (\gamma^\mu)_{ji}$ to Eq. (B.10). The fourth part of Fig. B.1, which corresponds to the third term of r.h.s. in Eq. (B.8), leads to the quark-gluon mixed condensate,

$$\frac{1}{2!} \langle (D_\mu D_\nu + D_\nu D_\mu) q_i^a(0) \bar{q}_j^b(0) \rangle = - \left(\frac{1}{96} g_s \langle \bar{q}\sigma \cdot Gq \rangle - \frac{m_q^2}{48} \langle \bar{q}q \rangle \right) g_{\mu\nu} \delta^{ab} \delta_{ij} . \tag{B.11}$$

Higher dimension operators are also obtained in the same way. Combining the

results, the expansion of the light quark propagator finally appears as

$$\begin{aligned}
 S_{ab}^{q,ij}(x) &\equiv \langle 0 | \mathcal{T} [q_a^i(x) \bar{q}_b^j(0)] | 0 \rangle \\
 &= \frac{i}{2\pi^2} \frac{\delta_{ab}}{x^4} \not{x}^{ij} - \frac{\delta_{ab} \delta^{ij}}{12} \langle \bar{q}q \rangle - \frac{\delta_{ab} \delta^{ij}}{192} x^2 g \langle \bar{q}\sigma \cdot Gq \rangle \\
 &\quad - \frac{i}{32\pi^2} \frac{1}{x^2} g_s G_{\mu\nu}^A t_{ab}^A (\not{x} \sigma^{\mu\nu} + \sigma^{\mu\nu} \not{x})^{ij} \\
 &\quad - \frac{\pi^2}{3^3 2^7} x^4 \delta_{ab} \delta^{ij} \langle \bar{q}q \rangle \left\langle \frac{\alpha_s}{\pi} G^2 \right\rangle \\
 &\quad - \frac{1}{4\pi^2} \frac{m_q}{x^2} \delta_{ab} \delta^{ij} + \frac{i}{48} \delta_{ab} m_q \langle \bar{q}q \rangle \not{x}^{ij} \\
 &\quad + \frac{i}{3^2 2^7} x^2 \delta_{ab} m_q g \langle \bar{q}\sigma \cdot Gq \rangle \not{x}^{ij} \\
 &\quad - \frac{1}{32\pi^2} \left[\ln \left(-\frac{x^2 \Lambda^2}{4} \right) + 2\gamma_{\text{EM}} \right] m_q g_s G_{\mu\nu}^A t_{ab}^A (\sigma^{\mu\nu})^{ij} \\
 &\quad + \frac{i}{8\pi^2} \frac{\delta_{ab}}{x^2} m_q^2 \not{x}^{ij} + \frac{\delta_{ab} \delta^{ij}}{96} x^2 m_q^2 \langle \bar{q}q \rangle \\
 &\quad + \frac{i}{2^7 \pi^2} \left[\ln \left(-\frac{x^2 \Lambda^2}{4} \right) + 2\gamma_{\text{EM}} \right] m_q^2 g_s G_{\mu\nu}^A t_{ab}^A (\not{x} \sigma^{\mu\nu} + \sigma^{\mu\nu} \not{x})^{ij} \\
 &\quad + \frac{\delta_{ab} \delta^{ij}}{3^2 2^8} x^4 m_q^2 g \langle \bar{q}\sigma \cdot Gq \rangle \\
 &\quad - \frac{i}{3^5 2^5} x^2 \delta_{ab} g_s^2 \langle \bar{q}q \rangle^2 \not{x}^{ij} - \frac{\delta_{ab} \delta^{ij}}{3^5 2^7} x^4 m_q g_s^2 \langle \bar{q}q \rangle^2 .
 \end{aligned} \tag{B.12}$$

In actual calculations, introducing the dual gluon tensor,

$$\tilde{G}^{\mu\nu} \equiv \frac{i}{2} \epsilon^{\mu\nu\alpha\beta} G_{\alpha\beta} , \quad \tilde{G}_{\mu\nu} = -\frac{i}{2} \epsilon_{\mu\nu\alpha\beta} G^{\alpha\beta} , \tag{B.13}$$

$$\tilde{G}_{\mu\nu} \tilde{G}_{\mu'\nu'} = \frac{1}{12} (g_{\mu\mu'} g_{\nu\nu'} - g_{\mu\nu'} g_{\nu\mu'}) \tilde{G}^2 , \tag{B.14}$$

$$\begin{aligned}
 \tilde{G}^2 &= \frac{1}{4} \epsilon_{\mu\nu\alpha\beta} G^{\alpha\beta} \epsilon^{\mu\nu\alpha'\beta'} G_{\alpha'\beta'} \\
 &= -\frac{1}{2} (\delta_{\alpha}^{\alpha'} \delta_{\beta}^{\beta'} - \delta_{\alpha}^{\beta'} \delta_{\beta}^{\alpha'}) G^{\alpha\beta} G_{\alpha'\beta'} \\
 &= -\frac{1}{2} (G^{\alpha\beta} G_{\alpha\beta} - G^{\alpha\beta} G_{\beta\alpha}) = -G^2 ,
 \end{aligned} \tag{B.15}$$

one can write the gluon term as follows,

$$-\frac{i}{32\pi^2} \frac{1}{x^2} g_s G_{\mu\nu}^A t_{ab}^A (\not{x} \sigma^{\mu\nu} + \sigma^{\mu\nu} \not{x}) = -\frac{i}{8\pi^2} \frac{1}{x^2} g_s \tilde{G}_{\mu\nu}^A t_{ab}^A \gamma^\nu \gamma_5 x^\mu . \tag{B.16}$$

C QCD corrections

Following Ref. [70], the expression for the n -th moment (with $n = 0, 1, 2$) of the spectral distribution in the isovector (ρ meson) channel is written

$$\int_0^{s_0} ds s^n R_\rho(s) = \frac{s_0^{n+1}}{n+1} \left(c_0 + \frac{3}{2} \varepsilon_n \right) + (-1)^n c_{n+1} - 12\pi^2 \Pi(0) \delta_{n0} . \quad (\text{C.1})$$

The leading perturbative QCD term on the r.h.s. has $c_0 = \frac{3}{2} \left(1 + \frac{\alpha_s}{\pi} \right)$. The corrections to $\mathcal{O}(\alpha_s^3)$ are

$$\varepsilon_n = a_n^{(2)} \left(\frac{\alpha_s}{\pi} \right)^2 + a_n^{(3)} \left(\frac{\alpha_s}{\pi} \right)^3 , \quad (\text{C.2})$$

with

$$\begin{aligned} a_n^{(2)} &= 1.641 + \frac{2.250}{n+1} , \\ a_n^{(3)} &= -10.28 + \frac{11.38}{n+1} + 1.69 \left(\frac{6}{(n+1)^2} - \pi^2 \right) . \end{aligned} \quad (\text{C.3})$$

In applications using Eq. (C.1) the relevant coupling is $\alpha_s(s_0)$ with $s_0 \sim 1 \text{ GeV}^2$. In practice we use $\alpha_s(1 \text{ GeV}^2) = 0.50 \pm 0.03$ [82, 83].

C.1 The running coupling $\alpha_s(\mu)$

To estimate the $\alpha_s(s_0)$ effectively optimized from sum rules for the moment with the theoretical (QCD) prediction, we consider the following form of $\alpha_s(\mu)$ up to NNLO.

$$\begin{aligned} \alpha_s(\mu) &= \frac{4\pi}{\beta_0 \ln(\mu^2/\Lambda^2)} \left[1 - \frac{2\beta_1 \ln[\ln(\mu^2/\Lambda^2)]}{\beta_0^2 \ln(\mu^2/\Lambda^2)} \right. \\ &\quad \left. + \frac{4\beta_1^2}{\beta_0^4 \ln^2(\mu^2/\Lambda^2)} \left(\left(\ln[\ln(\mu^2/\Lambda^2)] - \frac{1}{2} \right)^2 + \frac{\beta_2 \beta_0}{8\beta_0^2} - \frac{5}{4} \right) \right] , \end{aligned} \quad (\text{C.4})$$

where β_i 's are coefficients of the renormalization group beta function of which first three are given by

$$\begin{aligned} \beta_0 &= 11 - \frac{2}{3} n_f , \\ \beta_1 &= 51 - \frac{19}{3} n_f , \\ \beta_2 &= 2857 - \frac{5033}{9} n_f + \frac{325}{27} n_f^2 \quad \text{in } \overline{\text{MS}} \text{ scheme} , \end{aligned} \quad (\text{C.5})$$

with the number of active quark flavors n_f .

In order to calculate $\alpha_s(\mu = 1.16 \text{ GeV})$ we should choose first the dimensional parameter Λ at high energy region which usually use to be determined at $\mu = M_Z$, and then drift the Λ to certain energy scale we are interested in. Using the naive values ($\alpha_s(M_Z = 91.2 \text{ GeV}) \approx 0.12$), we obtain

$$\begin{aligned}\Lambda_L^{(5)} &= 0.099 \text{ GeV} , \\ \Lambda_{NL}^{(5)} &= 0.255 \text{ GeV} , \\ \Lambda_{NNL}^{(5)} &= 0.235 \text{ GeV} ,\end{aligned}\tag{C.6}$$

where the superscript of $\Lambda_i^{(5)}$ indicates n_f .

Ideally speaking, as the scale, μ , goes across quark mass thresholds, we can simply increase the n_f . Accordingly, since $m_s < \sqrt{s_0} = 1.16 \text{ GeV} < m_c$, we are interested in the $\Lambda_i^{(n_f)}$ ($i = L, NL$ and NNL) at $n_f = 3$.

Matching at b -quark mass threshold for continuity, $\alpha_{s,i}^{(4)}(m_b \sim 4.7 \text{ GeV}) = \alpha_{s,i}^{(5)}(4.7 \text{ GeV})$, we can obtain the $\Lambda_i^{(4)}$ and also $\alpha_{s,i}^{(4)}$ from Eq. (C.4):

$$\alpha_{s,i}^{(4)}(4.7 \text{ GeV}) = \begin{cases} 0.21 & \text{with } \Lambda_i^{(4)} = 0.130 \text{ GeV} \text{ for } i = L , \\ 0.22 & \text{with } \Lambda_i^{(4)} = 0.340 \text{ GeV} \text{ for } i = NL , \\ 0.22 & \text{with } \Lambda_i^{(4)} = 0.306 \text{ GeV} \text{ for } i = NNL . \end{cases}\tag{C.7}$$

If once again we repeat it at c -quark mass threshold, $\alpha_{s,i}^{(3)}(m_c \sim 1.5 \text{ GeV}) = \alpha_{s,i}^{(4)}(1.5 \text{ GeV})$, we obtain

$$\alpha_{s,i}^{(3)}(1.5 \text{ GeV}) = \begin{cases} 0.31 & \text{with } \Lambda_i^{(3)} = 0.158 \text{ GeV} \text{ for } i = L , \\ 0.37 & \text{with } \Lambda_i^{(3)} = 0.393 \text{ GeV} \text{ for } i = NL , \\ 0.36 & \text{with } \Lambda_i^{(3)} = 0.353 \text{ GeV} \text{ for } i = NNL . \end{cases}\tag{C.8}$$

With the parameter $\Lambda_i^{(3)}$,

$$\alpha_{s,i}^{(3)}(\sqrt{s_0} = 1.16 \text{ GeV}) = \begin{cases} 0.35 & \text{for } i = L , \\ 0.46 & \text{for } i = NL , \\ 0.44 & \text{for } i = NNL . \end{cases}\tag{C.9}$$

D First moment of quark distribution

An accurate value of A_1 ,

$$A_1 = 2 \int_0^1 dx x (u + \bar{u} + d + \bar{d}) , \quad (\text{D.1})$$

which determines the dominant part of the in-medium modifications in our sum rule analysis, is obtained from the MRST2001 fits [78]. In this analysis parton distributions of the proton are derived from measurements of structure functions by the H1 and ZEUS collaborations at HERA, and by the D0 and CDF collaborations at the Tevatron, performing DGLAP evolution. The parametrization of the parton distributions at $Q^2 = 1 \text{ GeV}^2$ is:

$$\begin{aligned} x u_v &= 0.158 x^{0.25} (1-x)^{3.33} (1 + 5.61x^{0.5} + 55.49x) , \\ x d_v &= 0.040 x^{0.27} (1-x)^{3.88} (1 + 52.73x^{0.5} + 30.65x) , \\ xS &= 0.222 x^{-0.26} (1-x)^{7.10} (1 + 3.42x^{0.5} + 10.30x) , \\ x\Delta &\equiv x(\bar{d} - \bar{u}) \\ &= 1.195 x^{1.24} (1-x)^{9.10} (1 + 14.05x - 45.52x^2) , \\ 2\bar{u} &= 0.4S - \Delta , \\ 2\bar{d} &= 0.4S + \Delta , \end{aligned} \quad (\text{D.2})$$

where u_v and d_v denote the valence u - and d -quark distributions while $2\bar{u}$ and $2\bar{d}$ are the sea quark distributions. Δ denotes the difference between \bar{d} and \bar{u} .

Using this parametrization, A_1 at a 1 GeV scale is directly calculated as

$$A_1 = 2 \int_0^1 dx x (u_v + d_v + 2\bar{u} + 2\bar{d}) = 1.2373 . \quad (\text{D.3})$$

List of Figures

2.1	Vector and axial-vector spectral functions in vacuum (curves) as parameterized in Ref. [25], compared to $e^+e^- \rightarrow n\pi$ data with n even [26, 27] and data from hadronic τ decays [28, 29].	8
2.2	The spectrum of low-mass hadronic excitations built on the condensed QCD ground state. The characteristic gap $\Lambda_{\text{CSB}} \sim 1$ GeV is indicated.	10
2.3	e^+e^- annihilation to $\pi^+\pi^-$. A virtual photon γ undergoes ρ -conversion with $g_{\rho\gamma}$ and ρ -meson dominates the process.	11
2.4	Schematic pictures in Ref. [44] to interpret possible patterns of chiral symmetry restoration in terms of vector and axial-vector spectral functions.	16
3.1	Contour integral in the complex q^2 -plane.	24
4.1	e^+e^- annihilation to $\pi^+\pi^-$. The pion-vertex has the form-factor that arises mainly through vector dominance.	39
4.2	Vector-isovector spectral function in vacuum showing the ρ resonance and continuum parts as described in the text and compared to $e^+e^- \rightarrow \pi^+\pi^-$ (ρ resonance region) and $e^+e^- \rightarrow n\pi$ data with n even [26, 27].	40
4.3	QCD sum rule analysis of the ρ meson spectral function in vacuum. First moment (solid line, left-hand side of Eq. (4.32)) is plotted versus right-hand side (grey band including uncertainties) as function of the gap scale $\sqrt{s_0}$ delineating low-mass resonance region from high-mass continuum.	41

- 4.4 Dependence of $\sqrt{s_0}$ [determined from Eqs. (4.37)-(4.39)] on the slope $(s_2 - s_1)^{-1}$ of the ramp function $W(s)$ describing the onset of the continuum in the vacuum sum rule. The grey band indicates the uncertainty range of the result obtained with step function parametrization of the continuum. 42
- 4.5 In-medium isovector vector spectral functions at nuclear matter density, $\rho_0 = 0.17 \text{ fm}^{-3}$, taken from Refs. [57] (KKW) and [41] (RW). The ρ meson spectrum in vacuum is also shown for comparison. . . 44
- 4.6 QCD sum rule analysis of the KKW in-medium ρ spectral function [57]. First moment [solid line, left-hand side of Eq. (4.41)] is plotted versus right-hand side [grey band including uncertainties] as function of the in-medium gap scale $\sqrt{s_0^*}$ 45
- 4.7 QCD sum rule analysis of the RW in-medium ρ spectral function [41]. First moment [solid line, left-hand side of Eq. (4.41)] is plotted versus right-hand side [grey band including uncertainties] as function of the in-medium gap scale $\sqrt{s_0^*}$ 46
- 4.8 Dependence of $\sqrt{s_0^*}$, as in Fig. 4.4, on the slope $(s_2 - s_1)^{-1}$ of the ramp function $W(s)$, now describing the onset of the continuum in the in-medium sum rules. Upper panel: result for the KKW spectral function. Lower panel: for the RW spectral function. The grey bands indicate the uncertainty ranges of the results obtained with step function parameterizations of the continuum. 47
- 4.9 In-medium isoscalar vector spectral functions at nuclear matter density, $\rho_0 = 0.17 \text{ fm}^{-3}$, taken from Refs. [57] (KKW) and [17] (LWF). The ω meson spectrum in vacuum is also shown for comparison. . . 49
- 4.10 QCD sum rule analysis of the KKW in-medium ω spectral function [57] at $\rho_N = \rho_0 = 0.17 \text{ fm}^{-3}$. First moment [solid line, left-hand side of Eq. (4.50)] is plotted versus right-hand side [grey band including uncertainties] as function of the in-medium gap scale $\sqrt{s_0^*}$. . 50
- 4.11 QCD sum rule analysis of the LWF in-medium ω spectral function [17] at $\rho_N = \rho_0 = 0.17 \text{ fm}^{-3}$. First moment [solid line, left-hand side of Eq. (4.50)] is plotted versus right-hand side [grey band including uncertainties] as function of the in-medium gap scale $\sqrt{s_0^*}$. . 51

5.1	Vector continuum threshold $\sqrt{s_V}$ as a function of T as obtained from <i>0th</i> (black solid line) and <i>1st</i> (red dashed line) moment of the sum rules. T -dependence of chiral scale $\Lambda_{CSB} \approx 4\pi f_\pi(T)$ (blue dotted line) is also displayed.	62
5.2	Axial-vector continuum threshold $\sqrt{s_A}$ (red dashed line) as a function of T as obtained from the sum rules. In contrast to the ρ meson mass, the a_1 -meson mass (black solid line) decreases with temperature.	64
5.3	Vector continuum threshold $\sqrt{s_V}$ as a function of T using Eq. (5.34).	65
5.4	Vector (black curve) and axial-vector (red curve) spectral distributions in vacuum, compared to $e^+e^- \rightarrow n\pi$ data with n even [26, 27] and data from hadronic τ decays [28, 29]. Here s_V and s_A stand for the continuum thresholds in the vector and axial-vector channels, respectively. The ramping function (blue dashed line) shows a different example of threshold modeling (see text).	66
5.5	ρ - (solid curve) and a_1 -meson (dashed curve) resonance at finite temperatures are obtained by inserting the vacuum spectral functions depicted in Fig. 5.4 into Eq. (5.26).	67
5.6	The average vector masses and its continuum threshold at various temperature are obtained by Eqs. (5.9) and (5.36). T -dependence of chiral scale $\Lambda_{CSB} \approx 4\pi f_\pi(T)$ (black dashed line) is also displayed.	68
5.7	Dependence of $\sqrt{s_V}$ (determined from Eqs. (5.43), (5.44) and (5.45)) on the slope $(s_2 - s_1)^{-1}$ of the ramp function $W(s)$ describing the onset of the continuum at $T = 100$ MeV. The grey band indicates the uncertainty range of the result obtained with step function parametrization of the continuum.	70
5.8	ρ -meson resonance at finite temperature from hidden local symmetry model.	71
5.9	Diagrams contributing to the V - A mixing at one loop. Vector and axial-vector fields are denoted by V and A and pion by ϕ_π . Here A represents the transverse components of the a_1 meson, while ϕ_q stands for the longitudinal one [102].	73
B.1	The light quark propagator.	85

List of Tables

4.1	Input summary	35
5.1	The average ρ -meson mass and its continuum threshold at various temperatures.	73

Bibliography

- [1] M. Cheng *et al.*, Phys. Rev. D **74**, 054507 (2006).
- [2] Y. Aoki, Z. Fodor, S. D. Katz and K. K. Szabo, Phys. Lett. B **643**, 46 (2006).
- [3] G. Agakishiev *et al.* [CERES/NA45 Collaboration], Phys. Lett. B **422**, 405 (1998).
- [4] G. Agakishiev *et al.* [CERES/NA45 Collaboration], Eur. Phys. J. C **41**, 475 (2005).
- [5] D. Adamova *et al.* [CERES/NA45 Collaboration], Phys. Rev. Lett. **91**, 042301 (2003).
- [6] D. Adamova *et al.* [CERES/NA45 Collaboration], Phys. Lett. B **666**, 425 (2008).
- [7] R. Arnaldi *et al.* [NA60 Collaboration], Phys. Rev. Lett. **96**, 162302 (2006).
- [8] S. Damjanovic *et al.* [NA60 Collaboration], Nucl. Phys. A **783**, 327 (2007).
- [9] R. Arnaldi *et al.* [NA60 Collaboration], Phys. Rev. Lett. **100**, 022302 (2008).
- [10] S. Damjanovic [NA60 Collaboration], J. Phys. G **35**, 104036 (2008).
- [11] R. Arnaldi *et al.* [NA60 Collaboration], Eur. Phys. J. C **59**, 607 (2009).
- [12] R. Arnaldi *et al.* [NA60 Collaboration], Eur. Phys. J. C **61**, 711 (2009).
- [13] G. E. Brown and M. Rho, Phys. Rev. Lett. **66**, 2720 (1991).
- [14] T. Hatsuda and S. H. Lee, Phys. Rev. C **46**, R34 (1992).
- [15] A. K. Dutt-Mazumder, R. Hofmann and M. Pospelov, Phys. Rev. C **63**, 015204 (2001).

- [16] M. Post and U. Mosel, Nucl. Phys. A **699**, 169 (2002).
- [17] M. F. M. Lutz, G. Wolf and B. Friman, Nucl. Phys. A **706**, 431 (2002).
- [18] K. G. Wilson, Phys. Rev. **179**, 1499 (1969).
- [19] K. G. Chetyrkin, N. V. Krasnikov and A. N. Tavkhelidze, Phys. Lett. B **76** (1978) 83.
- [20] N. V. Krasnikov and A. A. Pivovarov, Phys. Lett. B **112**, 397 (1982) [Sov. J. Nucl. Phys. **35**, 744.1982 YAFIA,35,1270 (1982 YAFIA,35,1270-1274.1982)].
- [21] N. V. Krasnikov, A. A. Pivovarov and N. N. Tavkhelidze, Z. Phys. C **19**, 301 (1983).
- [22] Y. Kwon, M. Procura and W. Weise, Phys. Rev. C **78**, 055203 (2008).
- [23] C. Amsler *et al.* [Particle Data Group], Phys. Lett. B **667**, 1 (2008).
- [24] J. Goldstone, Nuovo Cim. **19** (1961) 154.
- [25] E. Marco, R. Hofmann and W. Weise, Phys. Lett. B **530**, 88 (2002).
- [26] S. I. Dolinsky *et al.*, Phys. Rept. **202**, 99 (1991).
- [27] A. Aloisio *et al.* [KLOE Collaboration], Phys. Lett. B **606**, 12 (2005).
- [28] R. Barate *et al.* [ALEPH Collaboration], Eur. Phys. J. C **4**, 409 (1998).
- [29] K. Ackerstaff *et al.* [OPAL Collaboration], Eur. Phys. J. C **7**, 571 (1999).
- [30] M. Gell-Mann, R. J. Oakes and B. Renner, Phys. Rev. **175**, 2195 (1968).
- [31] A. Manohar and H. Georgi, Nucl. Phys. B **234**, 189 (1984).
- [32] Y. Nambu, Phys. Rev. **106**, 1366 (1957).
- [33] W. R. Frazer and J. R. Fulco, Phys. Rev. Lett. **2**, 365 (1959).
- [34] K. Kawarabayashi and M. Suzuki, Phys. Rev. Lett. **16**, 255 (1966).
- [35] Riazuddin and Fayyazuddin, Phys. Rev. **147**, 1071 (1966).
- [36] S. Weinberg, Phys. Rev. Lett. **18**, 507 (1967).

- [37] E. G. Drukarev and E. M. Levin, Nucl. Phys. A **511**, 679 (1990).
- [38] T. D. Cohen, R. J. Furnstahl and D. K. Griegel, Phys. Rev. C **45**, 1881 (1992).
- [39] C. M. Ko, V. Koch and G. Q. Li, Ann. Rev. Nucl. Part. Sci. **47**, 505 (1997).
- [40] G. E. Brown and M. Rho, Phys. Rept. **269**, 333 (1996).
- [41] R. Rapp and J. Wambach, Adv. Nucl. Phys. **25**, 1 (2000).
- [42] T. Hatsuda, Y. Koike and S. H. Lee, Nucl. Phys. B **394** (1993) 221.
- [43] C. Song, Phys. Rev. D **48**, 1375 (1993).
- [44] R. Rapp, J. Wambach and H. van Hees, arXiv:0901.3289 [hep-ph].
- [45] M. Dey, V. L. Eletsky and B. L. Ioffe, Phys. Lett. B **252**, 620 (1990).
- [46] M. A. Shifman, A. I. Vainshtein and V. I. Zakharov, Nucl. Phys. B **147**, 385, 448 (1979).
- [47] J. S. Schwinger, Phys. Rev. **82**, 664 (1951).
- [48] E. V. Shuryak and A. I. Vainshtein, Nucl. Phys. B **199**, 451 (1982).
- [49] I. I. Balitsky and V. M. Braun, Nucl. Phys. B **311**, 541 (1989).
- [50] G. Källén, Helv. Phys. Acta **25** (1952), 417.
- [51] H. Lehmann, Nuovo Cim. **11** (1954) 342.
- [52] P. Güttinger, Z. Phys. **73** (1932) 169.
- [53] J. C. Collins, A. Duncan and S. D. Joglekar, Phys. Rev. D **16**, 438 (1977).
- [54] J. Gasser and H. Leutwyler, Phys. Lett. B **184**, 83 (1987).
- [55] P. Gerber and H. Leutwyler, Nucl. Phys. B **321**, 387 (1989).
- [56] T. Hatsuda, S. H. Lee and H. Shiomi, Phys. Rev. C **52**, 3364 (1995).
- [57] F. Klingl, N. Kaiser and W. Weise, Nucl. Phys. A **624**, 527 (1997).
- [58] V. L. Eletsky and B. L. Ioffe, Phys. Rev. Lett. **78**, 1010 (1997).
- [59] T. Hatsuda and S. H. Lee, arXiv:nucl-th/9703022.

- [60] V. L. Eletsky and B. L. Ioffe, arXiv:hep-ph/9704236.
- [61] S. Leupold and U. Mosel, Phys. Rev. C **58**, 2939 (1998).
- [62] S. Zschocke, O. P. Pavlenko and B. Kämpfer, Eur. Phys. J. A **15**, 529 (2002).
- [63] B. Steinmueller and S. Leupold, Nucl. Phys. A **778**, 195 (2006).
- [64] R. Thomas, S. Zschocke and B. Kämpfer, Phys. Rev. Lett. **95**, 232301 (2005).
- [65] R. Thomas, T. Hilger and B. Kämpfer, Prog. Part. Nucl. Phys. **61**, 297 (2008).
- [66] R. Rapp, G. Chanfray and J. Wambach, Nucl. Phys. A **617**, 472 (1997).
- [67] M. Post and U. Mosel, Nucl. Phys. A **688**, 808 (2001).
- [68] J. Ruppert, T. Renk and B. Müller, Phys. Rev. C **73**, 034907 (2006).
- [69] F. Klingl and W. Weise, Eur. Phys. J. A **4**, 225 (1999).
- [70] E. Marco and W. Weise, Phys. Lett. B **482**, 87 (2000).
- [71] K. Maltman, Phys. Lett. B **440**, 367 (1998).
- [72] J. Bordes, C. A. Dominguez, J. Penarrocha and K. Schilcher, JHEP **0602**, 037 (2006).
- [73] T. Renk, R. A. Schneider and W. Weise, Phys. Rev. C **66**, 014902 (2002).
- [74] J. Ruppert, C. Gale, T. Renk, P. Lichard and J. I. Kapusta, Phys. Rev. Lett. **100**, 162301 (2008).
- [75] H. van Hees and R. Rapp, Nucl. Phys. A **806**, 339 (2008).
- [76] B. L. Ioffe, Prog. Part. Nucl. Phys. **56**, 232 (2006).
- [77] A. D. Martin, R. G. Roberts, W. J. Stirling and R. S. Thorne, Eur. Phys. J. C **4**, 463 (1998).
- [78] A. D. Martin, R. G. Roberts, W. J. Stirling and R. S. Thorne, Eur. Phys. J. C **23**, 73 (2002).
- [79] M. Procura, T. R. Hemmert and W. Weise, Phys. Rev. D **69**, 034505 (2004).

- [80] M. Procura, B. U. Musch, T. Wollenweber, T. R. Hemmert and W. Weise, Phys. Rev. D **73**, 114510 (2006).
- [81] J. Gasser, H. Leutwyler and M. E. Sainio, Phys. Lett. B **253**, 252 (1991).
- [82] S. Bethke, Prog. Part. Nucl. Phys. **58**, 351 (2007).
- [83] G. M. Prosperi, M. Raciti and C. Simolo, Prog. Part. Nucl. Phys. **58**, 387 (2007).
- [84] F. Klingl, N. Kaiser and W. Weise, Z. Phys. A **356**, 193 (1996).
- [85] U. G. Meissner, J. A. Oller and A. Wirzba, Annals Phys. **297**, 27 (2002).
- [86] H. C. Schröder *et al.*, Phys. Lett. B **469** (1999) 25.
- [87] K. Suzuki *et al.*, Phys. Rev. Lett. **92**, 072302 (2004).
- [88] E. E. Kolomeitsev, N. Kaiser and W. Weise, Phys. Rev. Lett. **90**, 092501 (2003).
- [89] E. E. Kolomeitsev, N. Kaiser and W. Weise, Nucl. Phys. A **721**, 835 (2003).
- [90] E. Friedman and A. Gal, Phys. Rept. **452**, 89 (2007).
- [91] D. Jido, T. Hatsuda and T. Kunihiro, Prog. Theor. Phys. Suppl. **168**, 478 (2007).
- [92] N. Kaiser, P. de Homont and W. Weise, Phys. Rev. C **77**, 025204 (2008).
- [93] R. Thomas, T. Hilger and B. Kämpfer, Nucl. Phys. A **795**, 19 (2007).
- [94] T. Hatsuda and T. Kunihiro, Nucl. Phys. B **387**, 715 (1992).
- [95] N. Kaiser, Phys. Rev. C **59**, 2945 (1999).
- [96] J. J. Sakurai, K. Schilcher and M. D. Tran, Phys. Lett. B **102**, 55 (1981).
- [97] M. Bando, T. Kugo and K. Yamawaki, Nucl. Phys. B **259**, 493 (1985).
- [98] M. Bando, T. Kugo and K. Yamawaki, Phys. Rept. **164**, 217 (1988).
- [99] M. Bando, T. Fujiwara and K. Yamawaki, Prog. Theor. Phys. **79**, 1140 (1988).
- [100] N. Kaiser and U. G. Meissner, Nucl. Phys. A **519**, 671 (1990).

- [101] M. Harada and C. Sasaki, Phys. Rev. D **73**, 036001 (2006).
- [102] M. Harada, C. Sasaki and W. Weise, Phys. Rev. D **78**, 114003 (2008).
- [103] V. L. Eletsky and B. L. Ioffe, Phys. Rev. D **51**, 2371 (1995)

Acknowledgments

I would like to take this opportunity to acknowledge those who have given me guidance, assistance and support for my doctoral study at TUM.

First of all I am greatly indebted to my thesis supervisor, Prof. Dr. Wolfram Weise in completing this dissertation. I sincerely appreciate his patience and endeavor on this work. I would like to notice that his comments have been always a great help and profound insight on the thesis at all the times.

To my collaborators, I would like to thank Dr. Massimiliano Procura and Dr. Chihiro Sasaki for fruitful and stimulating discussions. I also give my gratitude to Dr. Seung-il Nam at Chung-Yuan Christian University and Prof. Su Houng Lee at Yonsei University for their useful discussions.

I extend my sincere thanks to all members of T39, Thomas Hell, Alexander Laschka, Nino Bratovic, Dr. Bernhard Musch and others, who have given me warm hospitality.

Last but not least, I would like to stress my appreciation to my parents and sister who have been always on my side and supported me. Their love to me has been inspiration and strength for me to study by this far.